

UCLA

UCLA Electronic Theses and Dissertations

Title

Functional Characterization of Novel Cell Division Enzymes

Permalink

<https://escholarship.org/uc/item/68513775>

Author

Ramirez, Ivan

Publication Date

2021

Peer reviewed|Thesis/dissertation

UNIVERSITY OF CALIFORNIA
Los Angeles

Functional Characterization of Novel Cell Division Enzymes

A Dissertation submitted in satisfaction of the requirements for the degree Doctor of
Philosophy in Biochemistry and Molecular Biology

by

Ivan Ramirez

2021

© Copyright by

Ivan Ramirez

2021

ABSTRACT OF THE DISSERTATION

Functional Characterization of Novel Cell Division Enzymes

by

Ivan Ramirez

Doctor of Philosophy in Biochemistry and Molecular Biology

University of California, Los Angeles, 2021

Professor Jorge Z. Torres, Chair

The discovery of novel cell division proteins is important to further understand the basic mechanisms of cell division. Equally important is an understanding of how these proteins are misregulated to induce cell proliferation and the associated human diseases like cancer. Therefore, the discovery of novel cell division proteins and their functional characterization creates opportunities to define new cancer targets that can be used to develop new cancer therapeutics. The primary goal of this thesis was to identify new

enzymes that are misregulated in cancer cells and to understand their functions during cell division. The first enzyme that I analyzed was the previously uncharacterized protein Myl5, which is a myosin regulatory light chain (RLC). I determined that Myl5 localizes to the mitotic spindle and is important for cell division. Depletion of MYL5 in cancer cells led to mitotic defects and a slower transition through mitosis. In contrast, overexpression of MYL5 in cancer cells led to a faster mitosis. To my knowledge this the first myosin RLC that has been implicated in mitotic spindle assembly. The second protein that I analyzed was the cyclin dependent kinase Cdk14. Cdk14 has been linked to the cell cycle via the WNT signaling pathway. However, Cdk14 had not been implicated in cell division. My work showed that Cdk14 localizes to the mitotic spindle during mitosis and its down regulation resulted in severe mitotic defects and a faster cell division. This study enhanced our understanding of how the spindle assembly checkpoint (SAC) is regulated and how its dysregulation can impact cancer cell proliferation and anticancer drug resistance. Together, my work on Myl5 and Cdk14 has elucidated the function of these two previously underappreciated proteins in cell division.

The dissertation of Ivan Ramirez is approved.

Steven G. Clarke

Catherine F. Clarke

Kent L. Hill

Jorge Z. Torres, Committee Chair

University of California, Los Angeles

2021

Dedication

I would like to dedicate this work to my family.

Table of Contents

Abstract of Dissertation	ii-iii
Committee Page	iv
Dedication	v
Table of Contents	vi
List of Tables and Figures	vii-viii
Acknowledgements	ix-x
Curriculum Vitae	xi-xii
Chapter 1: Introduction to the cell cycle	1
References	9
Chapter 2: The myosin regulatory light chain Myl5 localizes to mitotic spindle poles and is required for proper cell division	15
References	51
Chapter 3: The role of Cdk14 in cell division	62
References	81
Chapter 4: Final thoughts	84
Appendix I: DUSP7 Regulates the Activity of ERK2 to Promote Proper Chromosome Alignment During Cell	86
References	94
Appendix II: Inducible LAP-tagged Stable Cell Lines for Investigating Protein Function, Spatiotemporal Localization and Protein Interaction Networks	96
References	104

List of Tables and Figures

Chapter 2

Figure 1	In silico analyses of Myl5	35
Figure 2	Myl5 localizes to mitotic spindle poles during mitosis	37
Figure 3	Depletion of Myl5 leads to spindle assembly and cell division defects	38
Figure 4	Modulation of Myl5 levels affects the time to cell division	39
Figure 5	Myl5 colocalizes with MYO10 at mitotic spindle poles during mitosis and binds to MYO10 <i>in vitro</i>	40
Figure 6	Myl5 localizes to the leading edge and filopodia	42
Figure S1	Expression of GFP-Myl5 and its localization to mitotic spindle poles during mitosis	43
Figure S2	Depletion of Myl5 leads to spindle assembly and cell division defects	44
Figure S3	Generation of a Myl5 siRNA-resistant clone for use in rescue experiments	45
Figure S4	Control immunoprecipitation (IP) experiment related to Figure 5c,d	46
Figure S5	Myl5 shares conserved S/T phosphorylation sites with other myosin regulatory light chains (RLCs)	47
Table S1	Reagents and resources	48
Table S2	List of cancer types analyzed for Myl5 and MYO10 differential gene expression	50

Chapter 3

Figure 1	Immunofluorescence microscopy of fixed cells overexpressing GFP-Cdk14	75
Figure 2	Cdk14 truncation analysis	76
Figure 3	Cdk14 protein associations	76
Figure 4	Cdk14 depletion analysis	77
Table S1	Reagents and resources	78

Appendix I

Figure 1	DUSP7 interacts with ERK2 and regulates the levels of phospho-ERK2	89
Figure 2	Knockdown of DUSP7 leads to chromosome alignment and segregation defects	90
Figure 3	DUSP7 promotes chromosome alignment in mitosis by regulating ERK2 activity	91
Figure 4	ERK2 interacts with DUSP7 independently of ERK2 phosphorylation	92

Appendix II

Figure 1	Overview of the Generation of LAP-tagged inducible Stable Cell Lines for any Protein of Interest	101
Figure 2	Overview of the Applications for LAP-tagged Stable Cell Lines	101
Figure 3	Overview of LAP-tagged Protein Expression, Purification for Mass Spectrometry	101
Figure 4	Verification of LAP-Tau expression	102
Table 1	Forward and Reverse Primers for Amplifying ORFs or Interest for Insertion into the Shuttle Vector	102
Table 2	PCR Conditions for Amplification of the ORDFs of Interest	102
Table 3	Forward and Reverse Sequencing Primers for the Shuttle Vector	103
Table 4	List of Available LAP/TAP Vectors with Variable Promoters, Epitope-tags, and Dox Inducible Expression Capabilities for N or C terminal Protein Tagging	103

Acknowledgements

This thesis would not have been possible without the invaluable involvement of a number of people. I would first like to thank all the faculty at Cal State University of Dominguez Hills who helped me get to this point of my career. I would like to give a special thanks to Gaby Gomez Dominguez from CSUDH, who recommended that I conduct summer research and ultimately sparked my interest in pursuing my graduate degree. I also need to thank Dr. Diana Azurdia who was instrumental in helping me get past some of my initial struggles in graduate school. She provided me with great advice that I will keep with me throughout my career and I am truly appreciative of all that she did for me.

Next, I would like to give my sincere thanks to the past and present lab-mates I have had the pleasure of knowing over the years and for helping with experiments while having lighthearted banter. I would especially like to thank Dr. Yenni Garcia who was always available for any experiment or career questions I had. I appreciate all of our conversations we had in the lab together that made the time pass by while conducting long experiments. I would also like to thank Dr. Xiao Guo who never failed to make me laugh, even when she wasn't trying too. I also need to thank my running mate Dr. Shahriyar Jahanbakhs who was ready to go for a run at a moment's notice whenever I needed to take a break from my research. Additionally, I would like to thank my Committee Members: Dr. Steve Clarke, Dr. Cathy Clarke, and Dr. Kent Hill. I appreciated all the feedback you provided me with about my research projects and career choices. I would like to thank all the undergraduate students that I have mentored in my time in the lab: Quynh Dam, Carlos Hernandez, Liliana Perez, and Daniel Lu for all their help. I would like to express my deepest gratitude to my mentor and supervisor Dr. Jorge Torres who

extended his assistance, support, and guidance in the process of my research and writing this thesis. I could never express how thankful I am for everything he has done for me during my time in graduate school. His door was always open for any question or concern I had and always made time for me.

I need to thank my parents and sister who always encouraged and supported me to get a graduate degree. Also, I would like to thank my aunts who would say that they were instrumental to me getting this degree.

Finally, I need to thank my partner Natalie, who always supported me throughout my graduate school career. Whenever I encountered a failure she would undoubtedly be there to support me and provide me with the encouragement I needed to continue with my work.

Thank you for everything.

Project: Identifying Protein Potential Binding Sites On BRCA1 using Bioinformatic Approaches and Verified by Peptide Array

Research Internship

Summer 2011

Indiana University-Purdue University Indianapolis

Mentor: Dr. Keith Dunker

Project: Identifying Potential Binding Sites In BRCA1 Using Bioinformatics

PUBLICATIONS

Guo X., **Ramirez I.**, Garcia Y.A., Velasquez E.F., Gholkar A.A., Cohn W., Whitelegge J.P., Tofig B., Damoiseaux R., and Torres, J.Z. "DUSP7 Regulates the Activity of ERK2 to Promote Proper Chromosome Alignment During Cell Division", *Journal of Biological Chemistry* 2021 April 15:100676. doi: 10.1016/j.jbc.2021.100676. Epub ahead of print. PMID: 33865857.

Ramirez I., Gholkar A.A., Velasquez E.F., Guo X., Bobby T., Damoiseaux R., and Torres, J.Z. "The Myosin Regulatory Light Chain Myl5 Localizes to Mitotic Spindle Poles and is Required for Proper Cell Division", *Cytoskeleton*, 2021.

Bradley M., **Ramirez I.**, Cheung K., Gholkar A.A., and Torres J.Z. "Inducible LAP-tagged Stable Cell Lines for Investigating Protein Function, Spatiotemporal Localization and Protein Interaction Networks", *Journal of Visualized Experiments* 2016 Dec. 24, (118):1-9, e54870, doi:10.3791/54870. PMID:28060263

Chapter 1

Introduction to the cell cycle

Overview of Cell Division:

The cell cycle is a sequence of events in which a cell will grow, duplicate its genome and divide into two identical daughter cells. This process is regulated by cyclins and cyclin dependent kinases (Cdk) whose presence and activity can speed up, slow down, or halt cell division (1). Eukaryotic cell division is encompassed by two major phases interphase and mitosis (M phase). Cells spend the majority of the time in interphase and do not divide during this time. Division of the genetic material occurs in mitosis which results in the formation of two new nuclei. Some cells may exit the cell cycle and enter a G0 phase where they are quiescent and do not divide (2). This phase can be temporary or permanent depending on whether or not they receive proliferative stimuli to re-enter the cell cycle (B). Interphase is composed of three phases Gap 1 (G1), DNA synthesis (S) and Gap 2 (G2). During G1 phase the cell will grow bigger and begin to synthesize the necessary proteins, RNA, and membranes needed for DNA synthesis (3). During S phase the cell will duplicate its genome and centrosomes (3). During G2 phase the cell will continue to grow and will synthesize the necessary proteins required to enter the mitotic M phase (4). During M phase the cell will segregate its duplicated DNA into two identical daughter cells by going through a series of subphases; Prophase, Metaphase, Anaphase/Telophase and Cytokinesis. Prophase can be further broken down into early prophase where the cell will begin to condense its DNA and prometaphase where the nuclear membrane starts to break down and centrosomes move to opposite sides of the cell. During Metaphase the chromosomes will begin to align at the metaphase plate and the centrosomes move to opposite sides of the cell. Microtubules then radiate out from the centrosomes, attach to the kinetochore region of the chromosomes, form the mitotic spindle, and align the chromosomes at the cell midplane. During anaphase the microtubules begin to pull the chromosomes to opposite ends of the cell and during telophase the DNA begins to unwind

and the nuclear envelope begins to reform. Finally, during cytokinesis the cell splits apart into two identical daughter cells completing the cell division cycle.

Cell Cycle Checkpoints:

The sequence of events that occur during the cell cycle are carefully monitored by a series of checkpoints that ensure proper cell division. These checkpoints ensure that cell has the necessary components to enter and exit each cell cycle phase. Without these checkpoints the cell could transition into the next phase without the necessary components, which could lead to cell defects and/or cell death. The three major cell cycle checkpoints are at the G1/S transition, G2/M transition, and the metaphase to anaphase transition (also known as the spindle assembly checkpoint, SAC). It is important for the cell to properly duplicate its DNA in G1/S before going into mitosis and not doing so can result in unequal genome distribution and cell death. The cell can also duplicate its chromosomes but not undergo cell divisions, which can also become problematic because it leads to polyploidy (5). Additionally, a cell can divide and have each cell inherit a different number of chromosomes called aneuploidy, which occurs when the SAC is dysfunctional and proper microtubule-kinetochore attachment cannot be monitored (6). Aneuploidy is a hallmark of many types of cancer cells, leading to the belief that accurate chromosome segregation is important for preventing proliferative diseases (7). Even if the cell transitions through all the checkpoints, if it is not able to divide during cytokinesis then the daughter cells may still become polyploidy (8). This doubling of the genome in the cell makes it more susceptible to chromosome segregation errors in future cell divisions. The mitotic microtubule-based spindle is responsible for congressing chromosomes to the metaphase plate and for separating sister chromatids into two identical pools for each daughter cell. Therefore, the spindle must be formed in a bipolar manner in order to carry out its

functions. Also the orientation and positioning of the mitotic spindle are important for establishing the cell division plane (6). Abnormal spindle assembly can result in a delayed mitosis and aneuploidy (6). Although many components involved in assembling and orienting the spindle are known, the molecular signaling pathways that govern these events are not well understood. Increasing evidence indicates that both the actin and microtubule cytoskeletal systems are necessary for proper cell division (9). For example, astral microtubules that emanate from the spindle poles are essential for the proper orientation of the spindle (10). Recently, the unconventional myosin 10 (Myo10), was shown to be an important factor for the architecture and function of the mitotic spindle; through its binding to both actin and microtubules (11).

Spindle Assembly Checkpoint:

Pivotal to cell division is the metaphase to anaphase transition, which is a highly regulated process involving a multitude of protein-protein interactions that are regulated by posttranslational modifications like phosphorylation and ubiquitination that function as switches to activate/inactivate protein function (12). For example, the multi-component spindle assembly checkpoint (SAC) is essential for maintaining the fidelity of chromosome segregation from a mother cell to the daughter cells. Misregulation of the spindle assembly checkpoint can lead to segregation errors, chromosomal instability, aneuploidy and tumorigenesis (13). However, there is currently no consensus as to the pathways and factors that are deregulated to induce aneuploidy, why it is prevalent in cancer and how it contributes to tumorigenesis. Many cancers will also down-regulate the SAC to bypass their sensitivity to antimetabolic agents (14). The SAC becomes activated when unattached kinetochores or nonproductive (monotelic, syntelic, and merotelic) microtubule attachments are sensed (15). The SAC then arrests cells

in metaphase to give time to correct these deficiencies and to generate proper microtubule-kinetochore attachments. A key factor in SAC activation is the mitotic checkpoint complex (composed of Mad2, BubR1/Mad3, and Bub3) that binds to the anaphase promoting complex, cyclosome (APC/C) ubiquitin ligase substrate adapter protein Cdc20 and inactivates the APC/C (12). Once proper microtubule-kinetochore attachment is sensed, the SAC is satisfied and the inhibitory effects of the MCC on the APC/C are relieved. Activated APC/C will then ubiquitinate Securin and target it for proteasome-dependent degradation, which in turn activates Separase. Separase subsequently cleaves the cohesion complex, allowing for chromosome segregation and marking the entry into anaphase.

Cyclin Dependent Kinases:

Cyclin-dependent kinases (Cdks) play an essential role in cell cycle regulation. They are the main machinery that drives cell cycle progression. Cdks are serine/threonine protein kinases that consist of a catalytic Cdk subunit and its corresponding activating cyclin subunit (16). Their activation by specific cyclin subunits coordinates the progression of the cell cycle from one stage to another. The ability of Cdks to phosphorylate different substrates allows them to regulate the cell cycle in response to different cellular cues (17). There are more than 20 CDK genes and more than 10 cyclin genes in the human genome (18,19). Cdks phosphorylate (and regulate the function of) a myriad of substrates with distinct functions that influence transcription, signal transduction, epigenetic regulation, metabolism, stem cell self-renewal, neuronal functions, and spermatogenesis (20). Each Cdk has a conserved catalytic core that is encompassed by the PSTAIRE domain, an activating T-loop, and an ATP binding pocket. Important for Cdk function is the binding of a cyclin to the Cdk via the PSTAIRE-like cyclin binding domain which in turn induces a structural shift in the Cdk exposing the substrate

binding interface and realigns residues in the active site. Most Cdks can bind different cyclins allowing them to interact with a wide range of substrates for phosphorylation. However, dysregulation of Cdks and cyclins can lead to the misregulation of the cell cycle, cell growth, and cell proliferation (21). Similarly, mutations that lead to hyperactivation of Cdk activity have been found in human cancer genomes and lead to selective growth advantage (22,23,24). Therefore, Cdks have been extensively studied within the context of cancer and are the subject of many ongoing cancer therapeutic studies. For example, over 30 small drug-like molecules have been developed to target hyper active Cdks in cancer cells (25).

Myosins:

Myosins perform a variety of functions in muscle contraction, cargo transport, cell adhesion, and cell division; including spindle assembly, spindle orientation and cytokinesis (26). There are about 40 different myosin genes in the human genome which categorized into 12 subfamilies (27). Myosins can be further divided into two major groups; conventional and unconventional (28). The only conventional myosin is myosin-II, which is highly expressed in muscle cells and is required for muscle contraction (29). Additionally, myosin-II can also be found in non-muscle cells at the contractile ring, which is necessary for physically dividing the cytoplasm of a dividing cell into two cells (30). Myosin-II contains a long coiled-coil dimerization domain at its C-termini that helps it form bipolar filaments (31,32). The remainder of the myosin motors form the unconventional myosin group and have varying domain compositions, outside of their conserved motor domain, which helps them carry out diverse functions like actin-based cytoplasmic transport of cargos (33,34).

Myosins in Cancer:

A number of unconventional myosin motors have been implicated in cellular processes that affect tumor progression and metastasis (35). Interestingly, myosins have been shown to function as tumor suppressors and are found mutated in 2-45% of tumor samples (36,37,38). This is very similar to other tumor suppressors like TP53 which is mutated in 5-50% of tumors, depending on the cancer type (39). For example, lower levels of myosin1a have been observed in patients with colorectal cancer, which has been correlated with faster tumor progression (40). Similarly, myosin1a is found mutated at a high frequency in patients with gastric tumors (40). Another example is myosin 5 that when sequestered to the actin cytoskeleton has been shown to promote cancer cell survival (41). Blocking of the myosin 5 sequestration in melanoma cells leads to apoptosis and a decrease in tumor growth in mice, indicating that myosin 5 may be involved in regulating tumor cell death (42).

Myosin Light Chains

The myosin holoenzyme consists of heavy and light chains. However less is known about myosin light chains in cell division. Myosin light chains are required for the structural integrity of the myosin holoenzyme and have regulatory functions that affect the activity of the protein complex (26). There are two major groups of myosin light chains, the Essential Light Chains (ELCs) and Regulatory Light Chains (RLCs). The regulatory light chains, as the name implies, are involved in the regulation of the enzymatic activity of the myosin (43). While the essential light chains are essential for the enzymatic activity of the myosin, which when removed under harsh conditions the enzyme activity of the myosin is lost (43). Myosin regulatory light chains have also been implicated in tumorigenesis via their phosphorylation. These MLC are usually phosphorylated by myosin light chain kinases (MLCK) and dephosphorylated by myosin phosphatases. Interestingly, low levels of MLC phosphorylation have been correlated with a

failure to undergo proper cytokinesis in cancer cells (44), which results in multinucleated cells (44). Additionally, overexpression of unphosphorylatable MLC in mammalian cells results in chromosome separation defects at the metaphase to anaphase transition and in cytokinetic defects that lead to a failure in cytokinesis (45).

References:

1. Malumbres, Marcos. "Cyclin-Dependent Kinases." *Genome Biology* 15, no. 6 (June 30, 2014): 122. <https://doi.org/10.1186/gb4184>.
2. Harper, Jane V., and Gavin Brooks. "The Mammalian Cell Cycle." In *Cell Cycle Control: Mechanisms and Protocols*, edited by Tim Humphrey and Gavin Brooks, 113–53. *Methods in Molecular Biology*TM. Totowa, NJ: Humana Press, 2005. <https://doi.org/10.1385/1-59259-857-9:113>.
3. Pardee, A. B. "G1 Events and Regulation of Cell Proliferation." *Science* 246, no. 4930 (November 3, 1989): 603–8. <https://doi.org/10.1126/science.2683075>.
4. Morgan, David. *The Cell Cycle : Principles of Control*. London ;Sunderland MA: New Science Press ;;Sinauer Associates, 2007.
5. Potapova, Tamara, and Gary J. Gorbsky. "The Consequences of Chromosome Segregation Errors in Mitosis and Meiosis." *Biology* 6, no. 1 (February 8, 2017). <https://doi.org/10.3390/biology6010012>.
6. Tanaka, Kozo, and Toru Hirota. "Chromosome Segregation Machinery and Cancer." *Cancer Science* 100, no. 7 (July 2009): 1158–65. <https://doi.org/10.1111/j.1349-7006.2009.01178.x>.
7. Potapova, Tamara A, Jin Zhu, and Rong Li. "Aneuploidy and Chromosomal Instability: A Vicious Cycle Driving Cellular Evolution and Cancer Genome Chaos." *Cancer Metastasis Reviews* 32, no. 0 (December 2013). <https://doi.org/10.1007/s10555-013-9436-6>.
8. Normand, Guillaume, and Randall W. King. "Understanding Cytokinesis Failure." *Advances in Experimental Medicine and Biology* 676 (2010): 27–55.
9. Fletcher, Daniel A., and R. Dyche Mullins. "Cell Mechanics and the Cytoskeleton." *Nature* 463, no. 7280 (January 28, 2010): 485. <https://doi.org/10.1038/nature08908>.

10. Chan, Po-Chao, Rosaline Y. C. Hsu, Chih-Wei Liu, Chien-Chen Lai, and Hong-Chen Chen. "Adducin-1 Is Essential for Mitotic Spindle Assembly through Its Interaction with Myosin-X." *The Journal of Cell Biology* 204, no. 1 (January 6, 2014): 19.
<https://doi.org/10.1083/jcb.201306083>.
11. Fletcher, Daniel A., and R. Dyche Mullins. "Cell Mechanics and the Cytoskeleton." *Nature* 463, no. 7280 (January 28, 2010): 485. <https://doi.org/10.1038/nature08908>.
12. Teixeira, José Henrique, Patrícia Manuela Silva, Rita Margarida Reis, Inês Moranguinho Moura, Sandra Marques, Joana Fonseca, Luís Silva Monteiro, and Hassan Bousbaa. "An Overview of the Spindle Assembly Checkpoint Status in Oral Cancer." *BioMed Research International* 2014 (2014). <https://doi.org/10.1155/2014/145289>.
13. Ciliberto, Andrea, and Jagesh V. Shah. "A Quantitative Systems View of the Spindle Assembly Checkpoint." *The EMBO Journal* 28, no. 15 (August 5, 2009): 2162.
<https://doi.org/10.1038/emboj.2009.186>.
14. Fang, Xiao, and Pumin Zhang. "Aneuploidy and Tumorigenesis." *Seminars in Cell & Developmental Biology* 22, no. 6 (August 2011): 595.
<https://doi.org/10.1016/j.semcdb.2011.03.002>.
15. Ba, Pinsky, and Biggins S. "The Spindle Checkpoint: Tension versus Attachment." *Trends in cell biology*. *Trends Cell Biol*, September 2005.
<https://doi.org/10.1016/j.tcb.2005.07.005>.
16. "Mechanisms of Cyclin-Dependent Kinase Regulation: Structures of Cdks, Their Cyclin Activators, and Cip and INK4 Inhibitors,." *Journal of Molecular Biology* 287, no. 5 (April 16, 1999): 821–28. <https://doi.org/10.1006/jmbi.1999.2640>.
17. Malumbres, Marcos. "Cyclin-Dependent Kinases." *Genome Biology* 15, no. 6 (2014): 122.
<https://doi.org/10.1186/gb4184>.

18. Malumbres, Marcos, Edward Harlow, Tim Hunt, Tony Hunter, Jill M. Lahti, Gerard Manning, David O. Morgan, Li-Huei Tsai, and Debra J. Wolgemuth. "Cyclin-Dependent Kinases: A Family Portrait." *Nature Cell Biology* 11, no. 11 (November 2009): 1275. <https://doi.org/10.1038/ncb1109-1275>.
19. S, Lim, and Kaldis P. "Cdks, Cyclins and CKIs: Roles beyond Cell Cycle Regulation." *Development* (Cambridge, England). *Development*, August 2013. <https://doi.org/10.1242/dev.091744>.
20. T, Ishidate, Elewa A, Kim S, Mello Cc, and Shirayama M. "Divide and Differentiate: CDK/Cyclins and the Art of Development." *Cell cycle* (Georgetown, Tex.). *Cell Cycle*, 2014. <https://doi.org/10.4161/cc.28656>.
21. Peyressatre, Marion, Camille Prével, Morgan Pellerano, and May C. Morris. "Targeting Cyclin-Dependent Kinases in Human Cancers: From Small Molecules to Peptide Inhibitors." *Cancers* 7, no. 1 (March 2015): 179. <https://doi.org/10.3390/cancers7010179>.
22. Malumbres, Marcos, and Mariano Barbacid. "Cell Cycle, CDKs and Cancer: A Changing Paradigm." *Nature Reviews. Cancer* 9, no. 3 (March 2009): 153–66. <https://doi.org/10.1038/nrc2602>.
23. Whitfield, Michael L., Lacy K. George, Gavin D. Grant, and Charles M. Perou. "Common Markers of Proliferation." *Nature Reviews. Cancer* 6, no. 2 (February 2006): 99–106. <https://doi.org/10.1038/nrc1802>.
24. Pérez de Castro, Ignacio, Guillermo de Cárcer, and Marcos Malumbres. "A Census of Mitotic Cancer Genes: New Insights into Tumor Cell Biology and Cancer Therapy." *Carcinogenesis* 28, no. 5 (May 2007): 899–912. <https://doi.org/10.1093/carcin/bgm019>.
25. A, Pumfery, de la Fuente C, Berro R, Nekhai S, Kashanchi F, and Chao Sh. "Potential Use of Pharmacological Cyclin-Dependent Kinase Inhibitors as Anti-HIV Therapeutics."

Current pharmaceutical design. *Curr Pharm Des*, 2006.

<https://doi.org/10.2174/138161206777442083>

26. Heissler, Sarah M., and James R. Sellers. "Myosin Light Chains: Teaching Old Dogs New Tricks." *Bioarchitecture* 4, no. 6 (2014): 169–88.
27. J, Li, Lu Q, and Zhang M. "Structural Basis of Cargo Recognition by Unconventional Myosins in Cellular Trafficking." *Traffic* (Copenhagen, Denmark). *Traffic*, August 2016.
<https://doi.org/10.1111/tra.12383>.
28. Js, Berg, Powell Bc, and Cheney Re. "A Millennial Myosin Census." *Molecular biology of the cell. Mol Biol Cell*, April 2001. <https://doi.org/10.1091/mbc.12.4.780>.
29. Vicente-Manzanares, Miguel, Xuefei Ma, Robert S. Adelstein, and Alan Rick Horwitz. "Non-Muscle Myosin II Takes Centre Stage in Cell Adhesion and Migration." *Nature Reviews. Molecular Cell Biology* 10, no. 11 (November 2009): 778–90.
<https://doi.org/10.1038/nrm2786>.
30. Lodish, Harvey, Arnold Berk, S. Lawrence Zipursky, Paul Matsudaira, David Baltimore, and James Darnell. "Actin and Myosin in Nonmuscle Cells." *Molecular Cell Biology*. 4th Edition, 2000. <https://www.ncbi.nlm.nih.gov/books/NBK21562/>.
31. Geeves, M. A., and K. C. Holmes. "Structural Mechanism of Muscle Contraction." *Annual Review of Biochemistry* 68 (1999): 687–728.
<https://doi.org/10.1146/annurev.biochem.68.1.687>.
32. Beach, Jordan R., and John A. Hammer. "Myosin II Isoform Co-Assembly and Differential Regulation in Mammalian Systems." *Experimental Cell Research* 334, no. 1 (May 15, 2015): 2–9. <https://doi.org/10.1016/j.yexcr.2015.01.012>.
33. Hartman, M. Amanda, Dina Finan, Sivaraj Sivaramakrishnan, and James A. Spudich. "Principles of Unconventional Myosin Function and Targeting." *Annual Review of Cell and*

Developmental Biology 27 (2011): 133–55. <https://doi.org/10.1146/annurev-cellbio-100809-151502>.

34. Ma, Hartman, and Spudich Ja. “The Myosin Superfamily at a Glance.” *Journal of cell science*. *J Cell Sci*, April 1, 2012. <https://doi.org/10.1242/jcs.094300>.
35. Ouderkirk, J. L., and M. Krendel. “Non-Muscle Myosins in Tumor Progression, Cancer Cell Invasion and Metastasis.” *Cytoskeleton (Hoboken, N.J.)* 71, no. 8 (August 2014): 447–63. <https://doi.org/10.1002/cm.21187>.
36. Mazzolini, Rocco, Paulo Rodrigues, Sarah Bazzocco, Higinio Dopeso, Ana M. Ferreira, Silvia Mateo-Lozano, Elena Andretta, et al. “Brush Border Myosin Ia Inactivation in Gastric but Not Endometrial Tumors.” *International Journal of Cancer* 132, no. 8 (April 15, 2013): 1790–99. <https://doi.org/10.1002/ijc.27856>.
37. Nakano, Tetsuhiro, Masachika Tani, Michiho Nishioka, Takashi Kohno, Ayaka Otsuka, Susumu Ohwada, and Jun Yokota. “Genetic and Epigenetic Alterations of the Candidate Tumor-Suppressor Gene MYO18B, on Chromosome Arm 22q, in Colorectal Cancer.” *Genes, Chromosomes & Cancer* 43, no. 2 (June 2005): 162–71. <https://doi.org/10.1002/gcc.20180>.
38. Yanaihara, Nozomu, Michiho Nishioka, Takashi Kohno, Ayaka Otsuka, Aikou Okamoto, Kazunori Ochiai, Tadao Tanaka, and Jun Yokota. “Reduced Expression of MYO18B, a Candidate Tumor-Suppressor Gene on Chromosome Arm 22q, in Ovarian Cancer.” *International Journal of Cancer* 112, no. 1 (October 20, 2004): 150–54. <https://doi.org/10.1002/ijc.20339>.
39. Olivier, Magali, Monica Hollstein, and Pierre Hainaut. “TP53 Mutations in Human Cancers: Origins, Consequences, and Clinical Use.” *Cold Spring Harbor Perspectives in Biology* 2, no. 1 (January 2010): a001008. <https://doi.org/10.1101/cshperspect.a001008>.

40. Ouderkirk, J. L., and M. Krendel. "Non-Muscle Myosins in Tumor Progression, Cancer Cell Invasion and Metastasis." *Cytoskeleton* (Hoboken, N.J.) 71, no. 8 (August 2014): 447–63. <https://doi.org/10.1002/cm.21187>.
41. Mazzolini, Rocco, Higinio Dopeso, Silvia Mateo-Lozano, Wakam Chang, Paulo Rodrigues, Sarah Bazzocco, Hafid Alazzouzi, et al. "Brush Border Myosin Ia Has Tumor Suppressor Activity in the Intestine." *Proceedings of the National Academy of Sciences of the United States of America* 109, no. 5 (January 31, 2012): 1530–35. <https://doi.org/10.1073/pnas.1108411109>.
42. Izidoro-Toledo, T. C., A. C. Borges, D. D. Araújo, D. P. S. Leitão Mazzi, F. O. Nascimento Júnior, J. F. Sousa, C. P. Alves, et al. "A Myosin-Va Tail Fragment Sequesters Dynein Light Chains Leading to Apoptosis in Melanoma Cells." *Cell Death & Disease* 4 (March 21, 2013): e547. <https://doi.org/10.1038/cddis.2013.45>.
43. Sellers, J. R., P. D. Chantler, and A. G. Szent-Györgyi. "Hybrid Formation between Scallop Myofibrils and Foreign Regulatory Light-Chains." *Journal of Molecular Biology* 144, no. 3 (December 15, 1980): 223–45. [https://doi.org/10.1016/0022-2836\(80\)90088-1](https://doi.org/10.1016/0022-2836(80)90088-1).
44. Wu, Qian, Ruta M. Sahasrabudhe, Li Z. Luo, Dale W. Lewis, Susanne M. Gollin, and William S. Saunders. "Deficiency in Myosin Light Chain Phosphorylation Causes Cytokinesis Failure and Multipolarity in Cancer Cells." *Oncogene* 29, no. 29 (July 22, 2010): 4183–93. <https://doi.org/10.1038/onc.2010.165>.
45. Komatsu, S., T. Yano, M. Shibata, R. A. Tuft, and M. Ikebe. "Effects of the Regulatory Light Chain Phosphorylation of Myosin II on Mitosis and Cytokinesis of Mammalian Cells." *The Journal of Biological Chemistry* 275, no. 44 (November 3, 2000): 34512–20. <https://doi.org/10.1074/jbc.M003019200>.

Chapter 2

The myosin regulatory light chain Myl5 localizes to mitotic spindle poles and is required for proper cell division

The myosin regulatory light chain Myl5 localizes to mitotic spindle poles and is required for proper cell division

Ivan Ramirez, Ankur A. Gholkar, Erick F. Velasquez, Xiao Guo, Bobby Tofig, Robert Damoiseaux and Jorge Z. Torres

ABSTRACT

Myosins are ATP-dependent actin-based molecular motors critical for diverse cellular processes like intracellular trafficking, cell motility, and cell invasion. During cell division, myosin MYO10 is important for proper mitotic spindle assembly, the anchoring of the spindle to the cortex, and positioning of the spindle to the cell mid-plane. However, myosins are regulated by myosin regulatory light chains (RLCs), and whether RLCs are important for cell division has remained unexplored. Here, we have determined that the previously uncharacterized myosin RLC Myl5 associates with the mitotic spindle and is required for cell division. We show that Myl5 localizes to the leading edge and filopodia during interphase and to mitotic spindle poles and spindle microtubules during early mitosis. Importantly, depletion of Myl5 led to defects in mitotic spindle assembly, chromosome congression, and chromosome segregation and to a slower transition through mitosis. Furthermore, Myl5 bound to MYO10 *in vitro* and co-localized with MYO10 at the spindle poles. These results suggest that Myl5 is important for cell division and that it may be performing its function through MYO10.

1 | INTRODUCTION

The proper assembly of the bipolar mitotic microtubule spindle is critical to the fidelity of chromosome congression and segregation during cell division (Walczak and Heald 2008). During development, the anchoring and positioning of the mitotic spindle regulates the establishment of the cell division plane that is critical for cell fate determination (Morin and Bellaiche 2011). Important to mitotic spindle anchoring and positioning are astral

microtubules that radiate out from the spindle poles and make contacts with the cell cortex (Nakajima 2018; di Pietro et al. 2016; Morin and Bellaiche 2011). Abnormal spindle assembly and orientation can result in defective cell divisions that can lead to developmental and proliferative diseases (Morin and Bellaiche 2011; di Pietro et al. 2016; Nakajima 2018). Although numerous components involved in assembling and orienting the spindle are known (Walczak and Heald 2008; Morin and Bellaiche 2011), the full complement of factors and the molecular signaling pathways that govern these events are not completely understood. Increasing evidence indicates that both the actin and microtubule cytoskeletal systems are necessary for proper cell division (Akhshi et al. 2014; Kita et al. 2019). Although actin has been highly studied within the context of interphase cells where it establishes the cellular architecture and regulates numerous important processes like cell motility, intracellular trafficking, cell signaling pathways, and gene expression (Hyrskyluoto and Vartiainen 2020; Moujaber and Stochaj 2020; Svitkina 2018; Titus 2018), less is known about its role during early cell division. However, actin has been shown to be critical for anchoring the spindle through microtubule-actin interactions at the cell cortex, for spindle positioning at the mid plane, and for actomyosin cellular constriction during cytokinesis (Akhshi et al. 2014; They and Bornens 2006; Uraji et al. 2018; Chaigne et al. 2016). Additionally, evidence indicates that an actin mesh assembly supports the bipolar meiotic and mitotic spindles, where actin provides rigidity and aids in focusing the spindle (Wuhr et al. 2008; Woolner et al. 2008; Mogessie and Schuh 2017; Kita et al. 2019). Therefore, actin plays an important role in ensuring the fidelity of cell division.

Myosins are ATP-dependent actin-based molecular motors that perform a variety of functions in muscle contraction, cargo transport, cell adhesion, and cell division; including spindle assembly, spindle orientation, and cytokinesis (Li et al. 2016; Hartman and Spudich 2012). During cell division, myosin-II is critical for acto-myosin ring contraction during cytokinesis, which is essential for bisecting one cell into two daughter cells (Murthy and Wadsworth 2005; Robinson and Spudich 2000). Of interest, the unconventional myosin-10 (MYO10) has been shown to be an important factor for establishing the architecture and function of the mitotic spindle through its binding to both actin and microtubules (Woolner et al. 2008; Wuhr et al. 2008; Sandquist et al. 2016; Weber et al. 2004; Kwon et al. 2015). MYO10 localizes to the spindle poles throughout mitosis and depletion of MYO10 leads to structural defects in the mitotic microtubule spindle, chromosome congression defects, and chromosome segregation defects (Woolner et al. 2008; Wuhr et al. 2008; Weber et al. 2004; Kwon et al. 2008). MYO10 also has important non-mitotic functions during interphase and in post-mitotic cells where it is important for filopodia formation and function (Sousa and Cheney 2005; Quintero and Yengo 2012; Kerber and Cheney 2011). The filopodia core is composed of actin filaments (Leijnse et al. 2015) and MYO10 has been shown to be recruited to focal adhesions at the leading edge, undergoes intrafilopodial motility, accumulates at the filopodial tips, and promotes the formation and extension of filopodia (Tokuo et al. 2007; Berg and Cheney 2002; Bohil et al. 2006; Kerber et al. 2009; He et al. 2017; Sato et al. 2017). Therefore, myosins perform important functions that are necessary for cell division and cell motility.

The unconventional myosin holoenzymes typically consists of heavy and light chains (Li et al. 2016). Myosin light chains are required for the structural integrity of the myosin

holoenzyme and have regulatory functions on the activity of the protein complex (Li et al. 2016; Heissler and Sellers 2016; Heissler and Sellers 2014). There are two major groups of myosin light chains, the Essential Light Chains (ELCs) and the Regulatory Light Chains (RLCs) (Heissler and Sellers 2016; Heissler and Sellers 2014). The ELCs are essential for the enzymatic activity of the myosin and removal or depletion of the ELCs from the myosin leads to a dramatic loss of myosin enzymatic activity (Heissler and Sellers 2016; Heissler and Sellers 2014). The RLCs are involved in regulating the enzymatic activity of the myosin and their removal or depletion typically leads to moderate effects on myosin activity (Heissler and Sellers 2016; Heissler and Sellers 2014). For example, both calmodulin (CaM) and calmodulin-like protein (CLP) have been shown to be MYO10 light chains that regulate MYO10 motility and function (Homma et al. 2001; Bennett et al. 2007; Bennett et al. 2008; Rogers and Strehler 2001). Although myosin-II and MYO10 have important roles in cell division, the role of RLCs (if any) in cell division has remained unexplored.

We recently performed a microscopy-based RNAi screen using an siRNA library (25,620 siRNAs) targeting the druggable genome in HeLa cells, that included enzymes like kinases and components of molecular motors like myosins, to identify novel factors whose depletion led to a slowed cell division (Torres lab unpublished). This screen identified 13 novel proteins that were not known to be important for cell division, among which was myosin light chain 5 (Myl5). Although Myl5 has remained poorly characterized, based on its protein sequence similarity it is predicted to be a myosin RLC (Collins et al. 1992). Dysregulation of *MYL5* mRNA levels has been observed in glioblastoma multiforme, cervical carcinoma, and breast cancer (Zhang et al. 2017; Alshabi et al. 2019; Savci-

Heijink et al. 2019). For example, *MYL5* mRNA levels are upregulated in late stage cervical cancer patients and is associated with poor survival (Zhang et al. 2017). Additionally, *MYL5* overexpression promoted tumor cell metastasis in a cervical cancer mouse model (Zhang et al. 2017). Here, we have discovered that Myl5 is important for mitotic spindle assembly, chromosome congression, and proper cell division. GFP-Myl5 localizes to the spindle poles during mitosis, indicating that its localization is cell cycle phase dependent. GFP-Myl5 co-localized with spindle pole proteins and MYO10 and bound to MYO10 *in vitro*. Importantly, depletion of Myl5 led to spindle assembly defects, chromosome congression defects, and chromosome segregation errors. These results suggest that Myl5 has important roles in spindle assembly and chromosome segregation and that it may be performing its function through its association with MYO10.

2 | RESULTS AND DISCUSSION

2.1 | *In silico* analysis of Myl5

Our recent genetic RNAi screen for novel cell division proteins led us to discover myosin light chain 5 (Myl5), an uncharacterized hypothetical myosin regulatory light chain (RLC) of the MLC2 type. Human Myl5 is a 173 amino acid protein with 3 EF hand domains predicted to be important for calcium binding in other myosin regulatory light chains (Figure 1a) (Heissler and Sellers 2014; Grabarek 2006). A phylogenetic tree (Hunt et al. 2018) analysis indicated that Myl5 was conserved among vertebrates (Figure 1b). An Online Mendelian Inheritance in Man (OMIM) search showed that the *MYL5* gene was within the 4p16.3 region where the Huntington Disease locus is located. However, *MYL5* has not been linked to inherited human diseases. Due to recent studies showing the

upregulation of *MYL5* expression in cervical cancer (Zhang et al. 2017) and the down regulation of *MYL5* expression in breast (Savci-Heijink et al. 2019) and brain cancers (Alshabi et al. 2019), we sought to determine if *MYL5* was widely dysregulated in other types of cancers. Interestingly, analysis of *MYL5* and *MYO10* differential gene expression across a broad array of cancers using the Gene Expression Profiling and Interactive Analysis (GEPIA) web server (Tang et al. 2017) showed that *MYL5* mRNA levels were lower in most cancers compared to matched normal samples, whereas *MYO10* mRNA levels were elevated in most cancers compared to normal samples (Figure 1c). Additionally, a GEPIA survival analysis showed that low *MYL5* mRNA levels and high *MYO10* mRNA levels related to an unfavorable overall survival (Figure 1d). Together, these analyses showed that the Myl5 protein is conserved among vertebrates and that *MYL5* and *MYO10* gene expression is widely dysregulated in cancer.

2.2 | Myl5 localizes to the spindle poles and spindle microtubules during cell division

Although previous genomic and bioinformatic studies had implicated Myl5 in myosin related functions and in tumorigenesis, its biological function had remained poorly characterized. To begin to understand the cellular role of Myl5 and its link to tumorigenesis, we analyzed its subcellular localization throughout the cell cycle. First, we generated a LAP(GFP-TEV-S-Peptide)-Myl5 inducible stable cell line that expressed GFP-Myl5 upon induction with Dox (Figure S1a) (Torres et al. 2009; Bradley et al. 2016). The LAP-Myl5 cell line was treated with Dox for 16 hours to express GFP-Myl5 and cells were fixed, stained with Hoechst 33342 DNA dye, and anti- α -Tubulin and anti-GFP

antibodies and imaged by immunofluorescence microscopy. During interphase GFP-Myl5 was dispersed throughout the nucleus and cytoplasm of the cell (Figure 2a). Interestingly, GFP-Myl5 localized to the spindle poles in early mitosis, and to a lesser extent the mitotic spindle, and remained associated with the poles until mitotic exit (Figure 2a). To further define the GFP-Myl5 subcellular localization in early mitosis, we performed immunofluorescence co-localization studies with centrosome and spindle pole markers. The GFP-Myl5 localization signal overlapped with NUMA at the spindle poles and encompassed the Pericentrin and Centrin signals, which stained the centrosomes (Figure 2b,c; Figure S1b). Furthermore, in cells with high levels of GFP-Myl5 expression, GFP-Myl5 also co-localized with TPX2 on the spindle microtubules (Figure S1c). Due to the change in GFP-Myl5 localization at mitotic entry, we next asked if endogenous Myl5 protein levels were also cell cycle regulated. HeLa cells were synchronized in G1/S with thymidine treatment, released into the cell cycle, cells were harvested every hour, and protein extracts were prepared. Immunoblot analysis of these samples with anti-Myl5 and anti-Cyclin B antibodies indicated that endogenous Myl5 protein levels remained steady in G1/S and G2/M and decreased slightly during mitotic exit, a time when mitotic Cyclin B levels decreased (Figure 2d). Additionally, the anti-Myl5 antibody recognized two protein bands that corresponded with the size of the two Myl5 isoforms (19.5 kD, UniProtKB-Q02045-1; 14.9 kD, UniProtKB-Q02045-2). Together, these results indicated that the Myl5 protein is abundant throughout the cell cycle and that it undergoes a dynamic cell cycle dependent change in subcellular localization where it redistributes from the nucleus and cytoplasm in interphase to the spindle poles during mitotic entry and remains associated with the poles throughout mitosis.

2.3 | Myl5 is required for proper cell division

Next, we asked if Myl5 was required for cell division by depleting Myl5 in HeLa cells. First, we sought to identify siRNA oligonucleotides which reduced Myl5 protein levels to less than 10% compared to non-targeting control siRNA. HeLa cells were transfected with non-targeting control siRNA (siCtrl) or siRNAs targeting Myl5 (siM1-siM4) for 72 hours and cell lysates were prepared and analyzed by immunoblotting. The siM1-siM4 oligonucleotides depleted Myl5 protein levels to undetectable levels (Figure 3a; Figure S2a). Next, we sought to analyze the consequences of depleting Myl5 protein levels during cell division. HeLa cells were transfected with siCtrl or siM1-siM4 siRNAs for 72 hours. The cells were then fixed and co-stained with Hoechst 33342 (to visualize the DNA) and anti- α -Tubulin antibodies to detect the mitotic microtubule spindle. Interestingly, depletion of Myl5 led to a significant increase in cells with a defective mitosis, including an increase in the percentage of prometaphase cells with multipolar spindles (siM1= $20.75 \pm 3.59\%$, $p=.0004$ compared to siCtrl= $7.5 \pm 1.29\%$) and anaphase cells with lagging chromosomes (siM1= $32.25 \pm 2.5\%$, $p<.0001$ compared to siCtrl= $8.25 \pm 3.1\%$) (Figure 3b-e; Figure S2b-f). Importantly, the mitotic defects (multipolar spindles and lagging chromosomes) observed upon siM1 treatment were rescued with the expression of a siRNA-resistant (siRes) version of GFP-Myl5 (for multipolar spindles- siM1+ GFP-Myl5-siRes= $3.0 \pm 1.0\%$, $p=.0270$ compared to siM1+ GFP-Myl5-WT= $8.33 \pm 2.51\%$; for lagging chromosomes- siM1+ GFP-Myl5-siRes= $9.67 \pm 1.5\%$, $p=.0026$ compared to siM1+ GFP-Myl5-WT= $19.67 \pm 2.08\%$) (Figure 3f,g; Figure S3). Together, these results indicated that Myl5 was required for proper cell division and that its depletion led to cell division errors.

2.4 | The levels of Myl5 affect the timing of cell division

Next, we asked if the overall time to cell division was affected by the depletion of Myl5. HeLa cells were transfected with non-targeting control siRNA (siCtrl) or siRNAs targeting Myl5 (siM1 and siM3) for 48 hours, synchronized in G1/S with thymidine treatment for 18 hours, and released in media containing the cell permeable DNA specific stain SiR-DNA (visible in the far-red channel). Five-hours post release live cells were imaged at 20X magnification at five-minute intervals for 18 hours. Movies were then analyzed and the time from nuclear DNA condensation to nuclear separation was quantified. This analysis showed that depletion of Myl5 led to a significant increase in the time that cells spent in mitosis with the average time from nuclear DNA condensation to nuclear separation for siM1= 55 ± 27.4 minutes ($p < .0001$) and siM3 = 46 ± 22 minutes ($p = .0288$) compared to siCtrl= 38.9 ± 21.6 minutes (Figure 4a,b; Supporting Videos S1-S3).

2.5 | Myl5 binds MYO10 and colocalizes with MYO10 to the spindle poles

Due to the ability of MYO10 to localize to the spindle poles in early mitosis and its functional importance in ensuring the fidelity of spindle assembly, chromosome congression, chromosome segregation, and cell division (Woolner et al. 2008), we asked if Myl5 and MYO10 shared a similar localization during mitosis. The LAP-Myl5 cell line was used to express GFP-Myl5 and cells were fixed, stained with Hoechst 33342 DNA dye, and anti- α -Tubulin, anti-MYO10, and anti-GFP antibodies and imaged by immunofluorescence microscopy. Indeed, the GFP-Myl5 and MYO10 localization signals overlapped at the spindle poles throughout mitosis (Figure 5a). Next, we sought to

determine if Myl5 and MYO10 could associate directly. *In vitro* binding experiments were performed with HA-Myl5 and FLAG-GFP or FLAG-MYO10. Indeed, MYO10 co-immunoprecipitated with Myl5 (Figure 5b). The IQ motifs of myosins are key sites for binding to regulatory light chains (Heissler and Sellers 2014), thus we asked if the IQ motifs of MYO10 were necessary for the MYO10-Myl5 interaction. To do this, we removed the three IQ motifs from MYO10 to generate MYO10 IQ-less (MYO10-IQL). *In vitro* binding experiments with HA-Myl5 or HA-CALM3 (Calmodulin 3, a known MYO10 regulatory light chain that binds to the MYO10 IQ motifs (Rogers and Strehler 2001)) and FLAG-GFP, FLAG-MYO10, or FLAG-MYO10-IQL showed that Myl5 was able to bind to both MYO10 and MYO10-IQL, while CALM3 only bound to MYO10 and not MYO10-IQL (Figure 5c,d; Figure S4). Together, these data indicated that Myl5 binds to MYO10, independent of the IQ motifs, and colocalizes with MYO10 at the spindle poles during mitosis.

2.6 | Myl5 localizes to the leading edge of the cell and to filopodia in interphase cells

Within the context of cancer, actin-based structures like filopodia are critical for cell migration, invasion, and metastasis (Caswell and Zech 2018; Jacquemet et al. 2015). Of interest, MYO10 has a critical role in filopodia formation and accumulates at the tips of filopodia (Bohil et al. 2006; Tokuo et al. 2007; Kerber et al. 2009) and has been linked to promoting cancer invasion and metastasis, including in breast cancer and melanomas (Arjonen et al. 2014; Courson and Cheney 2015; Tokuo et al. 2018; Cao et al. 2014). Due to the association of Myl5 with MYO10, we sought to determine whether Myl5 also

localized to filopodia like MYO10. The LAP-Myl5 or LAP-MYO10 cell lines was used to express GFP-Myl5 or GFP-MYO10 and cells were fixed, stained with Hoechst 33342 DNA dye, anti- α -Tubulin, anti-Fascin (marker for filopodia (Edwards and Bryan 1995; Otto et al. 1979)), and anti-GFP antibodies and imaged by immunofluorescence microscopy. Interestingly, GFP-Myl5 localized to the leading edge of the cell and throughout filopodia, but did not accumulate at the tips of filopodia like MYO10 (Figure 6a). Calcium binding and phosphorylation are two key mechanisms for regulating myosin RLC function (Heissler and Sellers 2016). RLCs typically have multiple EF hands that are generally thought bind calcium, however, only EF hands with a calcium binding consensus pattern of amino acids are predicted to have the ability to bind calcium (prosite prorule annotation rule: PRU00448, (Sigrist et al. 2005)) (Grabarek 2006). Specifically, Myl5 has three EF-hands, but only the N-terminal EF-hand contains the calcium binding consensus (amino acids 43-54) (Figure 1a). Additionally, RLCs are typically phosphorylated at consensus Ser/Thr residues in their N-terminus, which are conserved in Myl5 (Figure S5) (Yu et al. 2016). Therefore, we sought to determine whether deletion of the predicted Myl5 calcium binding site or mutation of the conserved RLC sites of phosphorylation (serines 20 and 21, Figure S5) would perturb the localization of GFP-Myl5 to cytoskeletal structures. To do this, we generated LAP-tagged inducible stable cell lines of Myl5 calcium binding site deletion (CAD), phospho-null (20A and 21A (AA)) and phospho-mimic (20E or 21E) mutants; although phospho-mimetic mutants in other RLCs do not always have the anticipated effect on myosin activity (Heissler and Sellers 2015; Vasquez et al. 2016). Immunofluorescence microscopy of HeLa cells overexpressing these GFP-Myl5 mutants, showed that they were capable of localizing to the leading edge, filopodia, and the spindle

poles, similar to wild type GFP-Myl5 (Figure 6b-e). Additionally, no major perturbations to the overall architecture of filopodia, spindles, and spindle poles were observed by the overexpression of these Myl5 mutants. Together, these results showed that GFP-Myl5 localizes to the leading edge and filopodia during interphase and that conserved residues in Myl5 that regulate the function of other RLCs are not required for its localization to these structures.

2.7 | CONCLUSION

Although actin and the unconventional myosin MYO10 had been implicated in ensuring the fidelity of mitotic spindle assembly and cell division, the role of myosin RLCs during cell division remained unknown. Here, we have determined that Myl5 is a novel and important factor necessary for proper cell division. GFP-Myl5 localized to the leading edge and filopodia in interphase cells and to the spindle poles and spindle microtubules during early mitosis. Depletion of Myl5 led to mitotic spindle defects, errors in chromosome congression and segregation, and a slowed progression through mitosis. These Myl5 depletion phenotypes were similar to those reported upon MYO10 depletion (Woolner et al. 2008), albeit less severe. Interestingly, the GFP-Myl5 immunofluorescence signal overlapped with MYO10 at the spindle poles throughout mitosis and Myl5 bound directly to MYO10 *in vitro*. Our results suggest that Myl5 is important for cell division and that it may function through MYO10. To our knowledge, Myl5 is the first myosin RLC family member that has been implicated in mitotic spindle assembly.

Of the ~40 myosins encoded in the human genome, at least ten (including MYO10) have been implicated in tumorigenesis (Li and Yang 2016). Our analysis showing that *MYL5*

and *MYO10* gene expression are frequently dysregulated in cancer compared to normal samples is intriguing and puzzling. While *MYL5* mRNA levels were lower in most cancers and related to unfavorable survival, *MYO10* mRNA levels were elevated in most cancers and related to unfavorable survival (Figure 1c,d). These results are consistent with reports showing low levels of *MYL5* mRNA in breast (Savci-Heijink et al. 2019) and brain cancers (Alshabi et al. 2019) and high *MYO10* mRNA levels in invasive and metastatic breast cancer and melanoma (Arjonen et al. 2014; Courson and Cheney 2015; Tokuo et al. 2018; Cao et al. 2014). However, others have reported that *MYL5* mRNA levels are elevated in late stage cervical cancer patients, are associated with poor survival, and can promote tumor cell metastasis in mouse models of cervical cancer (Zhang et al. 2017). Similarly, the upregulation of *MYO10* mRNA levels in invasive and metastatic cancers is consistent with its critical role in promoting filopodia formation, which are important for cell motility and invasion (Tokuo et al. 2007; Berg and Cheney 2002; Bohil et al. 2006; Kerber et al. 2009; He et al. 2017; Sato et al. 2017; Caswell and Zech 2018; Jacquemet et al. 2015). However, it is the depletion of *MYO10* that leads to cell division defects and genetic instability (Woolner et al. 2008; Wuhr et al. 2008; Weber et al. 2004; Kwon et al. 2008) and what role this may play in early stage cancers remains to be determined. Therefore, it is possible that *MYL5* and *MYO10* mRNA levels are differentially expressed in early versus late stage tumors and further research in this area is warranted. Although our data suggest that *Myl5* may be affecting cell division through *MYO10*, it is possible that *Myl5* may function independently or with other non-motor proteins. We also note that during interphase, myosin light chains have been implicated in regulating gene expression by binding to specific sequences within the promoter region of target genes (Zhang et al.

2015; Li and Sarna 2009) and that Myl5 has been shown to bind the promoter region of HIF-1alpha, an important factor in tumorigenesis, and regulates its expression (Rankin and Giaccia 2016; Zhang et al. 2017). Consistent with this function, GFP-Myl5 localized to both the cytoplasm and nucleus in interphase cells (Figure 6a). Therefore in addition to its cytoskeleton-related function, Myl5 has cytoskeleton unrelated functions in gene expression that may contribute to tumorigenesis.

3 | MATERIALS and METHODS

3.1 | Cell culture

HeLa cells were grown in F12:DMEM 50:50 (Hyclone) with 10% FBS, 2mM L-glutamine and antibiotics in 5% CO₂ at 37 °C. Cells were synchronized in G1/S by treatment with 2 mM thymidine (Sigma-Aldrich) for 18-hours. The following siRNAs were used for siRNA transfections: ThermoFisher Silencer Select 4390843 (control non-targeting siRNA) and S9187 and S9188 (M1 and M2 siRNAs targeting *MYL5*); Dharmacon ON-TARGETplus D-001810-10 (control non-targeting siRNA) and J-011739-03 and J-011739-04 (M3 and M4 siRNAs targeting *MYL5*) were used as described previously (Torres et al. 2010). See Table S1 for a list of key reagents and resources used in this study and their pertinent information.

3.2 | Generation of the LAP-Myl5 inducible stable cell line

The HeLa LAP(GFP-TEV-S-Peptide)-Myl5, -Myl5-AA, -Myl5-20E, -Myl5-21E, -Myl5-CAD, -Myl5-siRes, and -MYO10 inducible stable cell lines were generated as described previously (Torres et al. 2009; Bradley et al. 2016). Briefly, full-length *MYL5* (coding for

amino acid residues 1-173) and mutant derivatives (alanine mutations at both Ser20 and Ser21 (AA); Glu mutations at either Ser20 (20E) or Ser21 (21E); deletion of the calcium binding domain (amino acids 43-54, CAD)) and full-length MYO10 (coding for amino acid residues 1-2058) were cloned into pDONR221 and transferred to pGLAP1 through a Gateway reaction to generate the pGLAP1 vectors with these ORFs that were transfected into HeLa Flp-In T-Rex cells to generate their respective inducible stable cell lines.

3.3 | Immunoblotting

For Myl5 cell cycle protein expression analysis, HeLa cells were synchronized in G1/S with 2 mM thymidine for 18-hours. Cells were then washed with PBS three times and twice with F12:DMEM media with 10% FBS and released into the cell cycle. Cells were harvested at the indicated time points, lysed, and protein extracts were resolved on a 4-20% SDS-PAGE and transferred to a PVDF membrane. The membranes were immunoblotted with the indicated antibodies and imaged with a LiCOR system. The same approach was used to detect Myl5 protein depletion upon siRNA transfections without the cell synchronization step. Cell extract preparation and immunoblot analyses with the indicated antibodies were as described previously (Gholkar et al. 2016).

3. 4 | Fixed-cell immunofluorescence microscopy and live-cell time-lapse microscopy

Fixed-cell immunofluorescence microscopy was performed as described previously (Gholkar et al. 2016). Briefly, non-transfected cells or cells that had been transfected with the indicated siRNAs for 48 hours were arrested in G1/S with 2 mM thymidine for 18

hours, washed, and released into fresh media for eight hours. Cells were then fixed with 4% paraformaldehyde, permeabilized with 0.2% Triton X-100/PBS, and co-stained with 0.5 $\mu\text{g/ml}$ Hoechst 33342 (ThermoFisher) to visualize the DNA and the indicated antibodies. A Leica DMI6000 microscope (Leica DFC360 FX Camera, 63x/1.40-0.60 NA oil objective, Leica AF6000 software) was then used to capture the images, which were deconvolved with the Leica Application Suite 3D Deconvolution software and exported as TIFF files. For quantifying mitotic defects, the data from four independent experiments, with 100 cells counted for each, was used to quantify the average \pm standard deviation (SD). For time-lapse microscopy, HeLa cells were transfected with the indicated siRNAs for 48 hours, arrested in G1/S with 2 mM thymidine for 18 hours, washed, and released into fresh media containing 100 nM SiR-DNA stain (Cytoskeleton Inc.). Cells were imaged live five-hours post release for 18 hours using an ImageXpress XL imaging system (Molecular Devices) with a 20x air objective at 37 °C in 5% CO₂. Captured images were exported as a video at one half frames per second using Image J and the videos were saved as AVI movies. Each frame represents a five-minute interval. For quantifying the timing of cell division, the data from three independent experiments, with 30 cells counted for each, was used to quantify the average time in minutes from DNA condensation for nuclear separation \pm standard deviation (SD).

3.4.1 | Statistical analysis

All statistical data are presented as the average \pm SD from at least three independent experiments. Outliers were considered in time-lapse experiments by using Tukey's method in R (<https://www.r-project.org/>). For experiments where two groups were

compared, they were analyzed using unpaired Student's t test. Data was judged to be statistically significant when $p < 0.05$. For experiments where three or more groups were compared, they were first tested for significance using ANOVA statistical test. If p-value showed significance ($p < 0.05$), multiple pair-wise comparisons were performed between the means of groups using Tukey Honest Significant Difference and Dunnet's tests. All statistical figures were generated with GraphPad Prism 5.

3.5 | Generation of plasmids and *in vitro* binding assays

For *in vitro* binding assays, full-length human *MYL5* (encoding amino acid residues 1-173) or *CALM3* (encoding amino acid residues 1-149) were fused to the C-terminus of the HA-tag to generate the pCS2-HA-*MYL5* and pCS2-HA-*CALM3* vectors. Similarly full-length *MYO10* (encoding amino acid residues 1-2058) or *MYO10* lacking amino acids 742-817 that contain the IQ motifs (*MYO10-IQL*) were fused to the C-terminus of the FLAG-tag to generate the pCS2-FLAG-*MYO10* and pCS2-FLAG-*MYO10-IQL* vectors. *In vitro* binding assays were performed as described previously (Gholkar et al. 2016). Briefly, HA-MyI5, HA-CALM3, FLAG-MYO10, FLAG-MYO10-IQL, and FLAG-GFP (negative control) were *in vitro* transcribed and translated (IVT) using TNT® Quick Coupled Transcription/Translation System, (Promega) in 10 μ L reactions. Magnetic HA beads (MBL International) were washed three times and equilibrated with wash buffer (50 mM Tris pH 7.4, 200 mM KCl, 1 mM DTT, 0.5% NP-40, and Halt Protease and Phosphatase Inhibitor Cocktail). IVT reactions were added to the equilibrated HA beads and incubated for 1.5 hours at 30 °C with gentle shaking. Beads were washed three times with wash buffer and eluted by boiling for five minutes with 2X Laemmli SDS sample buffer. Samples

were resolved on a 4-20% gradient Tris gel with Tris-Glycine SDS running buffer, transferred to an Immobilon PVDF membrane (EMD Millipore), and membranes were analyzed with a PharosFX Plus molecular imaging system (Bio-Rad).

3.6 | *In silico* analysis of Myl5

The Myl5 phylogenetic tree was constructed by querying Ensembl (Hunt et al. 2018) (<https://www.ensembl.org/>) for Myl5 (ID: ENSGT00940000163023) and Figure 1b was generated by reconstructing the phylogenetic tree on Ensembl using images from LogoMarkr (<https://logomakr.com/>). For analysis of *MYL5* and *MYO10* differential gene expression in cancer cells compared to normal counterparts, their gene expression profiles were retrieved from the Gene Expression Profiling Interactive Analysis (GEPIA), an interactive web server for cancer genomics that compares cancer and normal gene expression (Tang et al., 2017). For a list of cancer types considered and their corresponding abbreviations refer to Table S2. The median gene expression for both tumor and matched normal samples were compared by subtracting median normal from tumor gene expression for each cancer type. Positive values represent higher gene expression in tumor samples compared to normal samples and negative values represent lower gene expression in tumor samples compared to normal samples. Figure 1c summarizes the gene expression compared to normal samples in different tumor types for both *MYL5* and *MYO10*. Correlation analysis between *MYL5* and *MYO10* mRNA levels and the overall survival of cancer patients was carried out using the Survival Plot tool in GEPIA with default parameters. Datasets for all cancers and matched normal

samples listed on Table S2 were used in the analysis. Survival plots were exported as PDF files.

3.7 | Antibodies

Immunofluorescence and immunoblotting were carried out using antibodies against: Myl5, MYO10, and Fascin (Proteintech: 14249-1-AP, 24565-1-AP, and 66321-1-Ig); Pericentrin (Novus Biologicals: NB-100-68277); GFP (Abcam: ab13970); Gapdh (GTX100118); α -Tubulin (Bio-Rad: MCA78G); Cyclin B (Santa Cruz: sc-245). Centrin antibodies were a gift from J. Salisbury and NUMA and TPX2 antibodies were gifts from D. Compton. Secondary antibodies conjugated to FITC, Cy3, and Cy5 were from Jackson Immuno Research and those conjugated to IRDye 680 and IRDye 800 were from LI-COR Biosciences.

ACKNOWLEDGMENTS

This material is based upon work supported by the National Science Foundation under Grant Number MCB1912837 to J.Z.T., any opinions, findings, and conclusions or recommendations expressed in this material are those of the authors and do not necessarily reflect the views of the National Science Foundation. This work was supported in part by a grant to The University of California, Los Angeles from the Howard Hughes Medical Institute through the James H. Gilliam Fellowships for Advanced Study program to E.F.V. This work was also supported by an NSF Louis Stokes Alliances for Minority Participation Bridge to the Doctorate Fellowship and Cota Robles Fellowship to I.R.

Figures

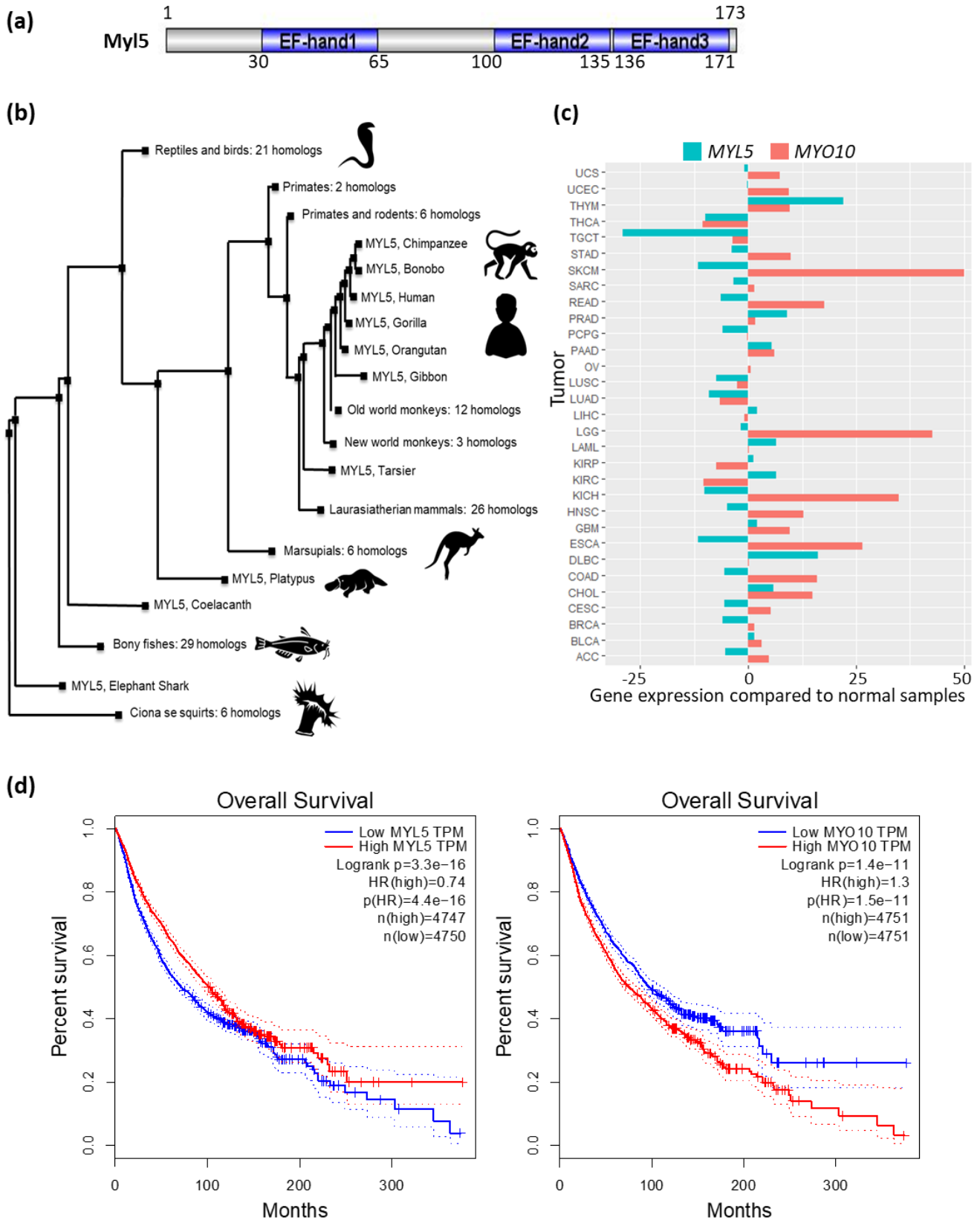


Figure 1 *In silico* analyses of Myl5. (a) Schematic of the human Myl5 (UniProtKB-Q02045) protein domain architecture with the EF hand domains highlighted in blue. The number of amino acid residues are indicated. (b) Phylogenetic tree analysis showing that Myl5 is conserved among vertebrates. (c) Analysis of *MYL5* and *MYO10* differential gene expression in a broad array of cancers versus matched normal samples with the Gene Expression Profiling and Interactive Analysis (GEPIA) web server. See Table S2 for a list of cancer types considered and their corresponding abbreviations. The median gene expression levels are on the x-axis and cancer type is on the y-axis. Positive values represent higher gene expression in tumor samples compared to normal samples and negative values represent lower gene expression in tumor samples compared to normal samples. (d) Correlation analysis between *MYL5* and *MYO10* mRNA levels and the overall survival of cancer patients using the GEPIA web server. Survival plots indicate time in months on the x-axis and percent survival on the y-axis. See materials and methods for analysis details.

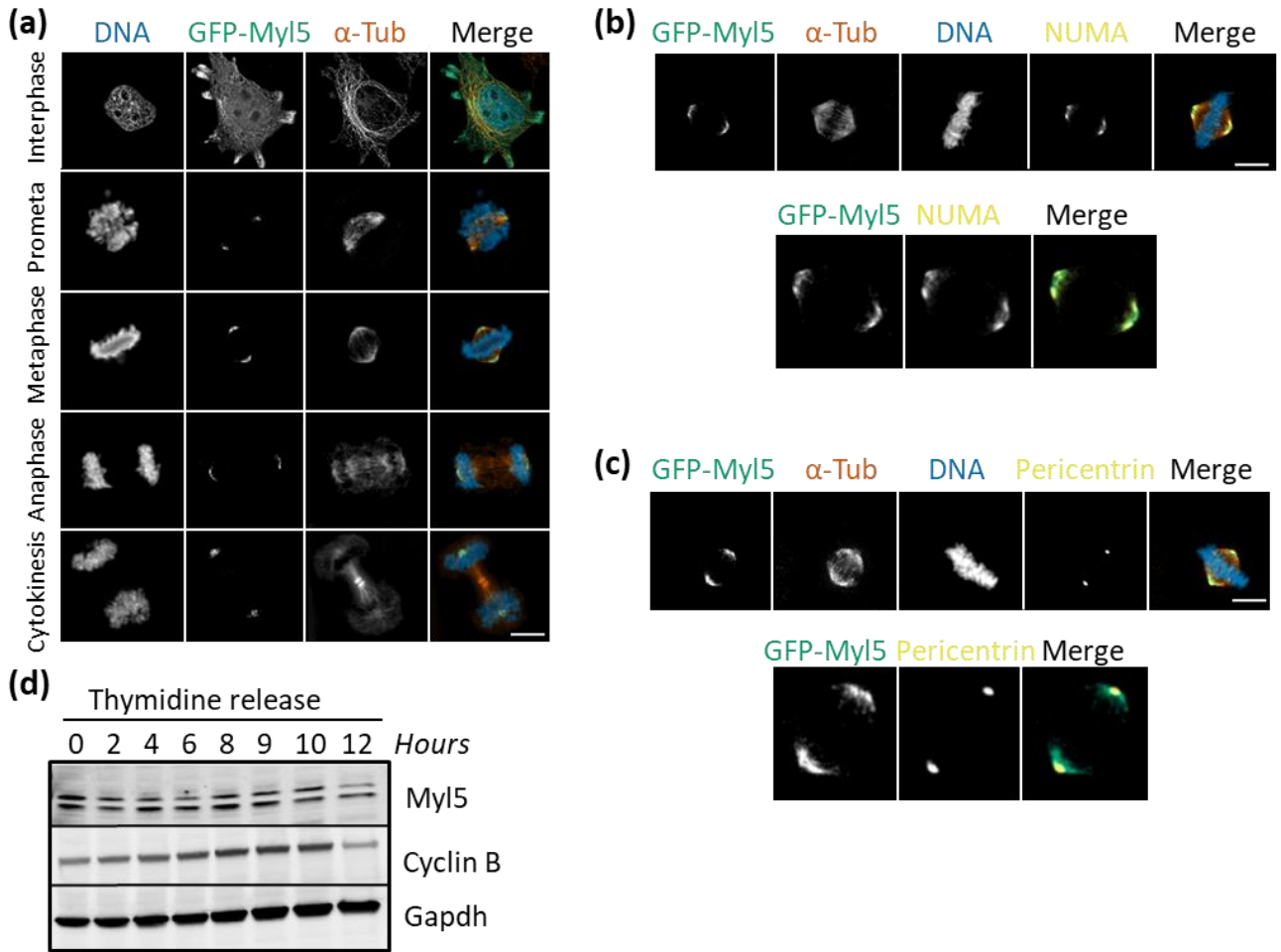


Figure 2 MyI5 localizes to mitotic spindle poles during mitosis. (a) The LAP (GFP-TEV-S-Peptide)-tagged-MyI5 HeLa inducible stable cell line was treated with Dox for 16 hours to express GFP-MyI5 and cells were fixed, stained with Hoechst 33342 DNA dye, and anti- α -Tubulin and anti-GFP antibodies and imaged by immunofluorescence microscopy. Images show the cell cycle subcellular localization of GFP-MyI5 during interphase, prometaphase, metaphase, anaphase and cytokinesis. Bar indicates 5 μ m. (b-c) Same as in (a), except that cells were also stained with anti-NUMA (b) or anti-Pericentrin (c) antibodies. Bar indicates 5 μ m. (d) Analysis of endogenous MyI5 protein levels throughout the cell cycle. HeLa cells were synchronized in G1/S, released into the cell cycle and cells

were harvested at the indicated time points. Protein extracts were prepared, resolved by SDS-PAGE, transferred to a PVDF membrane and immunoblotted with the indicated antibodies. Gapdh is used a loading control.

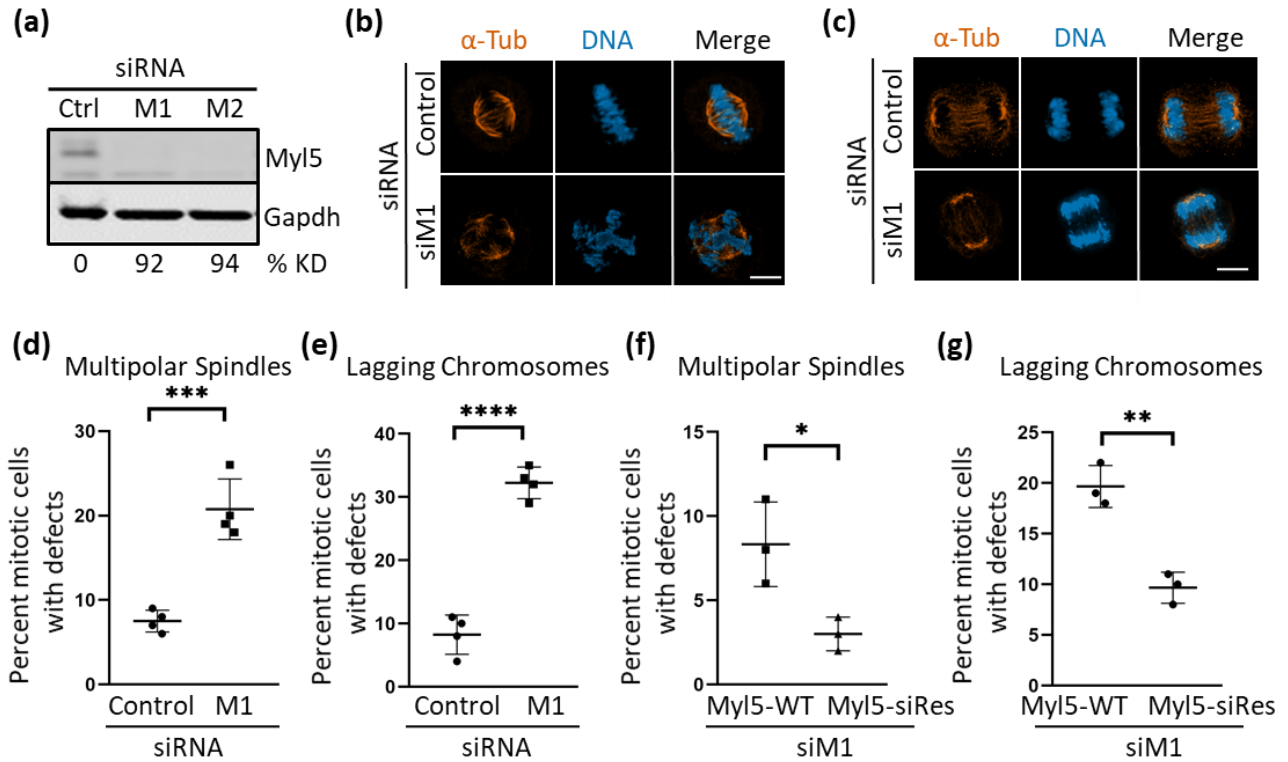


Figure 3 Depletion of Myl5 leads to spindle assembly and cell division defects. (a) Immunoblot analysis showing that siRNA oligonucleotides targeting *MYL5* (M1 and M2) expression deplete Myl5 protein levels in HeLa cells compared to non-targeting control siRNA (siCtrl). Percent Myl5 protein level knockdown (% KD) normalized to Gapdh is indicated for each oligonucleotide. (b-c) Immunofluorescence microscopy of HeLa cells transfected with siCtrl or siM1 for 72 hours, fixed, and stained with Hoechst 33342 DNA dye and anti- α -Tubulin antibodies. Scale bar indicates 5 μ m. (d-e) Quantitation of the percent mitotic cells with multipolar spindles (d) and lagging chromosomes (e) in siCtrl or

siM1 transfected cells. Data represent the average \pm SD of four independent experiments, 100 cells counted for each. *** indicates a p value =.0004 and **** a p value <.0001. (f-g) The LAP-MyI5-WT and LAP-MyI5-siRes (resistant to siM1 siRNA targeting MyI5) HeLa inducible stable cell lines were transfected with siM1 for 46 hours, synchronized in G1/S with thymidine for 18 hours, released into the cell cycle for 8 hours, and induced with Dox during the last 16 hours of the experiment to overexpress either GFP-MyI5-WT or GFP-MyI5-siRes. Cells were then fixed and analyzed by immunofluorescence microscopy and the percent mitotic cells with mitotic defects (multipolar spindles (f) and lagging chromosomes (g)) was quantified. Data represent the average \pm SD of three independent experiments, 100 cells counted for each. ** indicates a p value =.0026 and * indicates a p value =.0270.

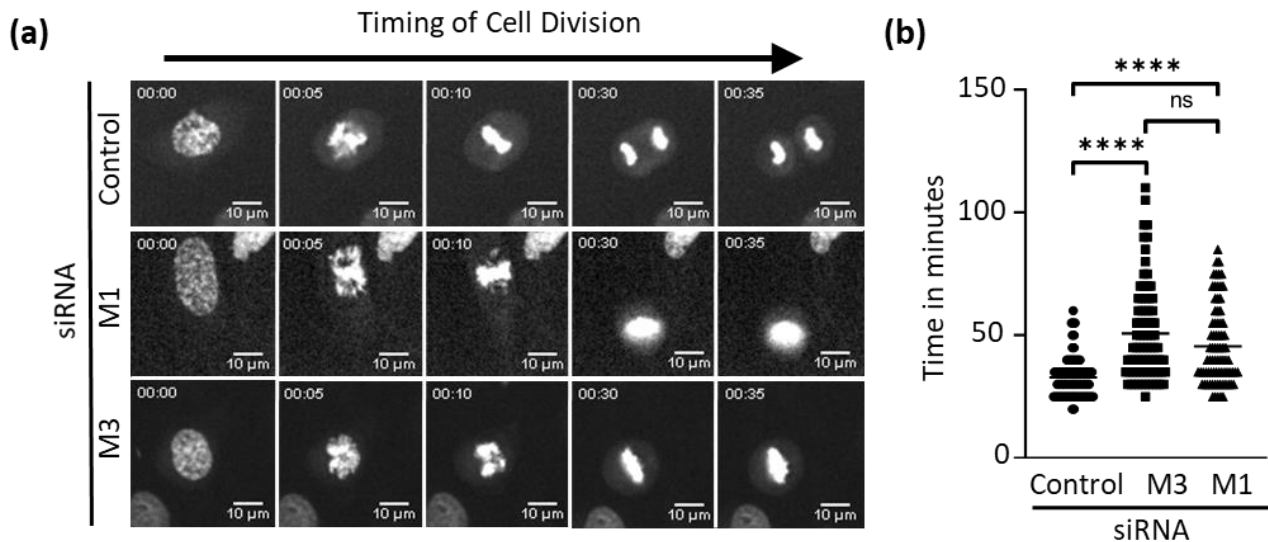


Figure 4 Modulation of MyI5 levels affects the time to cell division. (a) Live-cell time-lapse microscopy of HeLa cells transfected with siCtrl or siM1 or siM3 for 72 hours. Cells were then synchronized in G1/S with thymidine treatment for 18 hours, released, and imaged by staining the cells with SiR-DNA stain at five hours post-release. The indicated times

are in minutes. See Videos S1-S3. (b) Quantitation of the time cells spend in mitosis from DNA condensation to chromosome separation. Y-axis indicates time in minutes. X-axis indicates the siRNA transfections. Data represent the average \pm SD of three independent experiments, 30 cells counted for each. **** indicates p value $<.0001$.

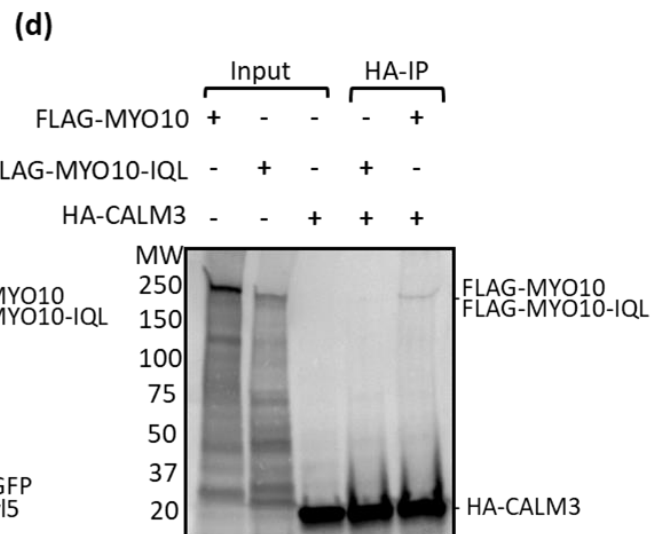
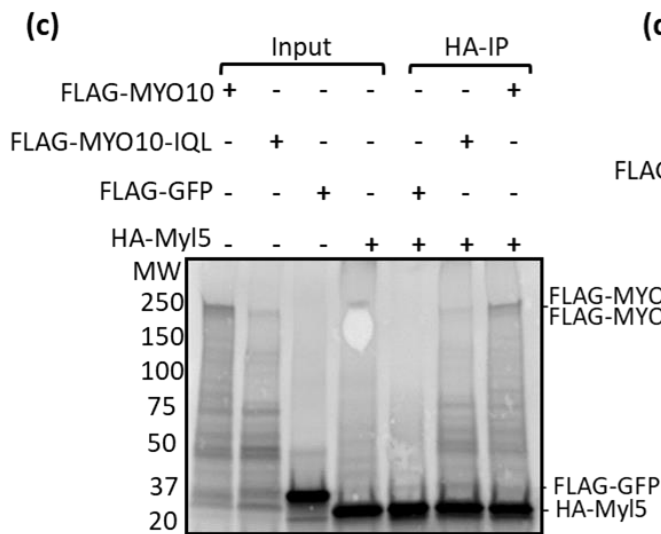
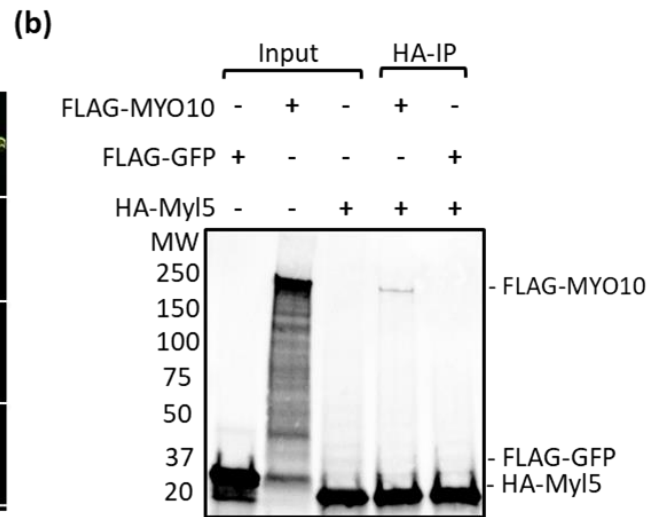
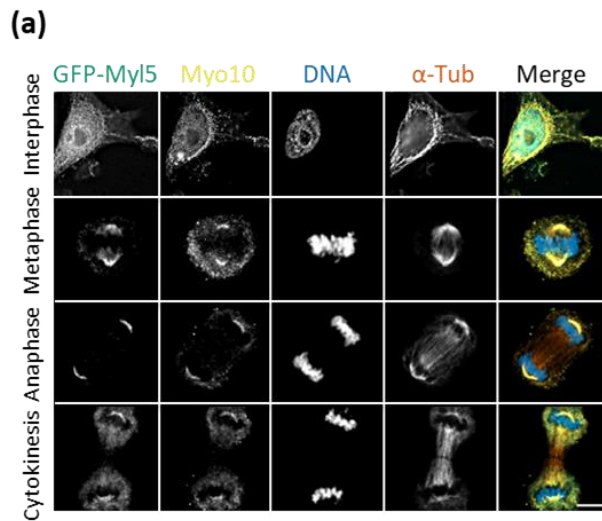


Figure 5 Myl5 colocalizes with MYO10 at mitotic spindle poles during mitosis and binds to MYO10 *in vitro*. (a) The LAP (GFP-TEV-S-Peptide)-tagged-Myl5 HeLa inducible stable cell line was treated with Dox for 16 hours to express GFP-Myl5 and cells were fixed, stained with Hoechst 33342 DNA dye, and anti- α -Tubulin and anti-MYO10 antibodies and imaged by immunofluorescence microscopy. Images show the cell cycle subcellular localization of GFP-Myl5 and MYO10 during interphase, metaphase, anaphase and cytokinesis. Bar indicates 5 μ m. (b) *In vitro* binding assays performed in the presence or absence of radiolabeled (³⁵S methionine) FLAG-MYO10, FLAG-GFP, or HA-Myl5. HA-Myl5 was immunoprecipitated (IP) and eluates were analyzed by radiometry. See materials and methods for experimental details. (c) Same as in (b), except that FLAG-MYO10-IQL (MYO10 IQ-less mutant) was added to the analysis. (d) Same as in (c), except that the binding of HA-CALM3 to FLAG-MYO10 or FLAG-MYO10-IQL was analyzed instead of HA-Myl5. See Figure S4 for control experiment showing that FLAG-MYO10 and FLAG-MYO10-IQL do not bind non-specifically to anti-HA beads.

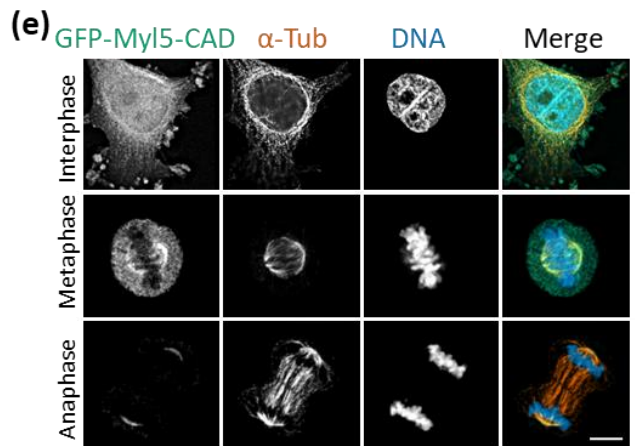
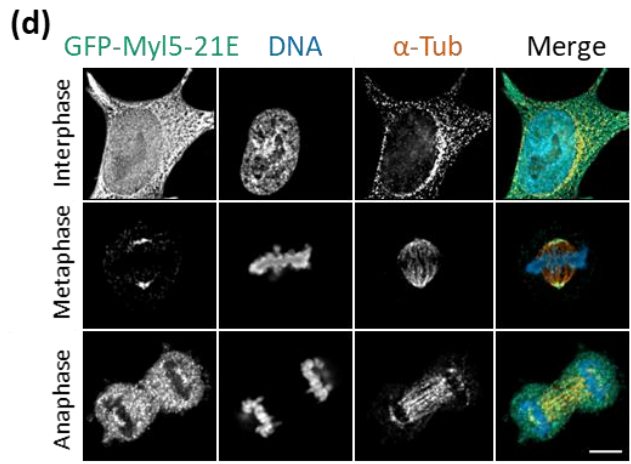
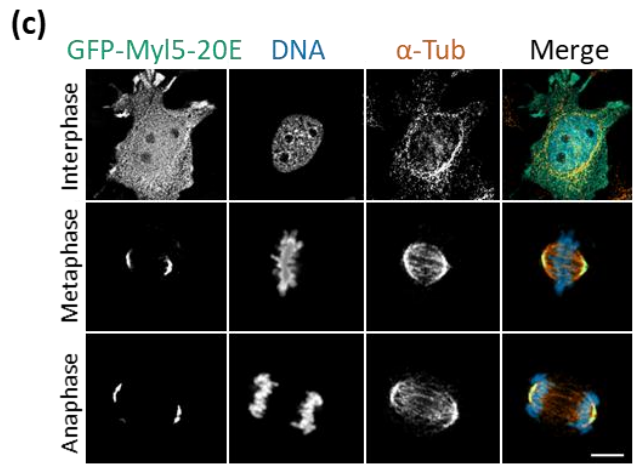
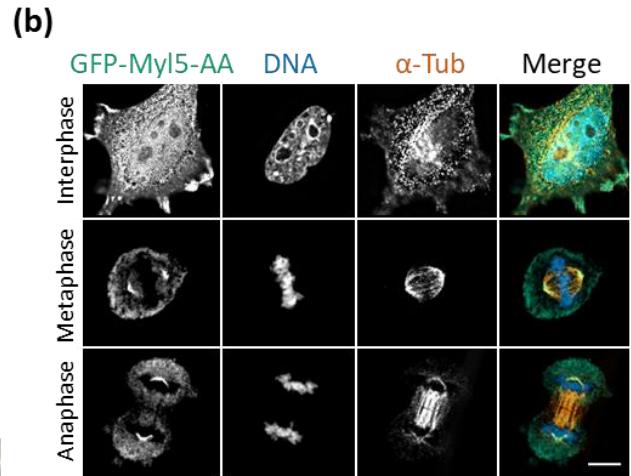
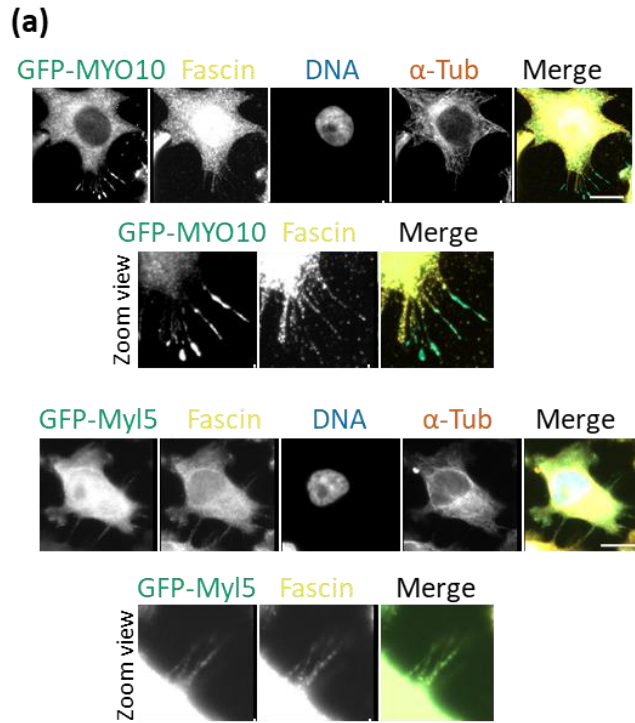


Figure 6 Myl5 localizes to the leading edge and filopodia. (a) The LAP (GFP-TEV-S-Peptide)-tagged-Myl5 or MYO10 HeLa inducible stable cell lines were treated with Dox for 16 hours to express GFP-Myl5 or GFP-MYO10 and cells were fixed, stained with Hoechst 33342 DNA dye, anti-GFP and anti- α -Tubulin, and anti-Fascin (filopodia marker) antibodies, and imaged by immunofluorescence (IF) microscopy. Bars indicate 5 μ m. Bottom panels of GFP-Myl5 and GFP-MYO10 IF images show magnified view of filopodia. (b-e) GFP-Myl5-AA (phospho-null), GFP-Myl5-20E and GFP-Myl5-21E (phospho-mimics), and GFP-Myl5-CAD (calcium-binding domain deletion) mutants were expressed in HeLa cells for 16 hours and cells were fixed, stained with Hoechst 33342 DNA dye, and anti- α -Tubulin and anti-GFP antibodies and imaged by IF microscopy. Bars indicate 5 μ m.

SUPPLEMENTAL MATERIAL

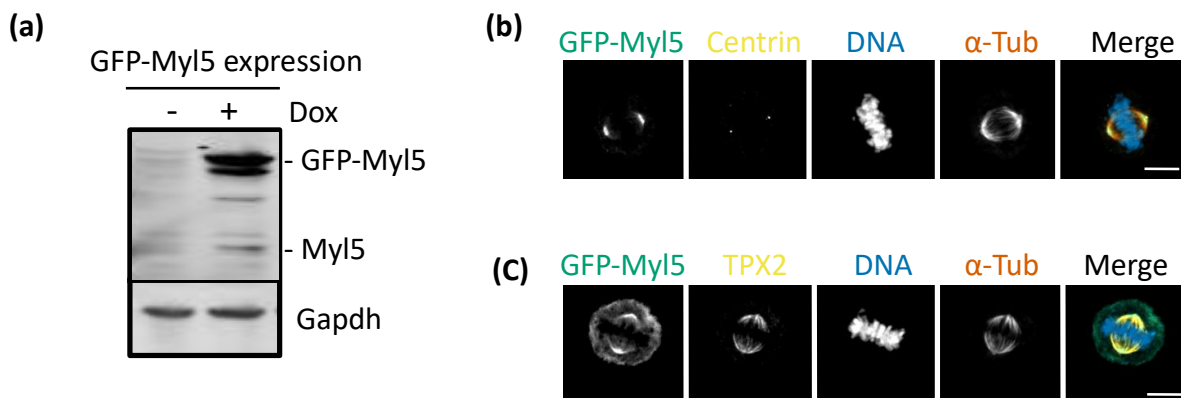


Figure S1 Expression of GFP-Myl5 and its localization to mitotic spindle poles during mitosis.

(a) Immunoblot analysis of protein extracts from the Dox inducible LAP (GFP-TEV-S-Peptide)-tagged-Myl5 stable cell line in the absence (-) or presence (+) of Dox. Blots

were probed with anti-Myl5 or anti-Gapdh antibodies. Immunoblot shows that GFP-Myl5 is expressed only when cells are treated with Dox. The level of GFP-Myl5 is ~5.8 times the level of endogenous Myl5. (b and c) The LAP (GFP-TEV-S-Peptide)-tagged-Myl5 HeLa inducible stable cell line was treated with Dox for 16 hours to express GFP-Myl5 and cells were fixed, stained with Hoechst 33342 DNA dye and anti- α -Tubulin, anti-GFP, anti-TPX2 (b), and anti-Centrin (c) antibodies and imaged by immunofluorescence microscopy. Images show the localization of GFP-Myl5 during metaphase in relation to TPX2 and Centrin. Bars indicate 5 μ m.

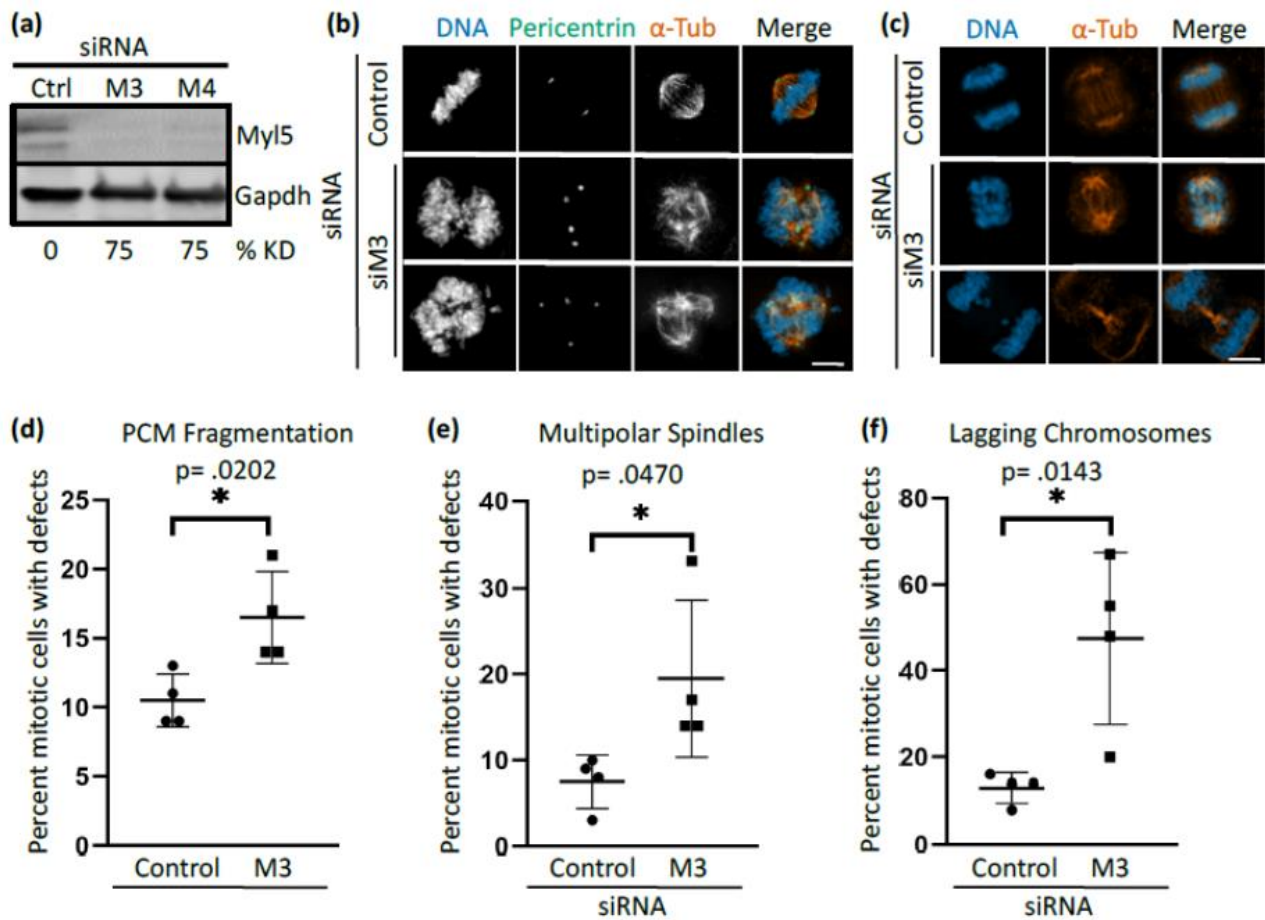


Figure S2 Depletion of Myl5 leads to spindle assembly and cell division defects.

(a) siRNA knockdown of Myl5 protein levels. Immunoblot analysis showing that siRNA oligonucleotides targeting *MYL5* (M3 and M4) expression deplete Myl5 protein levels in HeLa cells compared to non-targeting control siRNA (siCtrl). Percent Myl5 protein level knockdown (% KD) normalized to Gapdh is indicated for each oligonucleotide. (b-c) Immunofluorescence microscopy of HeLa cells treated with siCtrl or siM3 for 72 hours, fixed, and stained with Hoechst 33342 DNA dye and anti- α -Tubulin and anti-Pericentrin (b) antibodies. Note that siM3-treated cells display multipolar spindles in prometaphase (b), Pericentrin (marker for pericentriolar material- PCM) fragmentation with >2 foci (b), and lagging chromosomes (c) in anaphase. Scale bars indicate 5 μ m. (d-f) Quantitation of the percent mitotic cells with PCM fragmentation (d), multipolar spindles (e) and lagging chromosomes (f) in siCtrl or siM3 treated cells. Data represent the average \pm SD of 4 independent experiments, 100 cells counted for each. * indicates a p value <.05 as indicated above each asterisk.

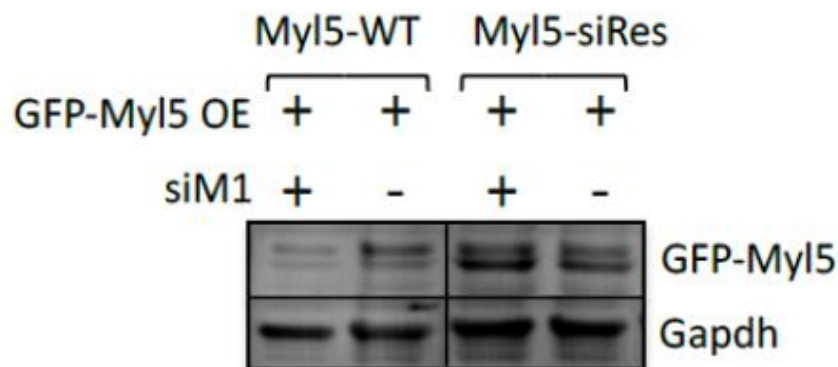


Figure S3 Generation of a Myl5 siRNA-resistant clone for use in rescue experiments. (a) HeLa cells were induced to overexpress (OE) an siRNA-sensitive wild type Myl5 (Myl5-WT) or an siRNA-resistant Myl5 (Myl5-siRes) mutant. Cells were transfected with or without siRNA targeting Myl5 (siM1) and immunoblot analysis was performed on cell extracts. Note that the overexpressed Myl5-WT is depleted upon treatment with siM1 (lane 1), while Myl5-siRes remains abundant (lane 3). Gapdh was used as a loading control and its levels remain unchanged.

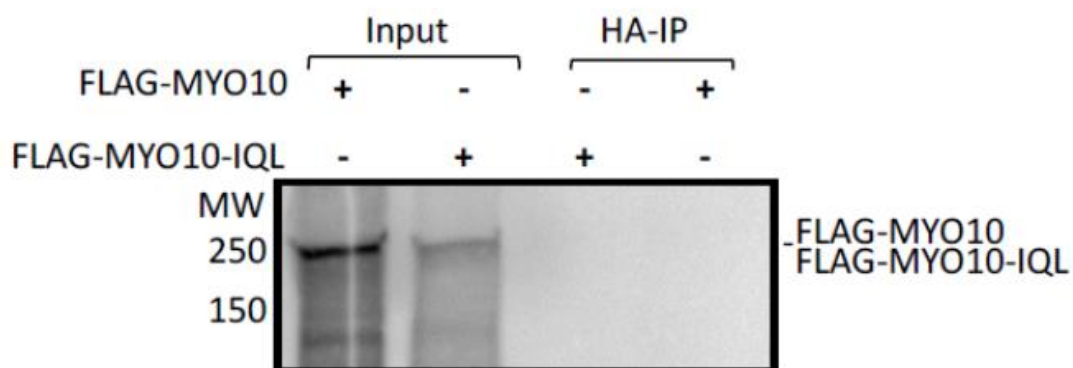


Figure S4 Control immunoprecipitation (IP) experiment related to Figure 5c,d.

The *in vitro* binding assay performed in the presence or absence of radiolabeled (³⁵S methionine) FLAG- MYO10 or FLAG-MYO10-IQL (MYO10 IQ-less mutant) and anti-HA beads. The anti-HA bead immunoprecipitation (HA-IP) shows that FLAG-MYO10 or FLAG-MYO10-IQL are not binding to the beads non-specifically. MW indicates molecular weight.

```

                                     ↓↓
sp|P24844|MYL9_HUMAN      -----MSSKRAK---AKTTKKRPQRATSNVVFAMFDQSQIQ 32
sp|P19105|ML12A_HUMAN    -----MSSKRTK---TKTKKRPQRATSNVVFAMFDQSQIQ 31
sp|O14950|ML12B_HUMAN    -----MSSKKAK---TKTKKRPQRATSNVVFAMFDQSQIQ 32
sp|Q01449|MYL7_HUMAN     -----MASRKAGTRGKVAATKQAQRGSSNVVFSMFEQAQIQ 35
sp|Q02045|MYL5_HUMAN     -----MASRKTKK--KEGGALRAQRASSNVVFSNFEQTQIQ 33
sp|P10916|MYL2_HUMAN     -----MAPKKAKK--R-----AGGANSNVVFSMFEQTQIQ 27
sp|Q9BUA6|MYL10_HUMAN    MLLRLVSNVSWPQVILPPRPPKVLGLQAPRRARK--RA-----EGTASSNVVFSMFDQSQIQ 53
                               :   ::
                               ..*****: *:*:***

sp|P24844|MYL9_HUMAN      EFKE-----AFNMIDQNRDGFIDKEDLHDML 58
sp|P19105|ML12A_HUMAN    EFKE-----AFNMIDQNRDGFIDKEDLHDML 57
sp|O14950|ML12B_HUMAN    EFKE-----AFNMIDQNRDGFIDKEDLHDML 58
sp|Q01449|MYL7_HUMAN     EFKE-----AFSCIDQNRDGIICKADLRETY 61
sp|Q02045|MYL5_HUMAN     EFKE-----AFTLMDQNRDGFIDKEDLKDITY 59
sp|P10916|MYL2_HUMAN     EFKE-----AFTIMDQNRDGFIDKNDLDRDTF 53
sp|Q9BUA6|MYL10_HUMAN    EFKESLALSPRLERNGMISAHCNLCITGSSNSPASASQAFTIMDQNRDGFIDKEDLDRDTF 113
*****
                               ** . :*****: * * **::

sp|P24844|MYL9_HUMAN      ASLGKN-PTDEYLEGMMSEAPGPINFTMFLTMFGEKLNQDPEDEVIRNAFACFDEEASGF 117
sp|P19105|ML12A_HUMAN    ASLGKN-PTDEYLDAMMNEAPGPINFTMFLTMFGEKLNQDPEDEVIRNAFACFDEEATGT 116
sp|O14950|ML12B_HUMAN    ASLGKN-PTDAYLDAMMNEAPGPINFTMFLTMFGEKLNQDPEDEVIRNAFACFDEEATGT 117
sp|Q01449|MYL7_HUMAN     SQLGKVSVPPEELDAMLQEGKGPINFTVFLTLFGEKLNQDPEEAILSAPRMFDPSGKGV 121
sp|Q02045|MYL5_HUMAN     ASLGKTNVKDELDELAMLKEASGPINFTMFLNLFGEKLSGTDAAEETILNAPKMLDPDGKGV 119
sp|P10916|MYL2_HUMAN     AALGRVNVKNEEIDEMIKEAPGPINFTVFLTMFGEKLNQDPEEETILNAPKVFDPGEGKV 113
sp|Q9BUA6|MYL10_HUMAN    AALGRINVKNEELEAMVKEAPGPINFTVFLTMFGEKLNQDPEEETILHAPKVFDPTEGKGV 173
: ** :   :   : : *:. * . *****: ** : *****: * * * : * * * *

sp|P24844|MYL9_HUMAN      IHEDHLRELLTTMGDRFTDEEVDEMYREAPIDKKGNFNHYEFTRILKHGAKDKDD 172
sp|P19105|ML12A_HUMAN    IQEDYLRELLTTMGDRFTDEEVDELYREAPIDKKGNFNHYEFTRILKHGAKDKDD 171
sp|O14950|ML12B_HUMAN    IQEDYLRELLTTMGDRFTDEEVDELYREAPIDKKGNFNHYEFTRILKHGAKDKDD 172
sp|Q01449|MYL7_HUMAN     VNKDEFKQLLLTQADKFSPAEVEQMPFALTPMDLAGNIDYKSLCYIITHGDEKEE- 175
sp|Q02045|MYL5_HUMAN     INKEYIKRLLMSQADKMTAEVVDQMPQFASIDVAGNLDYKALSIVITHGEEKEE- 173
sp|P10916|MYL2_HUMAN     LKADYVREMLTTQAERFSKEEVDQMPFAAFPDPVGTGNLDYKNLVHIITHGEEKD-- 166
sp|Q9BUA6|MYL10_HUMAN    VKADVIKEKLMTQADRFSEEEVKQMPFAAFPDPVCGNLDYRNLCYVITHGEEKD-- 226
: : : ... * : : : : ** : : : * ** : * : : : ** : :

```

Figure S5 Myl5 shares conserved S/T phosphorylation sites with other myosin regulatory light chains (RLCs). The indicated human myosin RLC protein sequences were derived from UniProt (UniProtKB ID numbers are indicated for each) and aligned using the Clustal Omega multiple sequence alignment tool with default parameters. The conserved myosin RLC Ser/Thr sites of phosphorylation are indicated with red arrows, which correspond to serine 20 and serine 21 in Myl5.

Table S1 Reagents and resources

REAGENT or RESOURCE	SOURCE	IDENTIFIER
Antibodies		
Chicken polyclonal anti-GFP	Abcam	Cat# ab13970; RRID: AB_300798
Rabbit polyclonal anti-HA	Proteintech	Cat# 51064-2-AP; RRID: AB_11042321
Rat monoclonal anti- α -Tubulin (clone YOL1/34)	Bio-Rad	Cat# MCA78G; RRID: AB_325005
Rabbit polyclonal anti-MYO10	Proteintech	Cat# 24565-1-AP
Rabbit polyclonal anti-Pericentrin	Novus	Cat# NB100-68277; RRID: AB_1109761
Rabbit polyclonal anti-GAPDH	Genetex	Cat# GTX100118; RRID: AB_1080976
Rabbit polyclonal anti-MYL5	Proteintech	Cat# 14249-1-AP; RRID: AB_2266762
Mouse monoclonal anti-Cyclin B1	Santa Cruz	Cat# sc-245; RRID: AB_627338
Rabbit polyclonal anti-NUMA	Gift from D. Compton	N/A
Rabbit polyclonal anti-TPX2	Gift from D. Compton	N/A
Rabbit polyclonal anti-Centrin	Gift from J. Salisbury	N/A
Rabbit polyclonal anti-Calmodulin	Proteintech	Cat# 10541-1-AP RRID: AB_2069442
Mouse monoclonal anti-Fascin	Proteintech	Cat# 66321-1-Ig RRID: AB_2881701
Donkey polyclonal anti-Human IgG (H+L), Fluorescein (FITC) AffiniPure	Jackson ImmunoResearch Labs	Cat# 709-095-149; RRID: AB_2340514
Donkey polyclonal anti-Rat IgG (H+L), Cy3 AffiniPure	Jackson ImmunoResearch Labs	Cat# 712-165-153; RRID: AB_2340667
Donkey polyclonal anti-Human IgG (H+L), Cy5 AffiniPure	Jackson ImmunoResearch Labs	Cat# 709-175-149; RRID: AB_2340539
Donkey polyclonal anti-Chicken IgY (IgG) (H+L), Fluorescein (FITC) AffiniPure	Jackson ImmunoResearch Labs	Cat# 703-095-155; RRID: AB_2340356
Donkey polyclonal anti-Rabbit IgG (H+L), Cy3 AffiniPure	Jackson ImmunoResearch Labs	Cat# 711-165-152; RRID: AB_2307443
Donkey polyclonal anti-Rabbit IgG (H+L), Fluorescein (FITC) AffiniPure	Jackson ImmunoResearch Labs	Cat# 711-095-152; RRID: AB_2315776
Donkey polyclonal anti-Mouse IgG (H+L), Fluorescein (FITC) AffiniPure	Jackson ImmunoResearch Labs	Cat# 715-095-151; RRID: AB_2335588
Donkey polyclonal anti-Mouse IgG (H+L), Cy3 AffiniPure	Jackson ImmunoResearch Labs	Cat# 715-165-151; RRID: AB_2315777
Donkey polyclonal anti-Goat IgG (H+L), IRDye 680RD	LI-COR Biosciences	Cat# 926-68074; RRID: AB_10956736
Donkey polyclonal anti-Mouse IgG (H+L), IRDye 680RD	LI-COR Biosciences	Cat# 926-68072; RRID: AB_10953628
Donkey polyclonal anti-Mouse IgG (H+L), IRDye 800CW	LI-COR Biosciences	Cat# 926-32212; RRID: AB_621847
Donkey polyclonal anti-Chicken IgG (H+L), IRDye 800CW	LI-COR Biosciences	Cat# 926-32218; RRID: AB_1850023
Donkey polyclonal anti-Rabbit IgG (H+L), IRDye 680RD	LI-COR Biosciences	Cat# 926-68073; RRID: AB_10954442
Donkey polyclonal anti-Rabbit IgG (H+L), IRDye 800CW	LI-COR Biosciences	Cat# 926-32213; RRID: AB_621848

Chemicals, Peptides, and Recombinant Proteins		
Paclitaxel	Sigma-Aldrich	Cat# T7191; CAS:33069-62-4
Nocodazole	Sigma-Aldrich	Cat# 1404; CAS:31430-18-9
Thymidine	Sigma-Aldrich	Cat# T1895; CAS:50-89-5
Doxycycline	Sigma-Aldrich	Cat# D9891; CAS:24390-14-5
Halt Protease Inhibitor Cocktail	Thermo Fisher Scientific	Cat# 87786
Hoechst 33342	Thermo Fisher Scientific	Cat# H1399; CAS:23491-52-3
ProLong Gold Antifade Mountant	Thermo Fisher Scientific	Cat# P36934
Lipofectamine RNAiMAX	Thermo Fisher Scientific	Cat# 13778150
FuGENE HD	Promega	Cat# E2311
FuGene 6	Promega	Cat# E2691
Critical Commercial Assays		
SP6 TnT Quick Coupled Transcription/Translation System	Promega	Cat# L2080
PureYield Plasmid Miniprep System	Promega	Cat# A1222
QIAprep Spin Miniprep Kit	QIAGEN	Cat# 27106
Experimental Models: Cell Lines		
Human: HeLa cells	ATCC	Cat# CCL-2; RRID: CVCL_0030
Human: HCT116-GFP-H2B Cells	Gift from P. Jackson	N/A
Human: HeLa Flp-In T-Rex Cells	Gift from S. Taylor	N/A
Oligonucleotides		
Silencer™ Select siRNA targeting <i>MYL5</i>	Thermo Fisher Scientific	Cat# 4392420; siRNA ID: s9187
Silencer™ Select siRNA targeting <i>MYL5</i>	Thermo Fisher Scientific	Cat# 4392420; siRNA ID: s9188
Silencer™ Select Negative Control siRNA	Thermo Fisher Scientific	Cat# 4390843
ON-TARGETplus Human <i>MYL5</i> siRNA	Dharmacon	Cat# J-011739-03
ON-TARGETplus Human <i>MYL5</i> siRNA	Dharmacon	Cat# J-011739-04
ON-TARGETplus Non-targeting Control	Dharmacon	Cat# D-001810-10
Recombinant DNA		
<i>MYL5</i> cDNA	GenScript	Clone ID: OHu30367
pDONR221-My15	This paper	N/A
pGLAP1-My15	This paper	N/A
pCS2-HA-My15	This paper	N/A
pDONR221-MYO10	This paper	N/A
EGFPC1-hMYO10	Addgene	Clone ID: 47608
pCS2-FLAG-MYO10	This paper	N/A
pDONR221-GFP	This paper	N/A
pCS2-FLAG-GFP	This paper	N/A
pDONR221	Thermo Fisher Scientific	Cat# 12536017
pGLAP1-My15-AA	This paper	N/A
pGLAP1- My15-20E	This paper	N/A
pGLAP1- My15-21E	This paper	N/A
pGLAP1- My15-CAD	This paper	N/A
pGLAP1-My15-siRes	This paper	N/A
pCS2-FLAG-MYO10-IQL	This paper	N/A
pLDNT7_nFLAG-CALM3	DNASU	Clone ID: HsCD00617973

pDONR221-CALM3	This paper	N/A
pCS2-HA-CALM3	This paper	N/A
Software and Algorithms		
GraphPad Prism 8	GraphPad	RRID: SCR_002798
ImageJ	NIH ImageJ	https://imagej.nih.gov/ij/index.html RRID:SCR_003070

Table S2 List of cancer types analyzed for *MYL5* and *MYO10* differential gene expression

Abbreviation	Cancer type
ACC	Adrenocortical carcinoma
BLCA	Bladder Urothelial Carcinoma
BRCA	Breast invasive carcinoma
CESC	Cervical squamous cell carcinoma & endocervical adenocarcinoma
CHOL	Cholangio carcinoma
COAD	Colon adenocarcinoma
DLBC	Lymphoid Neoplasm Diffuse Large B-cell Lymphoma
ESCA	Esophageal carcinoma
GBM	Glioblastoma multiforme
HNSC	Head and Neck squamous cell carcinoma
KICH	Kidney Chromophobe
KIRC	Kidney renal clear cell carcinoma
KIRP	Kidney renal papillary cell carcinoma
LAML	Acute Myeloid Leukemia
LGG	Brain Lower Grade Glioma
LIHC	Liver hepatocellular carcinoma
LUAD	Lung adenocarcinoma
LUSC	Lung squamous cell carcinoma
MESO	Mesothelioma
OV	Ovarian serous cystadenocarcinoma
PAAD	Pancreatic adenocarcinoma
PCPG	Pheochromocytoma and Paraganglioma
PRAD	Prostate adenocarcinoma
READ	Rectum adenocarcinoma
SARC	Sarcoma
SKCM	Skin Cutaneous Melanoma
STAD	Stomach adenocarcinoma
TGCT	Testicular Germ Cell Tumors
THCA	Thyroid carcinoma
THYM	Thymoma
UCEC	Uterine Corpus Endometrial Carcinoma
UCS	Uterine Carcinosarcoma
UVM	Uveal Melanoma

REFERENCES

1. AkhAkshshi TK, Wernike D and Piekny A. 2014. Microtubules and actin crosstalk in cell migration and division. *Cytoskeleton (Hoboken)* 71(1):1-23.
2. Alshabi AM, Vastrad B, Shaikh IA and Vastrad C. 2019. Identification of Crucial Candidate Genes and Pathways in Glioblastoma Multiform by Bioinformatics Analysis. *Biomolecules* 9(5).
3. Arjonen A, Kaukonen R, Mattila E, Rouhi P, Hognas G, Sihto H, Miller BW, Morton JP, Bucher E, Taimen P et al. 2014. Mutant p53-associated myosin-X upregulation promotes breast cancer invasion and metastasis. *J Clin Invest* 124(3):1069-82.
4. Bennett RD, Mauer AS and Strehler EE. 2007. Calmodulin-like protein increases filopodia-dependent cell motility via up-regulation of myosin-10. *J Biol Chem* 282(5):3205-12.
5. Bennett RD, Caride AJ, Mauer AS and Strehler EE. 2008. Interaction with the IQ3 motif of myosin-10 is required for calmodulin-like protein-dependent filopodial extension. *FEBS Lett* 582(16):2377-81.
6. Berg JS and Cheney RE. 2002. Myosin-X is an unconventional myosin that undergoes intrafilopodial motility. *Nat Cell Biol* 4(3):246-50.
7. Bohil AB, Robertson BW and Cheney RE. 2006. Myosin-X is a molecular motor that functions in filopodia formation. *Proc Natl Acad Sci U S A* 103(33):12411-6.
8. Bradley M, Ramirez I, Cheung K, Gholkar AA and Torres JZ. 2016. Inducible LAP-tagged Stable Cell Lines for Investigating Protein Function, Spatiotemporal Localization and Protein Interaction Networks. *J Vis Exp* 118(118):54870.
9. Cao R, Chen J, Zhang X, Zhai Y, Qing X, Xing W, Zhang L, Malik YS, Yu H and Zhu X. 2014. Elevated expression of myosin X in tumours contributes to breast cancer aggressiveness and metastasis. *Br J Cancer* 111(3):539-50.
10. Caswell PT and Zech T. 2018. Actin-Based Cell Protrusion in a 3D Matrix. *Trends Cell Biol* 28(10):823-34.
11. Chaigne A, Campillo C, Voituriez R, Gov NS, Sykes C, Verlhac MH and Terret ME. 2016. F-actin mechanics control spindle centring in the mouse zygote. *Nat Commun* 7:10253.

12. Collins C, Schappert K and Hayden MR. 1992. The genomic organization of a novel regulatory myosin light chain gene (MYL5) that maps to chromosome 4p16.3 and shows different patterns of expression between primates. *Hum Mol Genet* 1(9):727-33.
13. Courson DS and Cheney RE. 2015. Myosin-X and disease. *Exp Cell Res* 334(1):10-5.
14. di Pietro F, Echard A and Morin X. 2016. Regulation of mitotic spindle orientation: an integrated view. *EMBO Rep* 17(8):1106-30.
15. Edwards RA and Bryan J. 1995. Fascins, a family of actin bundling proteins. *Cell Motil Cytoskeleton* 32(1):1-9.
16. Gholkar AA, Senese S, Lo YC, Vides E, Contreras E, Hodara E, Capri J, Whitelegge JP and Torres JZ. 2016. The X-Linked-Intellectual-Disability-Associated Ubiquitin Ligase Mid2 Interacts with Astrin and Regulates Astrin Levels to Promote Cell Division. *Cell Rep* 14(2):180-8.
17. Grabarek Z. 2006. Structural basis for diversity of the EF-hand calcium-binding proteins. *J Mol Biol* 359(3):509-25.
18. Hartman MA and Spudich JA. 2012. The myosin superfamily at a glance. *J Cell Sci* 125(Pt 7):1627-32.
19. He K, Sakai T, Tsukasaki Y, Watanabe TM and Ikebe M. 2017. Myosin X is recruited to nascent focal adhesions at the leading edge and induces multi-cycle filopodial elongation. *Sci Rep* 7(1):13685.
20. Heissler SM and Sellers JR. 2014. Myosin light chains: Teaching old dogs new tricks. *Bioarchitecture* 4(6):169-88.
21. Heissler SM and Sellers JR. 2015. Four things to know about myosin light chains as reporters for non-muscle myosin-2 dynamics in live cells. *Cytoskeleton (Hoboken)* 72(2):65-70.
22. Heissler SM and Sellers JR. 2016. Various Themes of Myosin Regulation. *J Mol Biol* 428(9 Pt B):1927-46.
23. Homma K, Saito J, Ikebe R and Ikebe M. 2001. Motor function and regulation of myosin X. *J Biol Chem* 276(36):34348-54.

24. Hunt SE, McLaren W, Gil L, Thormann A, Schuilenburg H, Sheppard D, Parton A, Armean IM, Trevanion SJ, Flicek P et al. 2018. Ensembl variation resources. Database (Oxford) 2018.
25. Hyrskyluoto A and Vartiainen MK. 2020. Regulation of nuclear actin dynamics in development and disease. *Curr Opin Cell Biol* 64:18-24.
26. Jacquemet G, Hamidi H and Ivaska J. 2015. Filopodia in cell adhesion, 3D migration and cancer cell invasion. *Curr Opin Cell Biol* 36:23-31.
27. Kerber ML and Cheney RE. 2011. Myosin-X: a MyTH-FERM myosin at the tips of filopodia. *J Cell Sci* 124(Pt 22):3733-41.
28. Kerber ML, Jacobs DT, Campagnola L, Dunn BD, Yin T, Sousa AD, Quintero OA and Cheney RE. 2009. A novel form of motility in filopodia revealed by imaging myosin-X at the single-molecule level. *Curr Biol* 19(11):967-73.
29. Kita AM, Swider ZT, Erofeev I, Halloran MC, Goryachev AB and Bement WM. 2019. Spindle-F-actin interactions in mitotic spindles in an intact vertebrate epithelium. *Mol Biol Cell* 30(14):1645-54.
30. Kwon M, Bagonis M, Danuser G and Pellman D. 2015. Direct Microtubule-Binding by Myosin-10 Orients Centrosomes toward Retraction Fibers and Subcortical Actin Clouds. *Dev Cell* 34(3):323-37.
31. Kwon M, Godinho SA, Chandhok NS, Ganem NJ, Azioune A, Theyry M and Pellman D. 2008. Mechanisms to suppress multipolar divisions in cancer cells with extra centrosomes. *Genes Dev* 22(16):2189-203.
32. Leijnse N, Oddershede LB and Bendix PM. 2015. An updated look at actin dynamics in filopodia. *Cytoskeleton (Hoboken)* 72(2):71-9.
33. Li J, Lu Q and Zhang M. 2016. Structural Basis of Cargo Recognition by Unconventional Myosins in Cellular Trafficking. *Traffic* 17(8):822-38.
34. Li Q and Sarna SK. 2009. Nuclear myosin II regulates the assembly of preinitiation complex for ICAM-1 gene transcription. *Gastroenterology* 137(3):1051-60, 60 e1-3.
35. Li YR and Yang WX. 2016. Myosins as fundamental components during tumorigenesis: diverse and indispensable. *Oncotarget* 7(29):46785-812.
36. Mogessie B and Schuh M. 2017. Actin protects mammalian eggs against chromosome segregation errors. *Science* 357(6353).

37. Morin X and Bellaïche Y. 2011. Mitotic spindle orientation in asymmetric and symmetric cell divisions during animal development. *Dev Cell* 21(1):102-19.
38. Moujaber O and Stochaj U. 2020. The Cytoskeleton as Regulator of Cell Signaling Pathways. *Trends Biochem Sci* 45(2):96-107.
39. Murthy K and Wadsworth P. 2005. Myosin-II-dependent localization and dynamics of F-actin during cytokinesis. *Curr Biol* 15(8):724-31.
40. Nakajima YI. 2018. Mitotic spindle orientation in epithelial homeostasis and plasticity. *J Biochem* 164(4):277-84.
41. Otto JJ, Kane RE and Bryan J. 1979. Formation of filopodia in coelomocytes: localization of fascin, a 58,000 dalton actin cross-linking protein. *Cell* 17(2):285-93.
42. Quintero OA and Yengo CM. 2012. Myosin X dimerization and its impact on cellular functions. *Proc Natl Acad Sci U S A* 109(43):17313-4.
43. Rankin EB and Giaccia AJ. 2016. Hypoxic control of metastasis. *Science* 352(6282):175-80.
44. Robinson DN and Spudich JA. 2000. Towards a molecular understanding of cytokinesis. *Trends Cell Biol* 10(6):228-37.
45. Rogers MS and Strehler EE. 2001. The tumor-sensitive calmodulin-like protein is a specific light chain of human unconventional myosin X. *J Biol Chem* 276(15):12182-9.
46. Sandquist JC, Larson ME and Hine KJ. 2016. Myosin-10 independently influences mitotic spindle structure and mitotic progression. *Cytoskeleton (Hoboken)* 73(7):351-64.
47. Sato O, Jung HS, Komatsu S, Tsukasaki Y, Watanabe TM, Homma K and Ikebe M. 2017. Activated full-length myosin-X moves processively on filopodia with large steps toward diverse two-dimensional directions. *Sci Rep* 7:44237.
48. Savci-Heijink CD, Halfwerk H, Koster J, Horlings HM and van de Vijver MJ. 2019. A specific gene expression signature for visceral organ metastasis in breast cancer. *BMC Cancer* 19(1):333.
49. Sigrist CJ, De Castro E, Langendijk-Genevaux PS, Le Saux V, Bairoch A and Hulo N. 2005. ProRule: a new database containing functional and structural information on PROSITE profiles. *Bioinformatics* 21(21):4060-6.

50. Sousa AD and Cheney RE. 2005. Myosin-X: a molecular motor at the cell's fingertips. *Trends Cell Biol* 15(10):533-9.
51. Svitkina T. 2018. The Actin Cytoskeleton and Actin-Based Motility. *Cold Spring Harb Perspect Biol* 10(1).
52. Tang Z, Li C, Kang B, Gao G, Li C and Zhang Z. 2017. GEPIA: a web server for cancer and normal gene expression profiling and interactive analyses. *Nucleic Acids Res* 45(W1):W98-W102.
53. Thery M and Bornens M. 2006. Cell shape and cell division. *Curr Opin Cell Biol* 18(6):648-57.
54. Titus MA. 2018. Myosin-Driven Intracellular Transport. *Cold Spring Harb Perspect Biol* 10(3).
55. Tokuo H, Mabuchi K and Ikebe M. 2007. The motor activity of myosin-X promotes actin fiber convergence at the cell periphery to initiate filopodia formation. *J Cell Biol* 179(2):229-38.
56. Tokuo H, Bhawan J and Coluccio LM. 2018. Myosin X is required for efficient melanoblast migration and melanoma initiation and metastasis. *Sci Rep* 8(1):10449.
57. Torres JZ, Miller JJ and Jackson PK. 2009. High-throughput generation of tagged stable cell lines for proteomic analysis. *Proteomics* 9(10):2888-91.
58. Torres JZ, Ban KH and Jackson PK. 2010. A Specific Form of Phospho Protein Phosphatase 2 Regulates Anaphase-promoting Complex/Cyclosome Association with Spindle Poles. *Mol Biol Cell* 21(6):897-904.
59. Uraji J, Scheffler K and Schuh M. 2018. Functions of actin in mouse oocytes at a glance. *J Cell Sci* 131(22).
60. Vasquez CG, Heissler SM, Billington N, Sellers JR and Martin AC. 2016. *Drosophila* non-muscle myosin II motor activity determines the rate of tissue folding. *Elife* 5.
61. Walczak CE and Heald R. 2008. Mechanisms of mitotic spindle assembly and function. *Int Rev Cytol* 265:111-58.
62. Weber KL, Sokac AM, Berg JS, Cheney RE and Bement WM. 2004. A microtubule-binding myosin required for nuclear anchoring and spindle assembly. *Nature* 431(7006):325-9.

63. Woolner S, O'Brien LL, Wiese C and Bement WM. 2008. Myosin-10 and actin filaments are essential for mitotic spindle function. *J Cell Biol* 182(1):77-88.
64. Wuhr M, Mitchison TJ and Field CM. 2008. Mitosis: new roles for myosin-X and actin at the spindle. *Curr Biol* 18(19):R912-4.
65. Yu H, Chakravorty S, Song W and Ferenczi MA. 2016. Phosphorylation of the regulatory light chain of myosin in striated muscle: methodological perspectives. *Eur Biophys J* 45(8):779-805.
66. Zhang L, Huang ST, Feng YL, Wan T, Gu HF, Xu J, Yuan LJ, Zhou Y, Yu XJ, Huang L et al. 2017. The Bidirectional Regulation between MYL5 and HIF-1alpha Promotes Cervical Carcinoma Metastasis. *Theranostics* 7(15):3768-80.
67. Zhang YS, Liu B, Luo XJ, Li TB, Zhang JJ, Peng JJ, Zhang XJ, Ma QL, Hu CP, Li YJ et al. 2015. Nuclear cardiac myosin light chain 2 modulates NADPH oxidase 2 expression in myocardium: a novel function beyond muscle contraction. *Basic Res Cardiol* 110(4):38.
68. Shi TK, Wernike D and Piekny A. 2014. Microtubules and actin crosstalk in cell migration and division. *Cytoskeleton (Hoboken)* 71(1):1-23.
69. Alshabi AM, Vastrad B, Shaikh IA and Vastrad C. 2019. Identification of Crucial Candidate Genes and Pathways in Glioblastoma Multiform by Bioinformatics Analysis. *Biomolecules* 9(5).
70. Arjonen A, Kaukonen R, Mattila E, Rouhi P, Hognas G, Sihto H, Miller BW, Morton JP, Bucher E, Taimen P et al. 2014. Mutant p53-associated myosin-X upregulation promotes breast cancer invasion and metastasis. *J Clin Invest* 124(3):1069-82.
71. Bennett RD, Mauer AS and Strehler EE. 2007. Calmodulin-like protein increases filopodia-dependent cell motility via up-regulation of myosin-10. *J Biol Chem* 282(5):3205-12.
72. Bennett RD, Caride AJ, Mauer AS and Strehler EE. 2008. Interaction with the IQ3 motif of myosin-10 is required for calmodulin-like protein-dependent filopodial extension. *FEBS Lett* 582(16):2377-81.
73. Berg JS and Cheney RE. 2002. Myosin-X is an unconventional myosin that undergoes intrafilopodial motility. *Nat Cell Biol* 4(3):246-50.

74. Bohil AB, Robertson BW and Cheney RE. 2006. Myosin-X is a molecular motor that functions in filopodia formation. *Proc Natl Acad Sci U S A* 103(33):12411-6.
75. Bradley M, Ramirez I, Cheung K, Gholkar AA and Torres JZ. 2016. Inducible LAP-tagged Stable Cell Lines for Investigating Protein Function, Spatiotemporal Localization and Protein Interaction Networks. *J Vis Exp* 118(118):54870.
76. Cao R, Chen J, Zhang X, Zhai Y, Qing X, Xing W, Zhang L, Malik YS, Yu H and Zhu X. 2014. Elevated expression of myosin X in tumours contributes to breast cancer aggressiveness and metastasis. *Br J Cancer* 111(3):539-50.
77. Caswell PT and Zech T. 2018. Actin-Based Cell Protrusion in a 3D Matrix. *Trends Cell Biol* 28(10):823-34.
78. Chaigne A, Campillo C, Voituriez R, Gov NS, Sykes C, Verlhac MH and Terret ME. 2016. F-actin mechanics control spindle centring in the mouse zygote. *Nat Commun* 7:10253.
79. Collins C, Schappert K and Hayden MR. 1992. The genomic organization of a novel regulatory myosin light chain gene (MYL5) that maps to chromosome 4p16.3 and shows different patterns of expression between primates. *Hum Mol Genet* 1(9):727-33.
80. Courson DS and Cheney RE. 2015. Myosin-X and disease. *Exp Cell Res* 334(1):10-5.
81. di Pietro F, Echard A and Morin X. 2016. Regulation of mitotic spindle orientation: an integrated view. *EMBO Rep* 17(8):1106-30.
82. Gholkar AA, Senese S, Lo YC, Vides E, Contreras E, Hodara E, Capri J, Whitelegge JP and Torres JZ. 2016. The X-Linked-Intellectual-Disability-Associated Ubiquitin Ligase Mid2 Interacts with Astrin and Regulates Astrin Levels to Promote Cell Division. *Cell Rep* 14(2):180-8.
83. Grabarek Z. 2006. Structural basis for diversity of the EF-hand calcium-binding proteins. *J Mol Biol* 359(3):509-25.
84. Hartman MA and Spudich JA. 2012. The myosin superfamily at a glance. *J Cell Sci* 125(Pt 7):1627-32.

85. He K, Sakai T, Tsukasaki Y, Watanabe TM and Ikebe M. 2017. Myosin X is recruited to nascent focal adhesions at the leading edge and induces multi-cycle filopodial elongation. *Sci Rep* 7(1):13685.
86. Heissler SM and Sellers JR. 2014. Myosin light chains: Teaching old dogs new tricks. *Bioarchitecture* 4(6):169-88.
87. Heissler SM and Sellers JR. 2016. Various Themes of Myosin Regulation. *J Mol Biol* 428(9 Pt B):1927-46.
88. Homma K, Saito J, Ikebe R and Ikebe M. 2001. Motor function and regulation of myosin X. *J Biol Chem* 276(36):34348-54.
89. Hunt SE, McLaren W, Gil L, Thormann A, Schuilenburg H, Sheppard D, Parton A, Armean IM, Trevanion SJ, Flicek P et al. 2018. Ensembl variation resources. *Database (Oxford)* 2018.
90. Hyrskyluoto A and Vartiainen MK. 2020. Regulation of nuclear actin dynamics in development and disease. *Curr Opin Cell Biol* 64:18-24.
91. Jacquemet G, Hamidi H and Ivaska J. 2015. Filopodia in cell adhesion, 3D migration and cancer cell invasion. *Curr Opin Cell Biol* 36:23-31.
92. Kerber ML and Cheney RE. 2011. Myosin-X: a MyTH-FERM myosin at the tips of filopodia. *J Cell Sci* 124(Pt 22):3733-41.
93. Kerber ML, Jacobs DT, Campagnola L, Dunn BD, Yin T, Sousa AD, Quintero OA and Cheney RE. 2009. A novel form of motility in filopodia revealed by imaging myosin-X at the single-molecule level. *Curr Biol* 19(11):967-73.
94. Kita AM, Swider ZT, Erofeev I, Halloran MC, Goryachev AB and Bement WM. 2019. Spindle-F-actin interactions in mitotic spindles in an intact vertebrate epithelium. *Mol Biol Cell* 30(14):1645-54.
95. Kwon M, Bagonis M, Danuser G and Pellman D. 2015. Direct Microtubule-Binding by Myosin-10 Orients Centrosomes toward Retraction Fibers and Subcortical Actin Clouds. *Dev Cell* 34(3):323-37.
96. Kwon M, Godinho SA, Chandhok NS, Ganem NJ, Azioune A, They M and Pellman D. 2008. Mechanisms to suppress multipolar divisions in cancer cells with extra centrosomes. *Genes Dev* 22(16):2189-203.

97. Leijnse N, Oddershede LB and Bendix PM. 2015. An updated look at actin dynamics in filopodia. *Cytoskeleton (Hoboken)* 72(2):71-9.
98. Li J, Lu Q and Zhang M. 2016. Structural Basis of Cargo Recognition by Unconventional Myosins in Cellular Trafficking. *Traffic* 17(8):822-38.
99. Li Q and Sarna SK. 2009. Nuclear myosin II regulates the assembly of preinitiation complex for ICAM-1 gene transcription. *Gastroenterology* 137(3):1051-60, 60 e1-3.
100. Li YR and Yang WX. 2016. Myosins as fundamental components during tumorigenesis: diverse and indispensable. *Oncotarget* 7(29):46785-812.
101. Mogessie B and Schuh M. 2017. Actin protects mammalian eggs against chromosome segregation errors. *Science* 357(6353).
102. Morin X and Bellaiche Y. 2011. Mitotic spindle orientation in asymmetric and symmetric cell divisions during animal development. *Dev Cell* 21(1):102-19.
103. Moujaber O and Stochaj U. 2020. The Cytoskeleton as Regulator of Cell Signaling Pathways. *Trends Biochem Sci* 45(2):96-107.
104. Murthy K and Wadsworth P. 2005. Myosin-II-dependent localization and dynamics of F-actin during cytokinesis. *Curr Biol* 15(8):724-31.
105. Nakajima YI. 2018. Mitotic spindle orientation in epithelial homeostasis and plasticity. *J Biochem* 164(4):277-84.
106. Quintero OA and Yengo CM. 2012. Myosin X dimerization and its impact on cellular functions. *Proc Natl Acad Sci U S A* 109(43):17313-4.
107. Rankin EB and Giaccia AJ. 2016. Hypoxic control of metastasis. *Science* 352(6282):175-80.
108. Robinson DN and Spudich JA. 2000. Towards a molecular understanding of cytokinesis. *Trends Cell Biol* 10(6):228-37.
109. Rogers MS and Strehler EE. 2001. The tumor-sensitive calmodulin-like protein is a specific light chain of human unconventional myosin X. *J Biol Chem* 276(15):12182-9.
110. Sandquist JC, Larson ME and Hine KJ. 2016. Myosin-10 independently influences mitotic spindle structure and mitotic progression. *Cytoskeleton (Hoboken)* 73(7):351-64.

111. Sato O, Jung HS, Komatsu S, Tsukasaki Y, Watanabe TM, Homma K and Ikebe M. 2017. Activated full-length myosin-X moves processively on filopodia with large steps toward diverse two-dimensional directions. *Sci Rep* 7:44237.
112. Savci-Heijink CD, Halfwerk H, Koster J, Horlings HM and van de Vijver MJ. 2019. A specific gene expression signature for visceral organ metastasis in breast cancer. *BMC Cancer* 19(1):333.
113. Sousa AD and Cheney RE. 2005. Myosin-X: a molecular motor at the cell's fingertips. *Trends Cell Biol* 15(10):533-9.
114. Svitkina T. 2018. The Actin Cytoskeleton and Actin-Based Motility. *Cold Spring Harb Perspect Biol* 10(1).
115. Tang Z, Li C, Kang B, Gao G, Li C and Zhang Z. 2017. GEPIA: a web server for cancer and normal gene expression profiling and interactive analyses. *Nucleic Acids Res* 45(W1):W98-W102.
116. They M and Bornens M. 2006. Cell shape and cell division. *Curr Opin Cell Biol* 18(6):648-57.
117. Titus MA. 2018. Myosin-Driven Intracellular Transport. *Cold Spring Harb Perspect Biol* 10(3).
118. Tokuo H, Mabuchi K and Ikebe M. 2007. The motor activity of myosin-X promotes actin fiber convergence at the cell periphery to initiate filopodia formation. *J Cell Biol* 179(2):229-38.
119. Tokuo H, Bhawan J and Coluccio LM. 2018. Myosin X is required for efficient melanoblast migration and melanoma initiation and metastasis. *Sci Rep* 8(1):10449.
120. Torres JZ, Miller JJ and Jackson PK. 2009. High-throughput generation of tagged stable cell lines for proteomic analysis. *Proteomics* 9(10):2888-91.
121. Torres JZ, Ban KH and Jackson PK. 2010. A Specific Form of Phospho Protein Phosphatase 2 Regulates Anaphase-promoting Complex/Cyclosome Association with Spindle Poles. *Mol Biol Cell* 21(6):897-904.
122. Uraji J, Scheffler K and Schuh M. 2018. Functions of actin in mouse oocytes at a glance. *J Cell Sci* 131(22).
123. Walczak CE and Heald R. 2008. Mechanisms of mitotic spindle assembly and function. *Int Rev Cytol* 265:111-58.

124. Weber KL, Sokac AM, Berg JS, Cheney RE and Bement WM. 2004. A microtubule-binding myosin required for nuclear anchoring and spindle assembly. *Nature* 431(7006):325-9.
125. Woolner S, O'Brien LL, Wiese C and Bement WM. 2008. Myosin-10 and actin filaments are essential for mitotic spindle function. *J Cell Biol* 182(1):77-88.
126. Wuhr M, Mitchison TJ and Field CM. 2008. Mitosis: new roles for myosin-X and actin at the spindle. *Curr Biol* 18(19):R912-4.
127. Zhang L, Huang ST, Feng YL, Wan T, Gu HF, Xu J, Yuan LJ, Zhou Y, Yu XJ, Huang L et al. 2017. The Bidirectional Regulation between MYL5 and HIF-1alpha Promotes Cervical Carcinoma Metastasis. *Theranostics* 7(15):3768-80.
128. Zhang YS, Liu B, Luo XJ, Li TB, Zhang JJ, Peng JJ, Zhang XJ, Ma QL, Hu CP, Li YJ et al. 2015. Nuclear cardiac myosin light chain 2 modulates NADPH oxidase 2 expression in myocardium: a novel function beyond muscle contraction. *Basic Res Cardiol* 110(4):38.

Chapter 3:

The role of Cdk14 in cell division

Abstract

The spindle assembly checkpoint (SAC) plays a vital role in cell division by halting cell division until chromosomes are properly aligned at the metaphase plate and proper tension is sensed at the kinetochores. However, cancer cells are able to dysregulate the levels of SAC proteins, which enables them to bypass the SAC and continue with cell division, even when conditions are unfavorable. Through an siRNA screen we determined that depletion of cyclin dependent kinase 14 (Cdk14) allowed cancer cells to bypass the SAC. Cdks are known to play a role in signaling events that are necessary to start and complete cell division. Cdks have also been implicated in the Wnt signaling pathway through their ability to phosphorylate Wnt components, which has been shown to regulate G2/M phase progression. Although there are many factors that contribute to the establishment and maintenance of the SAC, our data indicates that Cdk14 may be a novel Cdk that is important for proper SAC functioning through the Wnt signaling pathway.

Introduction

The spindle assembly checkpoint (SAC) is important for the proper separation of sister chromatids during cell division. Dysregulation of SAC functioning can result in premature sister chromatid separation and in cases where the SAC is completely abolished can result in cell death (1). Many types of cancer cells have a weakened SAC that allows them to divide with mis-segregated chromosomes, as has been shown in human carcinomas (2). Experiments in mice have also shown that mutations in SAC genes can lead to aneuploidy and chromosomal instability, which later in life promotes tumor formation (3,4). Important for the functioning of the SAC is the mitotic checkpoint

complex (MCC) that is composed of cell division cycle protein 20 (Cdc20), mitotic arrest deficient 2 (Mad2), budding uninhibited by benzimidazole-related 1 (BubR1) and budding uninhibited by benzimidazole 3 (Bub3), which inhibits the anaphase-promoting complex/cyclosome (APC/C) activation (5). The MCC is activated when unattached kinetochores are present or when lack of tension across the kinetochore is sensed (6). Once the APC/C is activated, it is able to ubiquitinate securin (protein that holds sister chromatids together) and target it for degradation, thus allowing for sister chromatid separation (7).

In order to better understand the SAC and its regulation, the Torres lab sought to identify novel genes important for SAC function. We conducted a high throughput cell-based siRNA screen to define gene expression knockdowns that bypassed the SAC in response to low doses of the chemotherapeutic agent Taxol. This approach identified the novel cyclin dependent kinase 14 (Cdk14). Cdks are a large family of kinases that phosphorylate serine and threonine amino acids on proteins. They remain catalytically inactive until they bind to their cognate cyclin protein (8) and Cdk's can have multiple cyclin partners which modulate their function throughout the cell cycle (9).

Cdk14 was previously been shown to be involved in the Wnt signaling pathway (11). It was also shown to interact with cyclin Y (10) and through this interaction phosphorylate low-density lipoprotein receptor-related protein 5/6 (LRP5/6) (14). This phosphorylation was important for priming LRP5/6 for further incoming Wnt signals (12) that then illicit a stop to Wnt signaling called Wnt/STOP. The Wnt/STOP signal stabilizes proteins at the G2/M transition that would otherwise be phosphorylated by glycogen synthase kinase 3 β (GSK3 β) and targeted for degradation, which have a role in ensuring proper microtubule

dynamics (12). Interestingly, the blocking of LRP6 from further incoming Wnt signals has been shown to contribute to the pathology of Alzheimers disease (14).

Recently a relationship between Wnt signaling and mitotic progression was established (14), where numerous Wnt pathway components were found to be essential for regulating cell division (16). More specifically, the Wnt pathway components dishevelled (Dvl), Axis inhibition protein 1 (Axin-1), Axis inhibition protein 2 (Axin-2), GSK3 β , β -catenin, and APC are all important for centrosome and mitotic spindle homeostasis. Dvl localizes to the centrosomes and mitotic spindle where it can interact with polo like kinase 1 (Plk1) to regulate spindle orientation and kinetochore-microtubule attachment (17). Dvl's function in spindle orientation is dependent upon LRP6 activation (17). Axin 1 and 2 localize to the centrosomes where they play a role in centrosome cohesion and microtubule nucleation and stabilization (18). GSK3 β has been implicated in regulating microtubule dynamics as well as being required for proper chromosome alignment (19). β -catenin also localizes to the centrosome where it functions in proper spindle assembly and centrosome separation (20).

As very little was known about Cdk14 with regard to centrosome homeostasis and the SAC, we sought to better understand the function of Cdk14 in the Wnt signaling pathway and in cell division. First, we sought to determine the localization and protein levels of Cdk14 during mitosis. To do this, we generated Cdk14 truncations and determined their subcellular localization using immunofluorescence (IF) microscopy. We then utilized two complementary biochemical purification approaches to define the Cdk14 protein-protein interaction network. *In-vitro* binding experiments were then used to test and verify protein-protein interactions identified in the Cdk14 interactome. Finally, the

Cdk14 protein levels were depleted using different CRISPR sgRNAs and cell division defects were analyzed by IF microscopy. Our results indicate that Cdk14 is important for SAC function and proper cell division.

Results and Discussion

Cdk14 localizes to the mitotic spindle and Cdk14 protein levels increase during mitosis

To better understand the function of Cdk14, we first analyzed its subcellular localization. To do this, we established EGFP-tagged Cdk14 expression vectors and analyzed their localization throughout the cell cycle. We determined that Cdk14 localizes to the mitotic microtubule spindle during metaphase (Figure 1A). Additionally, we analyzed the Cdk14 protein levels throughout the cell cycle by arresting cells in G1/S with thymidine, in G2/M with nocodazole, and in prometaphase of mitosis with Taxol. The cells were then released into the cell cycle and harvested at various time points post release (Figure 1B-D). Next, cells were lysed and the extracts were immunoblotted for Cdk14, Cyclin B (protein levels accumulate in mitosis, a mitotic marker), and Gapdh (loading control). Interestingly, all three synchronization and release experiments showed that Cdk14 protein levels increased as the cells entered mitosis and decreased as the cells exited mitosis (Figure 1B-D). These results indicated that the protein stability of Cdk14 was regulated in a cell cycle dependent manner and that Cdk14 levels were the highest during mitosis.

Full length CDK14 required for proper spindle localization

Next, we developed a truncation series of EGFP-tagged Cdk14 and analyzed the ability of these truncations to localize to the mitotic spindle during metaphase. This included an N-terminal domain (NT), the N-terminal and kinase domain (NTKD), the kinase domain (KD), the kinase and C-terminal domain (KDCT), and the C-terminal domain (CT). These experiments showed that the Cdk14 NTKD was the only truncation that retained the ability to localize to the spindle and the rest of the Cdk14 truncations were mislocalized from the spindle microtubules to the spindle poles (Figure 2A-B). Interestingly, the N-terminal region or C-terminal regions of Cdk14 alone were able to localize to the spindle poles, indicating that Cdk14 may have multiple domains that interact with spindle pole proteins (Figure 2B).

Cdk14 protein associations

Next, we established inducible LAP and BioID2-tagged Cdk14 stable cell lines. These cell lines were utilized to map the associations of Cdk14 through affinity (LAP-Tag) and proximity (BioID2-Tag) based proteomic approaches. Briefly, cells were induced with Dox to express LAP-tagged or BioID2-tagged Cdk14 and LAP and BioID2 biochemical purifications were performed, followed by mass spectrometry analyses of the purifications. The mass spectrometry data was analyzed to identify statistically significant associations and these associations were visualized as an interaction network using Cytoscape (Figure 3A). This preliminary analysis identified two mitotic kinases as potential Cdk14 interactors, the Polo-like kinase 1 (Plk1) and the Aurora Kinase A (AurkA) (Figure 3A). Plk1 localizes to kinetochores and regulates kinetochore-microtubule attachment (Liu 2018), while AurkA localizes to spindle poles and is involved in

centrosome function (Dutertre 2002). Additionally, we identified several other proteins involved in mitotic spindle assembly and the SAC, including Bub3 and the Bub3 interacting protein ZNF207, TPX2, SGO2, Survivin, and KIF23. Due to the importance of these proteins to the SAC and to spindle formation we decided to test the binding of some of these proteins to Cdk14. To do this, we performed in-vitro binding experiments with HA-Cdk14 and FLAG-TPX2, FLAG-SGO2, FLAG-KIF23, FLAG-Cyclin Y, FLAG-PLK1, FLAG- Survivin, and FLAG-LCMT1A. Interestingly, Cdk14 bound to SGO2, CyclinY, Plk1, and Survivin.

Cdk14 is important for SAC function

To further understand the function of Cdk14 in the SAC, we first defined siRNA oligos that were able to deplete the levels of Cdk14 in cells (Figure 4A). We also established Dox inducible CRISPR-Cas9 stable cell lines that were able to deplete Cdk14 protein levels upon Dox treatment (Figure 4B). These cell lines contained a Dox inducible Cas9 and constitutive sgRNAs that targeted Cdk14 expression. An initial characterization of one of the Cdk14 knockout cell lines, indicated that deletion of Cdk14 led to defects in chromosome congression, chromosome segregation, and to the generation of multinucleated cells (Figure 4C-E). Although preliminary, these results indicate that Cdk14 is indeed important for SAC function.

Conclusions and future perspectives

We have determined that Cdk14 localizes to the mitotic spindle during metaphase and is important for SAC function (Figure 1A). Cdk14 protein levels peaked during mitosis

and decreased after mitotic exit (Figure 1B) Truncation analysis of Cdk14 showed that the N terminus fragment containing the kinase domain (NTKD) contained the minimal sequences required for spindle localization. (Figure 2B), while the rest of the truncations localized to the spindle poles (Figure 2B). The establishment of inducible LAP and BioID2-tagged Cdk14 stable cell lines and subsequent biochemical purifications followed by mass spectrometry analyses of the purifications yielded interesting putative protein-protein interactions. Of interest, we identified two mitotic kinases as potential Cdk14 interactors; PLK1 and Aurka (Figure 3A). Finally, depletion of Cdk14 led to mitotic chromosome congression and segregation errors indicating it may have a role in the SAC (Figure 4).

As the Cdk14 depletion and phenotypic analysis results are preliminary, future studies should focus on validating siRNAs and CRISPR sgRNAs that deplete Cdk14 and analyzing the resulting cell division defects via fixed-cell and live-cell time-lapse microscopy. Although we have identified and validated several novel Cdk14 interacting proteins, future studies should focus on determining whether these proteins are substrates of Cdk14 and/or if they are regulating Cdk14 localization and/or activity through phosphorylation. Additionally, it will be important to determine which domains of Cdk14 are important for binding to these novel interactors and what the importance of these interactions are to mitotic spindle assembly and the SAC.

Materials and Methods

Cell culture

HeLa cells were grown in F12:DMEM 50:50 (Hyclone) with 10% FBS, 2mM L-glutamine and antibiotics in 5% CO₂ at 37 °C. Cells were synchronized in G1/S by treatment with 2 mM thymidine (Sigma-Aldrich) for 18-hours. The following siRNAs were used for siRNA transfections: Thermo Fisher Silencer Select 4390843 (control non-targeting siRNA) and (M1, M2, M3, and M4 siRNAs targeting *Cdk14*) were used as described previously (Torres et al. 2010).

Generation of the LAP/BioID2-Cdk14 inducible stable cell line

The HeLa BioID2-Cdk14 and HeLa LAP(GFP-TEV-S-Peptide)-Cdk14, -Cdk14-NT, -Cdk14-NTKD, -Cdk14-Kd, -Cdk14-KDCT, and -Cdk14-CT inducible stable cell lines were generated as described previously (Torres et al. 2009; Bradley et al. 2016). Briefly, full-length *Cdk14* (coding for amino acid residues 1-469) and truncation derivatives NT (coding for amino acid residues 1-134), NTKD (coding for amino acid residues 1-419), KD (coding for amino acid residues 135-419), KDCT (coding for amino acid residues 135-469), CT (coding for amino acid residues 419-469), were cloned into pDONR221 and transferred to pGLAP1 through a Gateway reaction to generate the pGLAP1 vectors with these ORFs that were transfected into HeLa Flp-In T-Rex cells to generate their respective inducible stable cell lines.

Immunoblotting

For *Cdk14* cell cycle protein expression analysis, HeLa cells were synchronized in G1/S with 2 mM thymidine for 18-hours. Cells were then washed with PBS three times and twice with F12:DMEM media with 10% FBS and released into the cell cycle. Cells were

harvested at the indicated time points, lysed, and protein extracts were resolved on a 4-20% SDS-PAGE and transferred to a PVDF membrane. The membranes were immunoblotted with the indicated antibodies and imaged with a LiCOR system. The same approach was used to detect Cdk14 protein depletion upon siRNA transfections without the cell synchronization step. Cell extract preparation and immunoblot analyses with the indicated antibodies were as described previously (Gholkar et al. 2016).

Fixed-cell immunofluorescence microscopy

Fixed-cell immunofluorescence microscopy was performed as described previously (Gholkar et al. 2016). Briefly, non-transfected cells or cells that had been transfected with the indicated siRNAs for 48 hours were arrested in G1/S with 2 mM thymidine for 18 hours, washed, and released into fresh media for eight hours. Cells were then fixed with 4% paraformaldehyde, permeabilized with 0.2% Triton X-100/PBS, and co-stained with 0.5 μ g/ml Hoechst 33342 (Thermo Fisher) to visualize the DNA and the indicated antibodies. A Leica DMI6000 microscope (Leica DFC360 FX Camera, 63x/1.40-0.60 NA oil objective, Leica AF6000 software) was then used to capture the images, which were deconvolved with the Leica Application Suite 3D Deconvolution software and exported as TIFF files. For quantifying mitotic defects, the data from four independent experiments, with 100 cells counted for each, was used to quantify the average \pm standard deviation (SD).

LAP/BioID2 Purifications and LC-MS/MS Analyses

For LAP purifications, GFP as the negative control and Cdk14 were purified from LAP-tagged inducible stable cell lines as previously described (Torres et al., 2009). Briefly, LAP-GFP and LAP-Cdk14 stable cell lines were induced with 0.1µg/ml doxycycline and lysed. The cell lysates were subjected to tandem affinity purification by incubating with anti-GFP antibody beads; the bound eluates were incubated with S-protein Agarose. The final eluates were resolved on a 4-20% gradient SDS PAGE gel; the gel was excised and prepared for LC-MS/MS analysis. For BioID2 purifications, biotinylated proteins were purified from BioID2-tagged inducible stable cell lines using protocols described previously with modifications (Gupta et al., 2015; Kim et al., 2016). Briefly, BioID2-only and BioID2-Cdk14 stable cell lines were washed with PBS and DMEM/Ham's F-12 before being shifted into DMEM/Ham's F-12 supplemented with 10% Dynabeads treated FBS (FBS was incubated with Dynabeads at 4°C overnight and the Dynabeads were removed with magnetic stand the following day). The cells were induced with 0.1µg/ml doxycycline and 50 µM Biotin for 16 hours before being lysed in lysis buffer (50 mM Tris-HCl pH 7.5, 150 mM NaCl, 1 mM EDTA, 1 mM EGTA, 1% Triton-X-100, 0.1% SDS, protease inhibitor cocktail) for 1 hour at 4°C with gentle rotation. The cell lysates were centrifuged at 15,000 rpm for 15 minutes and transferred to TLA-100.3 tubes for a second high speed centrifuge at 45,000 rpm for 1 hour at 4°C. The supernatants were incubated with Dynabeads at 4°C overnight with gentle rotation. The beads were washed twice with 2% SDS, one time with WB1 (0.1% sodium deoxycholate, 1% Triton X-100, 500 mM NaCl, 1 mM EDTA, 50 mM HEPES), one time with WB2 (250 mM LiCl, 0.5% deoxycholate, 1 mM EDTA, 10 mM Tris-HCl pH 8.0), and a final wash with 50 mM Tris-HCl pH 7.5 before being resuspended in elution buffer (50 mM triethyl ammonium bicarbonate, 12 mM sodium lauroyl sarcosine,

0.5% sodium deoxycholate). The resuspended beads were proceeded to on-bead digestion and LC-MS/MS analysis. Mass spectrometry analysis was performed at the UCLA Pasarow Mass Spectrometry Laboratory on a Thermo LTQ-Orbitrap XL as described previously (Patananan et al., 2014).

Statistical analysis

All statistical data are presented as the average \pm SD from at least three independent experiments. The data was analyzed using an unpaired Student's t test. Data was judged to be statistically significant when $p < 0.05$. All statistical figures were generated with GraphPad Prism 5.

Generation of plasmids and *in vitro* binding assays

For *in vitro* binding assays, full-length human *CDK14* (encoding amino acid residues 1-469) was fused to the C-terminus of the HA-tag to generate the pCS2-HA-*CDK14* vector. Similarly, full-length *TPX2*, *KIF23*, *Cyclin Y*, *PLK1*, *Survivin*, *LCMT1A* were fused to the C-terminus of the FLAG-tag to generate the pCS2-FLAG-*TPX2*, pCS2-FLAG-*SGO2*, pCS2-FLAG-*KIF23*, pCS2-FLAG-*CCNY*, pCS2-FLAG-*PLK1*, pCS2-FLAG-*Survivin* (*BIRC5*) and pCS2-FLAG-*LCMT1A* vectors. *In vitro* binding assays were performed as described previously (Gholkar et al. 2016). Briefly, HA-Cdk14, FLAG-*TPX2*, FLAG-*SGO2*, FLAG-*KIF23*, FLAG-*Cyclin Y*, FLAG-*PLK1*, FLAG-*Survivin* and FLAG-*LCMT1A* (negative control) were *in vitro* transcribed and translated (IVT) using TNT® Quick Coupled Transcription/Translation System, (Promega) in 10 μ L reactions. Magnetic HA beads (MBL International) were washed three times and equilibrated with wash buffer (50

mM Tris pH 7.4, 200 mM KCl, 1 mM DTT, 0.5% NP-40, and Halt Protease and Phosphatase Inhibitor Cocktail). IVT reactions were added to the equilibrated HA beads and incubated for 1.5 hours at 30 °C with gentle shaking. Beads were washed three times with wash buffer and eluted by boiling for five minutes with 2X Laemmli SDS sample buffer. Samples were resolved on a 4-20% gradient Tris gel with Tris-Glycine SDS running buffer, transferred to an Immobilon PVDF membrane (EMD Millipore), and membranes were analyzed with a PharosFX Plus molecular imaging system (Bio-Rad).

Antibodies

Immunofluorescence and immunoblotting were carried out using antibodies against: Cdk14 (21612-1-AP), Cas9 (); GFP (Abcam: ab13970); Gapdh (GTX100118); α -Tubulin (Bio-Rad: MCA78G); Cyclin B (Santa Cruz: sc-245). Secondary antibodies conjugated to FITC, Cy3, and Cy5 were from Jackson Immuno Research and those conjugated to IRDye 680 and IRDye 800 were from LI-COR Biosciences.

Figures

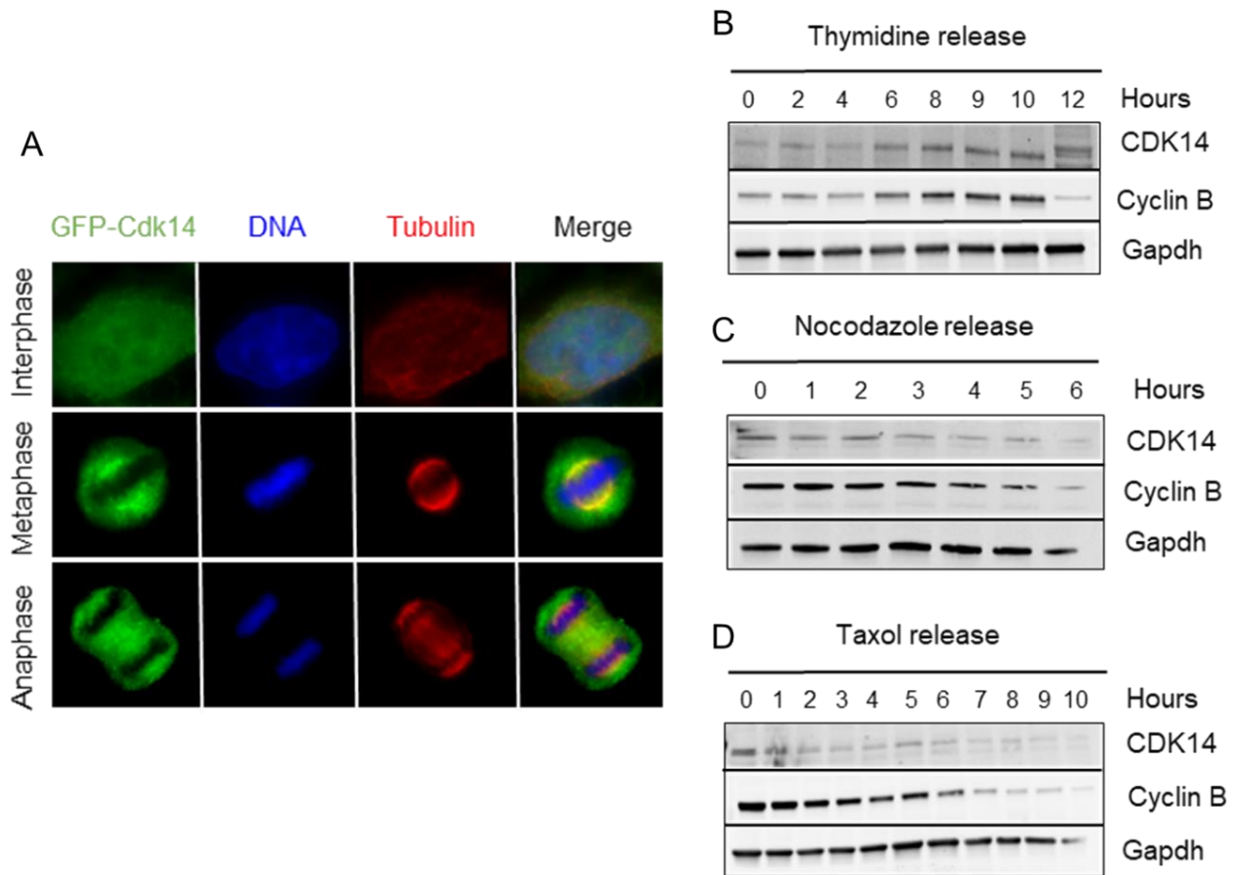


Figure 1. (A) Immunofluorescence microscopy of fixed cells overexpressing GFP-Cdk14 stained with Hoechst 33342 DNA dye, anti- α -tubulin, and anti-GFP. Images show the localization of Cdk14 in interphase and mitosis. (B-D) Immunoblot analysis of Cdk14 protein levels throughout the cell cycle. HeLa cells were synchronized in G1/S (Thymidine), G2/M (Nocodazole), metaphase (Taxol), released into the cell cycle and cells were harvested at the indicated time points. Cyclin B is used as a mitotic marker since it is highly expressed during mitosis and Gapdh is a loading control.

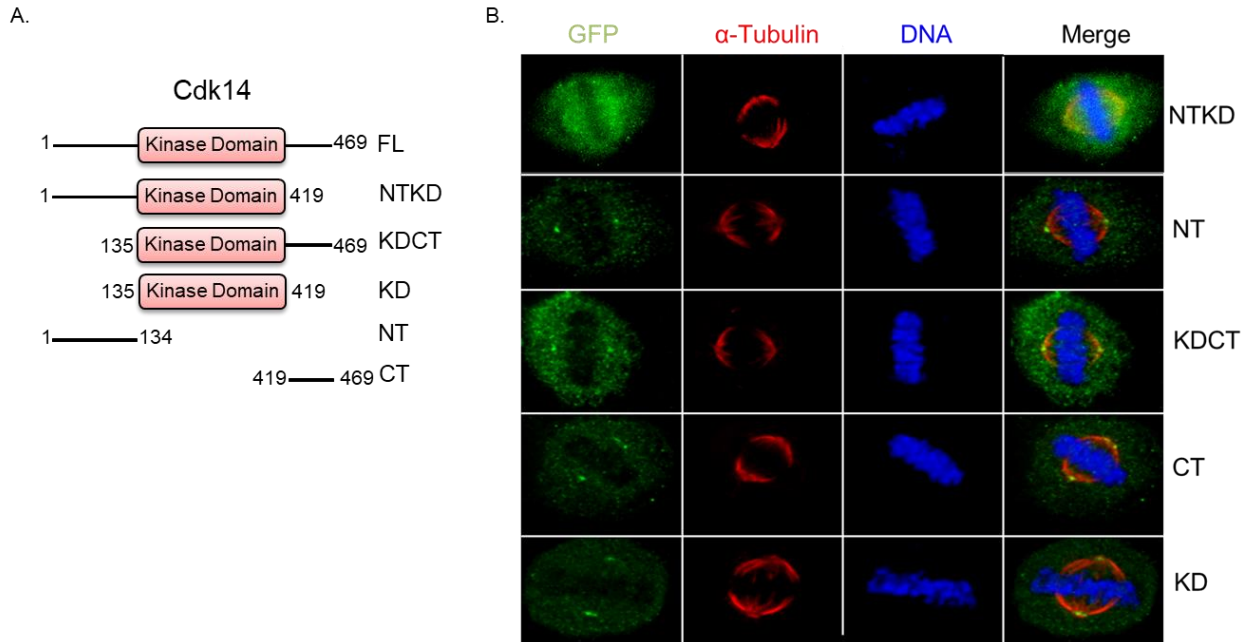


Figure 2. Cdk14 truncation analysis. (A) Schematic figure of the Cdk14 truncations that were generated. (B) Immunofluorescence microscopy of fixed cells overexpressing truncated versions of GFP-Cdk14 stained with Hoechst 33342 DNA dye, anti- α -tubulin, and anti-GFP. Images show the localization of the GFP-Cdk14 truncations during metaphase.

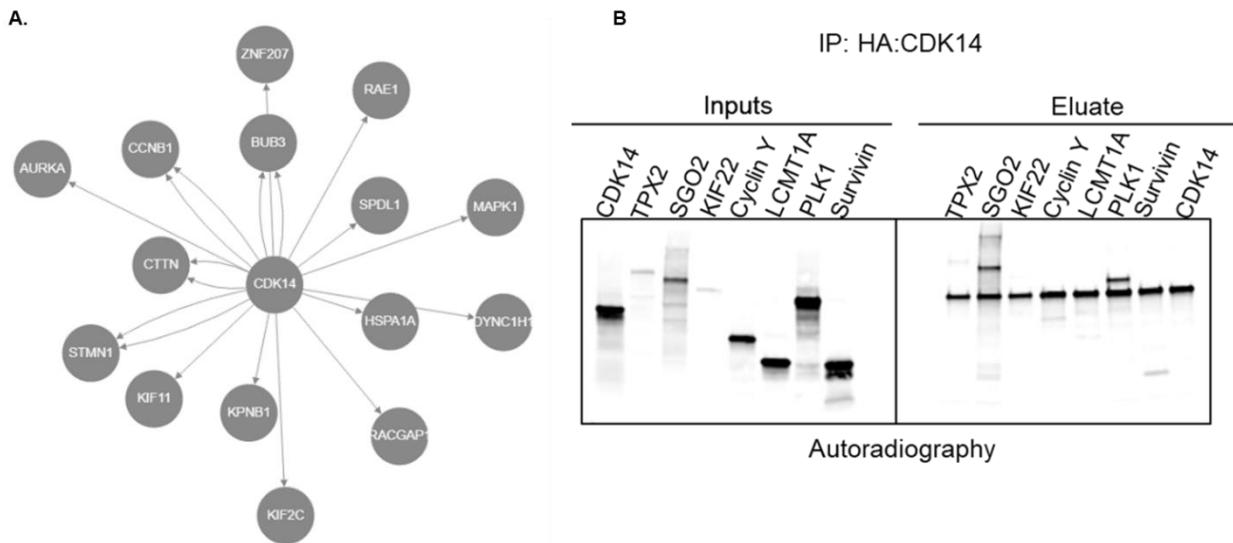


Figure 3. Cdk14 protein associations. (A) Cdk14 protein association network comprised of kinetochore and spindle pole proteins identified in a Cdk14-BioID2 purification by mass spectrometry. (B) Shows immunoprecipitation of [35S] methionine-labeled proteins using HA-tagged Cdk14. Cdk14 co-precipitates with SGO2, CyclinY, Plk1, and Survivin, but not with the negative control LCMT1A.

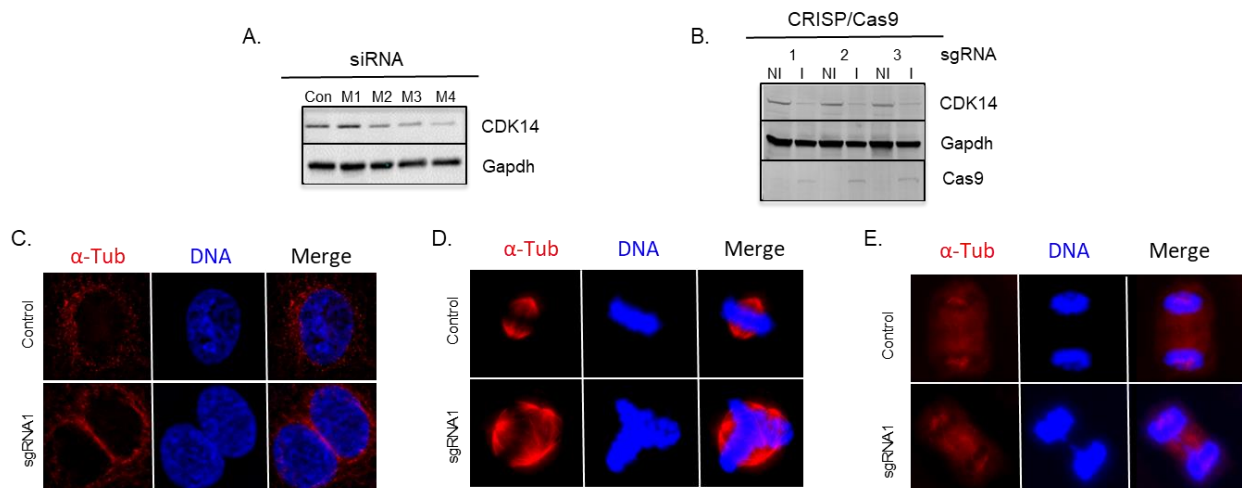


Figure 4. Cdk14 depletion analysis. (A) Immunoblot analysis showing knockdown of Cdk14 with different siRNA oligos targeting different regions of Cdk14 and Gapdh is used as a loading control. (B) Immunoblot analysis showing knockdown of Cdk14 using different guide RNAs targeting different regions of Cdk14 and Gapdh is a loading control and Cas9 shows proper induction of Cas9. (C-E) Immunofluorescence microscopy of fixed cells showing phenotypes of CRIPR/Cas9 depletion of Cdk14. HeLa cells were synchronized in G1/S, released into the cell cycle, and then stained with Hoechst 33342 DNA dye and anti- α -tubulin. (C-E) Shows phenotypes that arise upon depletion of Cdk14

using sgRNA1 that targets Cdk14. Cdk14 knockdown leads to multinucleated cells (C), multipolar spindles (D), and lagging chromosomes (E) when compared to the control.

Table S1 Reagents and resources

REAGENT or RESOURCE	SOURCE	IDENTIFIER
Antibodies		
Chicken polyclonal anti-GFP	Abcam	Cat# ab13970; RRID: AB_300798
Rabbit polyclonal anti-HA	Proteintech	Cat# 51064-2-AP; RRID: AB_11042321
Rat monoclonal anti- α -Tubulin (clone YOL1/34)	Bio-Rad	Cat# MCA78G; RRID: AB_325005
Rabbit polyclonal anti-GAPDH	Genetex	Cat# GTX100118; RRID: AB_1080976
Mouse monoclonal anti-Cyclin B1	Santa Cruz	Cat# sc-245; RRID: AB_627338
Rabbit polyclonal anti-Cdk14	Proteintech	Cat# 21612-1-AP
Anti-CRISPR-Cas9	Abcam	Cat# ab191468 RRID# AB_2692325
Rabbit polyclonal anti-Centrin	Gift from J. Salisbury	N/A
Donkey polyclonal anti-Human IgG (H+L), Fluorescein (FITC) AffiniPure	Jackson ImmunoResearch Labs	Cat# 709-095-149; RRID: AB_2340514
Donkey polyclonal anti-Rat IgG (H+L), Cy3 AffiniPure	Jackson ImmunoResearch Labs	Cat# 712-165-153; RRID: AB_2340667
Donkey polyclonal anti-Human IgG (H+L), Cy5 AffiniPure	Jackson ImmunoResearch Labs	Cat# 709-175-149; RRID: AB_2340539
Donkey polyclonal anti-Chicken IgY (IgG) (H+L), Fluorescein (FITC) AffiniPure	Jackson ImmunoResearch Labs	Cat# 703-095-155; RRID: AB_2340356
Donkey polyclonal anti-Rabbit IgG (H+L), Cy3 AffiniPure	Jackson ImmunoResearch Labs	Cat# 711-165-152; RRID: AB_2307443
Donkey polyclonal anti-Rabbit IgG (H+L), Fluorescein (FITC) AffiniPure	Jackson ImmunoResearch Labs	Cat# 711-095-152; RRID: AB_2315776
Donkey polyclonal anti-Mouse IgG (H+L), Fluorescein (FITC) AffiniPure	Jackson ImmunoResearch Labs	Cat# 715-095-151; RRID: AB_2335588
Donkey polyclonal anti-Mouse IgG (H+L), Cy3 AffiniPure	Jackson ImmunoResearch Labs	Cat# 715-165-151; RRID: AB_2315777
Donkey polyclonal anti-Goat IgG (H+L), IRDye 680RD	LI-COR Biosciences	Cat# 926-68074; RRID: AB_10956736

Donkey polyclonal anti-Mouse IgG (H+L), IRDye 680RD	LI-COR Biosciences	Cat# 926-68072; RRID: AB_10953628
Donkey polyclonal anti-Mouse IgG (H+L), IRDye 800CW	LI-COR Biosciences	Cat# 926-32212; RRID: AB_621847
Donkey polyclonal anti-Chicken IgG (H+L), IRDye 800CW	LI-COR Biosciences	Cat# 926-32218; RRID: AB_1850023
Donkey polyclonal anti-Rabbit IgG (H+L), IRDye 680RD	LI-COR Biosciences	Cat# 926-68073; RRID: AB_10954442
Donkey polyclonal anti-Rabbit IgG (H+L), IRDye 800CW	LI-COR Biosciences	Cat# 926-32213; RRID: AB_621848
Chemicals, Peptides, and Recombinant Proteins		
Paclitaxel	Sigma-Aldrich	Cat# T7191; CAS:33069-62-4
Nocodazole	Sigma-Aldrich	Cat# 1404; CAS:31430-18-9
Thymidine	Sigma-Aldrich	Cat# T1895; CAS:50-89-5
Doxycycline	Sigma-Aldrich	Cat# D9891; CAS:24390-14-5
Halt Protease Inhibitor Cocktail	Thermo Fisher Scientific	Cat# 87786
Hoechst 33342	Thermo Fisher Scientific	Cat# H1399; CAS:23491-52-3
ProLong Gold Antifade Mountant	Thermo Fisher Scientific	Cat# P36934
Lipofectamine RNAiMAX	Thermo Fisher Scientific	Cat# 13778150
FuGENE HD	Promega	Cat# E2311
FuGene 6	Promega	Cat# E2691
Critical Commercial Assays		
SP6 TnT Quick Coupled Transcription/Translation System	Promega	Cat# L2080
PureYield Plasmid Miniprep System	Promega	Cat# A1222
QIAprep Spin Miniprep Kit	QIAGEN	Cat# 27106
Experimental Models: Cell Lines		
Human: HeLa cells	ATCC	Cat# CCL-2; RRID: CVCL_0030
Human: HCT116-GFP-H2B Cells	Gift from P. Jackson	N/A
Human: HeLa Flp-In T-Rex Cells	Gift from S. Taylor	N/A
Oligonucleotides		

Silencer™ Select siRNA targeting <i>Cdk14</i>	Thermo Fisher Scientific	Cat# 4392420; siRNA ID: 004837-06-0002
Silencer™ Select siRNA targeting <i>Cdk14</i>	Thermo Fisher Scientific	Cat# 4392420; siRNA ID: J-004837-07-0002
Silencer™ Select Negative Control siRNA	Thermo Fisher Scientific	Cat# 4390843
Recombinant DNA		
<i>Cdk14</i> cDNA	GenScript	Clone ID: OHu01143C
pDONR221- <i>Cdk14</i>	This paper	N/A
pGLAP1- <i>Cdk14</i>	This paper	N/A
pCS2-HA- <i>Cdk14</i>	This paper	N/A
pCS2-FLAG-TPX2	This paper	N/A
pCS2-FLAG-SGO2	This paper	N/A
pCS2-FLAG-KIF23	This paper	N/A
pCS2-FLAG-CCNY	This paper	N/A
pCS2-FLAG-PLK1	This paper	N/A
pCS2-FLAG-BIRC5	This paper	N/A
pCS2-FLAG-LCMT1A	This paper	N/A
pDONR221-GFP	This paper	N/A
pCS2-FLAG-GFP	This paper	N/A
pDONR221	Thermo Fisher	Cat# 12536017
pGLAP1- <i>Cdk14</i> -NT	This paper	N/A
pGLAP1- <i>Cdk14</i> -NTKD	This paper	N/A
pGLAP1- <i>Cdk14</i> -KD	This paper	N/A
pGLAP1- <i>Cdk14</i> -KDCT	This paper	N/A
pGLAP1- <i>Cdk14</i> -CT	This paper	N/A
Software and Algorithms		
GraphPad Prism 8	GraphPad	RRID: SCR_002798
ImageJ	NIH ImageJ	https://imagej.nih.gov/ij/index.html RRID:SCR_003070

References

1. Ricke, Robin M., Janine H. van Ree, and Jan M. van Deursen. "Whole Chromosome Instability and Cancer: A Complex Relationship." *Trends in Genetics: TIG* 24, no. 9 (September 2008): 457–66. <https://doi.org/10.1016/j.tig.2008.07.002>.
2. Weaver, Beth A. A., and Don W. Cleveland. "Does Aneuploidy Cause Cancer?" *Current Opinion in Cell Biology* 18, no. 6 (December 2006): 658–67. <https://doi.org/10.1016/j.ceb.2006.10.002>.
3. "MAD2 Haplo-Insufficiency Causes Premature Anaphase and Chromosome Instability in Mammalian Cells - PubMed." Accessed April 26, 2021. <https://pubmed.ncbi.nlm.nih.gov/11201745/>.
4. Iwanaga, Yoichi, Ya-Hui Chi, Akiko Miyazato, Sergey Sheleg, Kerstin Haller, Jean-Marie Peloponese, Yan Li, Jerrold M. Ward, Robert Benezra, and Kuan-Teh Jeang. "Heterozygous Deletion of Mitotic Arrest-Deficient Protein 1 (MAD1) Increases the Incidence of Tumors in Mice." *Cancer Research* 67, no. 1 (January 1, 2007): 160–66. <https://doi.org/10.1158/0008-5472.CAN-06-3326>.
5. Sudakin, V., G. K. Chan, and T. J. Yen. "Checkpoint Inhibition of the APC/C in HeLa Cells Is Mediated by a Complex of BUBR1, BUB3, CDC20, and MAD2." *The Journal of Cell Biology* 154, no. 5 (September 3, 2001): 925–36. <https://doi.org/10.1083/jcb.200102093>.
6. Foley, Emily A., and Tarun M. Kapoor. "Microtubule Attachment and Spindle Assembly Checkpoint Signalling at the Kinetochores." *Nature Reviews. Molecular Cell Biology* 14, no. 1 (January 2013): 25–37. <https://doi.org/10.1038/nrm3494>.
7. Peters, Jan-Michael. "The Anaphase Promoting Complex/Cyclosome: A Machine Designed to Destroy." *Nature Reviews Molecular Cell Biology* 7, no. 9 (September 2006): 644–56. <https://doi.org/10.1038/nrm1988>.
8. Malumbres, Marcos, Edward Harlow, Tim Hunt, Tony Hunter, Jill M. Lahti, Gerard Manning, David O. Morgan, Li-Huei Tsai, and Debra J. Wolgemuth. "Cyclin-Dependent Kinases: A Family Portrait." *Nature Cell Biology* 11, no. 11 (November 2009): 1275–76. <https://doi.org/10.1038/ncb1109-1275>.

9. Morgan, D. O. "Cyclin-Dependent Kinases: Engines, Clocks, and Microprocessors." *Annual Review of Cell and Developmental Biology* 13 (1997): 261–91.
<https://doi.org/10.1146/annurev.cellbio.13.1.261>.
10. Davidson, Gary, and Christof Niehrs. "Emerging Links between CDK Cell Cycle Regulators and Wnt Signaling." *Trends in Cell Biology* 20, no. 8 (August 2010): 453–60. <https://doi.org/10.1016/j.tcb.2010.05.002>.
11. Jiang, Mei, Yankun Gao, Tao Yang, Xueliang Zhu, and Jiangye Chen. "Cyclin Y, a Novel Membrane-Associated Cyclin, Interacts with PFTK1." *FEBS Letters* 583, no. 13 (July 7, 2009): 2171–78. <https://doi.org/10.1016/j.febslet.2009.06.010>.
12. Davidson, Gary, Jinlong Shen, Ya-Lin Huang, Yi Su, Emil Karaulanov, Kerstin Bartscherer, Christine Hassler, Peter Stannek, Michael Boutros, and Christof Niehrs. "Cell Cycle Control of Wnt Receptor Activation." *Developmental Cell* 17, no. 6 (December 2009): 788–99. <https://doi.org/10.1016/j.devcel.2009.11.006>.
13. Stolz, Ailine, Norman Ertych, and Holger Bastians. "A Phenotypic Screen Identifies Microtubule plus End Assembly Regulators That Can Function in Mitotic Spindle Orientation." *Cell Cycle (Georgetown, Tex.)* 14, no. 6 (2015): 827–37.
<https://doi.org/10.1080/15384101.2014.1000693>
14. Niehrs, Christof, and Sergio P. Acebron. "Mitotic and Mitogenic Wnt Signalling." *The EMBO Journal* 31, no. 12 (June 13, 2012): 2705–13.
<https://doi.org/10.1038/emboj.2012.124>.
15. Kikuchi, Koji, Yohei Niikura, Katsumi Kitagawa, and Akira Kikuchi. "Dishevelled, a Wnt Signalling Component, Is Involved in Mitotic Progression in Cooperation with Plk1." *The EMBO Journal* 29, no. 20 (October 20, 2010): 3470–83.
<https://doi.org/10.1038/emboj.2010.221>.
16. Hadjihannas, Michel V., Martina Brückner, and Jürgen Behrens. "Conductin/Axin2 and Wnt Signalling Regulates Centrosome Cohesion." *EMBO Reports* 11, no. 4 (April 2010): 317–24. <https://doi.org/10.1038/embor.2010.23>.
17. Wakefield, James G., David J. Stephens, and Jeremy M. Tavaré. "A Role for Glycogen Synthase Kinase-3 in Mitotic Spindle Dynamics and Chromosome Alignment." *Journal of Cell Science* 116, no. Pt 4 (February 15, 2003): 637–46.
<https://doi.org/10.1242/jcs.00273>.

18. Kaplan, Daniel D., Thomas E. Meigs, Patrick Kelly, and Patrick J. Casey.
“Identification of a Role for Beta-Catenin in the Establishment of a Bipolar Mitotic Spindle.” *The Journal of Biological Chemistry* 279, no. 12 (March 19, 2004): 10829–32. <https://doi.org/10.1074/jbc.C400035200>.

Chapter 4

Final Thoughts

The Myl5 research studies have demonstrated that a myosin light chain can interact with a myosin in a region outside of a myosin binding site. This leads to new questions about whether there are other unconventional myosin RLCs and whether other non-canonical mechanisms exist to regulate myosin activity. Future research studies should address these pressing questions and whether these processes regulate cell division. Similar to cyclins, which can bind to different Cdk's to either activate or target for degradation different substrates during different cell cycle phases, it will be interesting to determine if Myl5 interacts with and regulates different myosins during different phases of the cell cycle. This could be accomplished by using cell synchronization experiments coupled to proximity-based proteomics approaches to generation cell cycle phase-specific interaction networks.

The Cdk14 research studies have shed light on the function of a new cyclin dependent kinase whose roll in cell division is still not fully understood. Moving forward, it will be important to validate Cdk14s role in the sac, to determine if the identified interacting kinases are Cdk14 substrates or if Cdk14 is a substrate of these enzymes, and more importantly how this phospho-regulation interplay is important for proper cell division.

Appendix Chapter 1

DUSP7 Regulates the Activity of ERK2 to Promote Proper Chromosome Alignment
During Cell



DUSP7 regulates the activity of ERK2 to promote proper chromosome alignment during cell division

Received for publication, November 10, 2020, and in revised form, April 10, 2021. Published, Papers in Press, April 16, 2021.
<https://doi.org/10.1016/j.jbc.2021.100676>

Xiao Guo¹, Ivan Ramirez¹, Yenni A. Garcia¹, Erick F. Velasquez¹, Ankur A. Gholkar¹, Whitaker Cohn², Julian P. Whitelegge^{2,3,4}, Bobby Tofig⁵, Robert Damoiseaux^{5,6}, and Jorge Z. Torres^{1,3,4,*}

From the ¹Department of Chemistry and Biochemistry, ²Pasarow Mass Spectrometry Laboratory, The Jane and Terry Semel Institute for Neuroscience and Human Behavior, David Geffen School of Medicine, ³Molecular Biology Institute, ⁴Jonsson Comprehensive Cancer Center, ⁵California NanoSystems Institute, and ⁶Department of Molecular and Medical Pharmacology, University of California, Los Angeles, California, USA

Edited by Enrique De La Cruz

Human cell division is a highly regulated process that relies on the accurate capture and movement of chromosomes to the metaphase plate. Errors in the fidelity of chromosome congression and alignment can lead to improper chromosome segregation, which is correlated with aneuploidy and tumorigenesis. These processes are known to be regulated by extracellular signal-regulated kinase 2 (ERK2) in other species, but the role of ERK2 in mitosis in mammals remains unclear. Here, we have identified the dual-specificity phosphatase 7 (DUSP7), known to display selectivity for ERK2, as important in regulating chromosome alignment. During mitosis, DUSP7 bound to ERK2 and regulated the abundance of active phospho-ERK2 through its phosphatase activity. Overexpression of DUSP7, but not catalytically inactive mutants, led to a decrease in the levels of phospho-ERK2 and mitotic chromosome misalignment, while knockdown of DUSP7 also led to defective chromosome congression that resulted in a prolonged mitosis. Consistently, knockdown or chemical inhibition of ERK2 or chemical inhibition of the MEK kinase that phosphorylates ERK2 led to chromosome alignment defects. Our results support a model wherein MEK-mediated phosphorylation and DUSP7-mediated dephosphorylation regulate the levels of active phospho-ERK2 to promote proper cell division.

Critical to the fidelity of cell division is the accurate movement and alignment of chromosomes at the metaphase plate and their segregation during anaphase. Errors in these processes are linked to human developmental disorders and tumorigenesis (1). Previous research has underscored the importance of protein phosphorylation as a molecular switch to regulate the activity of cell division enzymes (2, 3). This is highlighted by the growing list of essential mitotic kinases and their substrates that carry out functions related to bipolar spindle assembly, kinetochore-microtubule attachment, chromosome congression, and chromosome segregation (4–6). Beyond well-established mitotic kinases, less studied phospho signaling pathways have been implicated in cell division including the

Wnt, mTOR, and MAPK/ERK pathways, among which MAPK/ERK is phosphorylated by MEKs (mitogen-activated protein kinase or extracellular signal-regulated kinase) to regulate downstream transcription factors (7–9). In *Xenopus laevis* ERK2 (extracellular signal-regulated kinase 2) is critical for the spindle assembly checkpoint (10–12). In mammalian cells ERK1/2 activity is necessary for the G1/S transition and early G2 events for timely entry into mitosis (13, 14). However, whether human ERK2 is active in mitosis and what roles it plays in human somatic cell division remains ambiguous.

Our RNAi screen for novel factors important for cell division identified the dual-specificity phosphatase 7 (DUSP7/MKP-X). DUSP7, DUSP6/MKP-3, and DUSP9/MKP-4 are members of the cytoplasmic ERK specific mitogen-activated protein kinase phosphatases (MKPs) subfamily that share similar amino acid sequences, subcellular localizations, and substrate preferences (15–17). DUSPs can dephosphorylate both tyrosine and serine/threonine residues and are important modulators of signaling pathways that regulate cellular processes such as proliferation and apoptosis (16, 17). DUSP7 exhibits selectivity toward ERK1/2 (18–20) and is a regulator of oocyte meiosis (21–23). DUSP7 contains an N terminal noncatalytic Rhodanese-like domain and a C-terminal dual-phosphatase domain. A conserved Kinase Interaction Motif (KIM) in the noncatalytic domain is essential for the interaction between MKPs and ERK (19, 24). Two key amino acid residues within the conserved catalytic sequence (H/V)C(X₅)R(S/T) of the phosphatase domain, C331 and R337, are important for DUSP7's phosphatase activity (25, 26). However, in contrast to MKPs such as DUSP6 and DUSP9, little is known about the physiological functions of DUSP7.

Here, we have determined that MEK phosphorylation activity and DUSP7 phosphatase activity regulate the levels of active phospho-ERK2, which is important for the fidelity of chromosome alignment and segregation during cell division.

Results

DUSP7 interacts with ERK2 and regulates the levels of phospho-ERK2

To understand the role of DUSP7 during cell division, we began by defining the protein–protein interaction and protein

* For correspondence: Jorge Z. Torres, torres@chem.ucla.edu.

ACCELERATED COMMUNICATION: DUSP7 regulates ERK2 to promote cell division

proximity networks of DUSP7 in mitotic cells. Localization and affinity purification (LAP = GFP-Tev-S-tag)-tagged and biotin identification 2 (BioID2)-tagged DUSP7 inducible HeLa stable cell lines were used to express LAP/BioID2-DUSP7 and biochemical purifications were analyzed by mass spectrometry. In-house R scripts were used to analyze the mass spectrometry data and protein interaction and proximity networks were visualized with RCytoscape JS (Fig. S1, A and B). Further, we applied Gene Ontology (GO) terms (mitotic spindle; kinetochore and chromosome segregation) (Fig. S1C) and CORUM complex annotation analyses to these networks (see [Experimental procedures](#) for details). These analyses determined that ERK2 (aka MAPK1) was also associating with DUSP7 in mitosis (Fig. 1, A and B). Next, we validated the DUSP7-ERK2 mitotic interaction by immunoprecipitation (IP) experiments using mitotic cell extracts from Taxol- or nocodazole-arrested LAP-DUSP7 stable cell lines (Fig. 1C).

The KIM domain was shown to be essential for the interaction of some DUSPs (DUSP1, 4, 6) with ERK2 (24, 27, 28), but it remained unknown which domain of DUSP7 bound to ERK2 and whether its KIM was required for binding to ERK2 or its ability to dephosphorylate ERK2. To better understand the DUSP7-ERK2 interaction, we generated DUSP7 KIM mutants R102A, R103A, and R102,103A double mutants (Fig. 1D and Fig. S2, A–C). IP experiments from mitotic cells transiently transfected with DUSP7 or DUSP7 KIM mutants showed that ERK2 IPed with DUSP7 but not DUSP7 KIM mutants (Fig. 1E). To further define the interaction domains of DUSP7 involved in ERK2 binding, we generated a series of LAP-DUSP7 stable cell lines expressing DUSP7 truncations (Fig. S3A). ERK2 failed to associate with DUSP7 truncations (Fig. S3B), likely due to DUSP7 destabilization. Next, we sought to determine the significance of the DUSP7-ERK2 interaction. Consistent with the abolished interaction between DUSP7 KIM mutants and ERK2 (Fig. 1E), DUSP7-R103A and DUSP7-R102,103A double mutants showed a slightly reduced ability to dephosphorylate ERK2 in mitotic HeLa cells (Fig. 1F and Fig. S3, C–E). However, DUSP7-R102A could still dephosphorylate ERK2 (Fig. 1F); this phenomenon was also observed for conserved KIM mutations in DUSP6 (29). Similarly, IP experiments using *in vitro* expressed proteins or mitotic cell extracts from DUSP7 or DUSP7 catalytic dead mutant (C331A and R337A) (Fig. S2, D–G) cell lines showed that ERK2 IPed with DUSP7 and DUSP7-R337A but not DUSP7-C331A (Fig. 1, G and H, Fig. S3, F–H). While overexpression of DUSP7 led to the absence of phospho-ERK2, overexpressed DUSP7-R337A or DUSP7-C331A showed a reduced ability to dephosphorylate ERK2 in mitotic HeLa cells (Fig. 1I). Together, these results showed that DUSP7 was binding to ERK2 during mitosis and that the DUSP7 KIM was required for this interaction, while the DUSP7 catalytic sites (C331 and R337) within its phosphatase domain were important for regulating the levels of active phospho-ERK2.

Knockdown of DUSP7 leads to chromosome alignment and segregation defects

To understand the importance of DUSP7's function in regulating the levels of active phospho-ERK2 during cell

division, we first identified siRNAs capable of depleting DUSP7 levels by immunoblot analysis (Fig. 2A and Fig. S4A) and DUSP7 mRNA expression by RT-qPCR (Fig. S4, B and C). Knockdown of DUSP7 led to a failure to dephosphorylate ERK2 and an increase in phospho-ERK2 levels (Fig. 2A). We then analyzed the consequences of depleting DUSP7 during metaphase (Fig. 2B) and postmetaphase (Fig. 2E) with immunofluorescence (IF) microscopy. DUSP7 depletion led to an increased percentage of defective mitotic cells with chromosome misalignment (siDUSP7 = 44.6 ± 5.6 , $p < 0.05$ compared with siControl = 29.1 ± 2.9) (Fig. 2, C and D). These defective cells also showed defects in spindle organization including unfocused and multipolar spindles (Fig. 2C). The chromosome misalignments defects in siDUSP7 cells translated into an increase in the percentage of lagging chromosomes during anaphase (siDUSP7 = 24.9 ± 3.7 , $p < 0.05$ compared with siControl = 13.45 ± 3.1) (Fig. 2, F and G). The mitotic defects were rescued by an siRNA resistant DUSP7 (Fig. S2H) expressed at near endogenous levels but not DUSP7 catalytic dead mutants (Fig. S4, D–F). Similar results were observed and statistically analyzed in U2OS cells (Fig. S4, G–I) and HCT116 cells (Fig. S4, J–L).

Next, we analyzed whether DUSP7 depletion could affect the timing of cell division by live-cell time-lapse microscopy in HCT116 GFP-H2B cells (Fig. 2H). This analysis showed that depletion of DUSP7 led to a marked increase in the time from chromosome condensation to chromosome segregation (siDUSP7 = 54.0 ± 38.3 min, $p < 0.01$ compared with siControl = 38.0 ± 19.1 min) (Fig. 2, I–K; [Movies S1–S4](#)). Together, these results showed that depletion of DUSP7 led to a slowed mitosis where cells failed to properly align and segregate chromosomes.

Downregulation of ERK2 leads to chromosome alignment defects

Next, we sought to determine if ERK2 was important for human cell division. First, we depleted endogenous ERK2 by RNAi (Fig. 3A) and analyzed the consequences during cell division (Fig. 3B) with IF microscopy. Depletion of ERK2 led to an increased number of cells with defects in chromosome alignment during metaphase (siERK2 = 52.1 ± 2.8 , $p < 0.01$ compared with siControl = 30.6 ± 3.5) (Fig. 3, C and D), which was consistent in U2OS cells (Fig. S5, A and B) and HCT116 cells (Fig. S5, C and D). ERK2 depletion also led to an increase in interphase cells that were multinucleated or contained micronuclei (siERK2 = 22.6 ± 6.2 , $p < 0.01$ compared with siControl = 3.8 ± 0.8) (Fig. S5, E and F).

Since phospho-ERK2 levels were lower in mitosis than in G1/S phase (Fig. S5, G–I), we asked if ERK2 phosphorylation or ERK2 kinase activity was important for cell division. HeLa cells were treated with a MEK inhibitor U0126 (30, 31) or the ERK2 ATP-competitive inhibitor FR180204 (32) and analyzed by western blotting and IF microscopy (Fig. 3E). Phospho-ERK2 levels decreased in U0126-treated cells, but were not affected in FR180204-treated cells (Fig. 3F). In comparison to the control DMSO treatment, cells treated with U0126 or FR180204 showed an increase in chromosome alignment

ACCELERATED COMMUNICATION: *DUSP7* regulates ERK2 to promote cell division

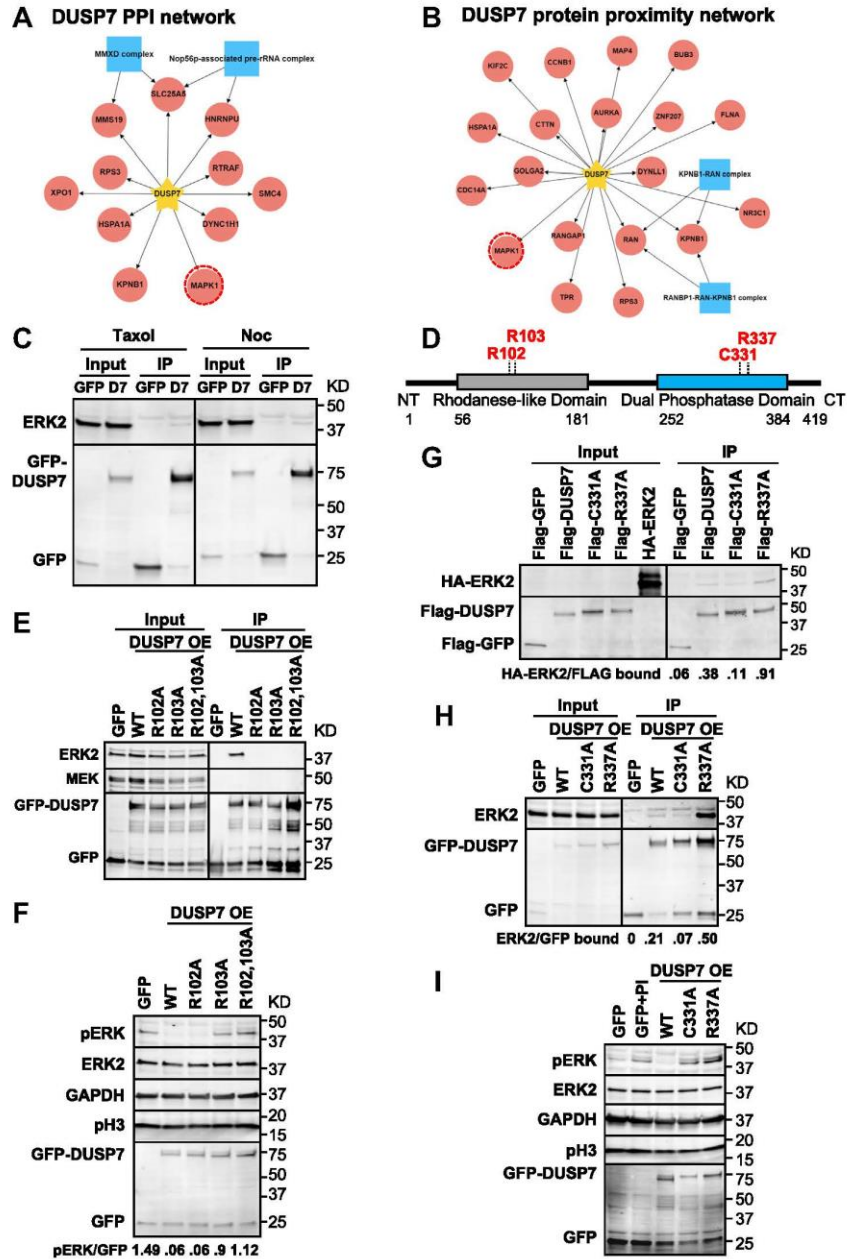


Figure 1. *DUSP7* interacts with ERK2 and regulates the levels of phospho-ERK2. *A* and *B*, *DUSP7* protein–protein interaction (PPI) (*A*) and protein proximity (*B*) networks generated using mitotic spindle GO annotations and CORUM complex annotation analyses. *Yellow stars* indicate the bait protein *DUSP7*; *red circles* indicate putative interactors; *blue squares* indicate protein complexes; *red dashed circles* highlight ERK2 (aka MAPK1). *C*, ERK2 immunoprecipitates (IPs) with *DUSP7* (D7) in early (nocodazole (Noc) arrested cells) and mid (taxol (Tax) arrested cells) mitosis. *D*, schematic of *DUSP7* domain structure and key sites. The number of amino acids are indicated for each domain. *DUSP7* KIM (R102, R103) and catalytic sites (C331, R337) are in *red*. *E*, the *DUSP7* KIM mediates the *DUSP7*–ERK2 mitotic interaction. *F*, the *DUSP7* KIM is dispensable for its phosphatase activity. Ratios below immunoblots indicate normalized phospho-ERK2 levels. *G* and *H*, the *DUSP7*–ERK2 mitotic interaction is influenced by *DUSP7*'s catalytic activity. In (*G*) HA-ERK2, Flag-*DUSP7*, Flag-C331A, Flag-R337A and Flag-GFP (negative control) were IVT expressed and incubated with anti-FLAG M2 magnetic beads in IP assays. In (*H*) LAP-only, LAP-*DUSP7*-WT, LAP-C331A, and LAP-R337A stable cell lines were induced before being harvested for S-tag pull downs. Ratios below immunoblots indicate relative protein–protein binding affinity. *I*, *DUSP7* regulates mitotic phospho-ERK2 levels through its phosphatase activity. Phosphatase inhibitor (PI) in the second lane was added when lysing the cells. Numbers on the right side of immunoblots indicate molecular weights of proteins. All cell-based experiments and immunoprecipitations were carried out in HeLa cells.

ACCELERATED COMMUNICATION: DUSP7 regulates ERK2 to promote cell division

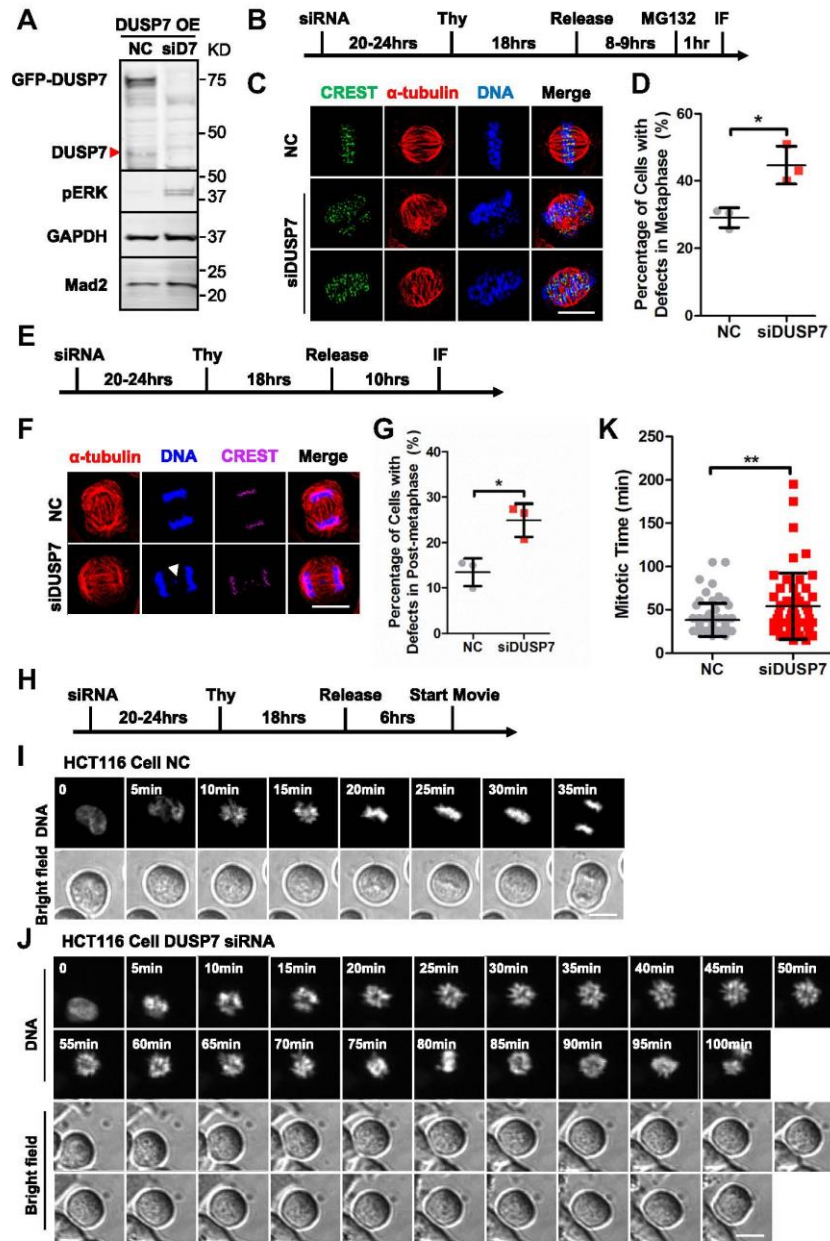


Figure 2. Knockdown of DUSP7 leads to chromosome alignment and segregation defects. *A*, siRNA knockdown of endogenous and overexpressed DUSP7. Numbers on the right side of immunoblots indicate molecular weights of proteins. *Red arrow* indicates endogenous DUSP7 band. *B*, schematic of IF microscopy experiment performed in (*C*). *C*, knockdown of DUSP7 leads to chromosome misalignment in metaphase. HeLa cells were treated with negative control siRNA or siDUSP7 before being fixed and costained with anti-CREST and anti- α -tubulin antibodies and the DNA dye Hoechst 33342. *D*, quantification of the percentage of cells with chromosome misalignment in metaphase (y-axis) for conditions shown in (*C*) (x-axis). *E*, schematic of IF microscopy experiment performed in (*F*). *F*, knockdown of DUSP7 leads to an increase in lagging chromosomes in anaphase. HeLa cells were treated with negative control siRNA or siDUSP7 before being fixed and costained with anti-CREST and anti- α -tubulin antibodies and the DNA dye Hoechst 33342. *White arrow* shows the lagging chromosome. *G*, quantification of the percentage of cells with lagging chromosomes in anaphase (y-axis) for conditions shown in (*F*) (x-axis). *H*, schematic of live-cell time-lapse microscopy experiment performed in (*I*) and (*J*). *I* and *J*, knockdown of DUSP7 leads to a slowed mitosis. Live-cell time-lapse microscopy of HCT116 GFP-H2B cells treated with negative control siRNA (*I*) and siDUSP7 (*J*) undergoing cell division. *K*, quantification of the timing of mitosis from chromosome condensation to chromosome segregation (y-axis) for the conditions shown in (*I*) and (*J*) (x-axis). Scale bars: 10 μ m. * p < 0.05, ** p < 0.01 (unpaired two-tailed Student's *t*-test).

errors (U0126 = 48.7 ± 12.7 , p < 0.05 and FR180204 = 45.6 ± 6.5 , p < 0.05 compared with DMSO = 25.8 ± 3.9) (Fig. 3, *G* and *H*), which was consistent in U2OS cells (Fig. S5, *K* and *L*) and

HCT116 cells (Fig. S5, *M* and *N*). These results showed that inhibiting ERK2 phosphorylation, and thereby its activation, or ERK2's kinase activity led to chromosome alignment defects.

ACCELERATED COMMUNICATION: DUSP7 regulates ERK2 to promote cell division

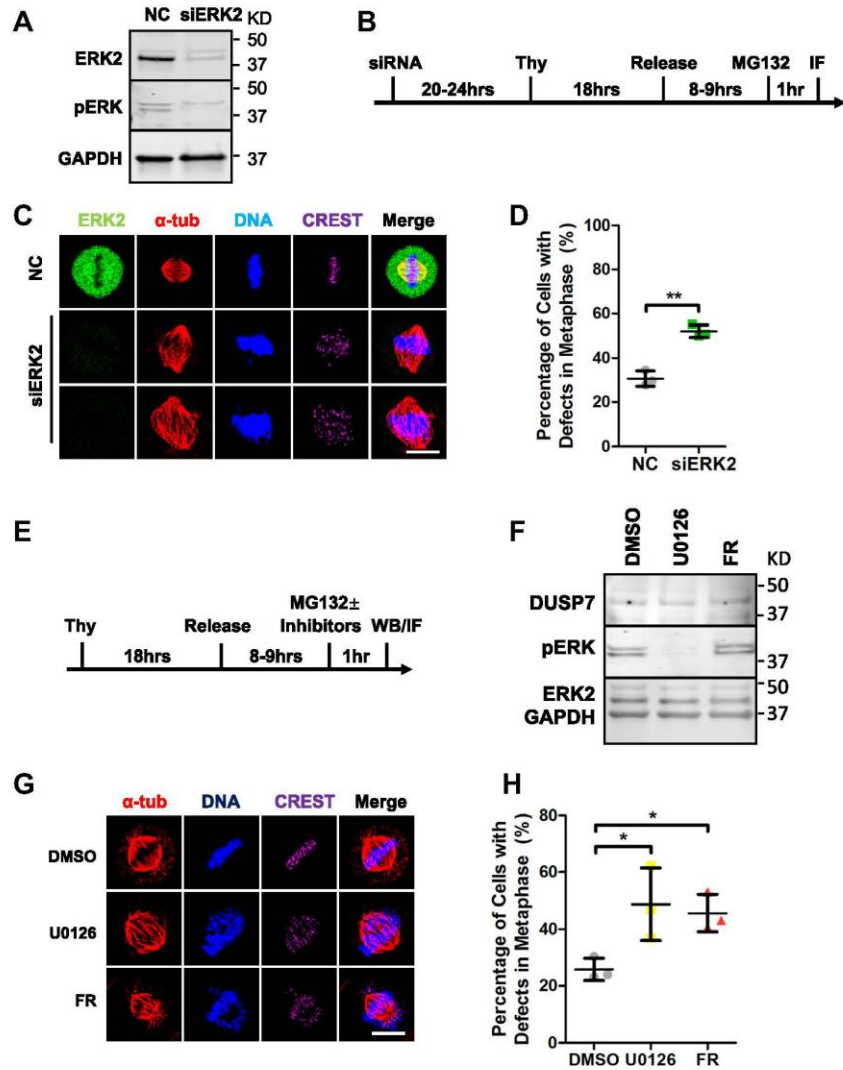


Figure 3. Downregulation of ERK2 leads to chromosome alignment defects. *A*, siRNA knockdown of ERK2. *B*, schematic of IF microscopy experiment performed in *C*. *C*, knockdown of ERK2 leads to chromosome misalignment in metaphase. HeLa cells were treated with negative control siRNA or siERK2 before being fixed and costained with anti-ERK2, anti-CREST and anti- α -tubulin antibodies and the DNA dye Hoechst 33342. *D*, quantification of the percentage of cells with chromosome misalignment in metaphase (y-axis) for conditions shown in *C* (x-axis). *E*, schematic of western blotting experiment performed in *F* and IF microscopy experiment performed in *G*. *F*, HeLa cells were treated with DMSO (as negative control), 50 μ M U0126, or 50 μ M FR180204 before being lysed and analyzed by immunoblot. *G*, inhibition of MEK kinase activity or ERK2 kinase activity leads to chromosome misalignment in metaphase. HeLa cells were treated with DMSO or the indicated inhibitors, fixed, and costained with anti-CREST and anti- α -tubulin antibodies and the DNA dye Hoechst 33342. *H*, quantification of the percentage of cells with chromosome misalignment in metaphase (y-axis) for the conditions shown in *G* (x-axis). Numbers on the right side of immunoblots indicate molecular weights of proteins. Scale bars: 10 μ m. * p < 0.05, ** p < 0.01 (unpaired two-tailed Student's *t*-test).

DUSP7 promotes chromosome alignment in mitosis by regulating the activity of ERK2

Since DUSP7 dephosphorylated ERK2 (Fig. 1E), we hypothesized that overexpression of DUSP7 would lead to similar chromosome alignment defects to those observed in cells treated with the MEK inhibitor U0126. To test this, we overexpressed GFP-tagged DUSP7 (validated to decrease phospho-ERK2 levels, Fig. 1, F and I) or the catalytic dead DUSP7-C331A or DUSP7-R337A mutants (showed minimal effects on phospho-ERK2 levels, Fig. 1I) and analyzed the cells by IF

microscopy (Fig. 4A). While DUSP7 overexpression led to a significant increase in chromosome alignment defects, overexpression of DUSP7-R337A or DUSP7-C331A did not (DUSP7 = 42.1 \pm 6.9, p < 0.05; DUSP7-C331A = 30.6 \pm 3.5, p = 0.3183; and DUSP7-R337A = 34.4 \pm 5.7, p = 0.1386; compared to the GFP control = 27.3 \pm 3.5) (Fig. 4, B and C), which was consistent in U2OS cells (Fig. S6A) and HCT116 cells (Fig. S6B). These results showed that an overabundance of DUSP7 phosphatase activity led to chromosome alignment defects.

ACCELERATED COMMUNICATION: DUSP7 regulates ERK2 to promote cell division

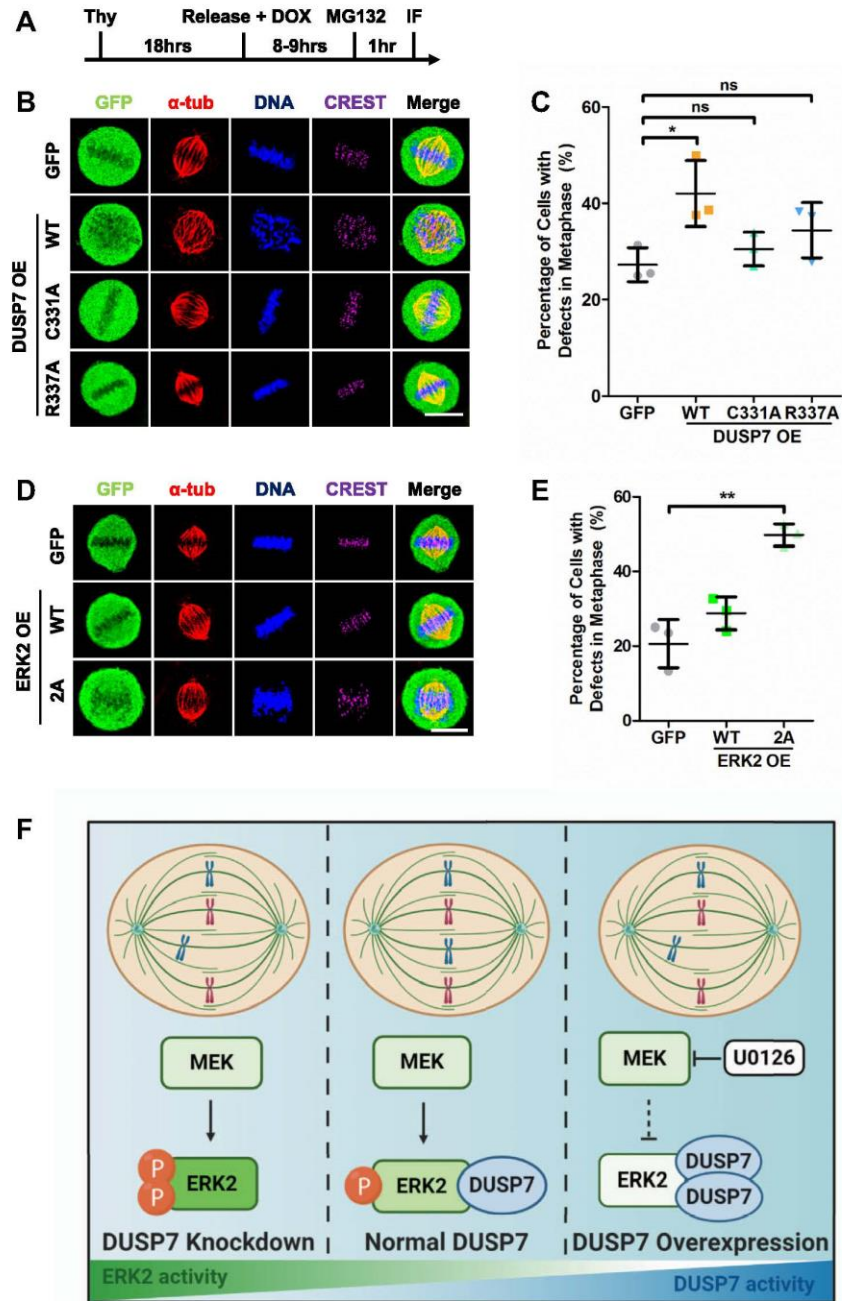


Figure 4. DUSP7 promotes chromosome alignment in mitosis by regulating the activity of ERK2. *A*, schematic of IF microscopy experiment performed in *(B)* and *(D)*. *B*, overexpression of DUSP7 wild type, but not catalytic dead mutants, leads to chromosome misalignment in metaphase. LAP-only, LAP-DUSP7-WT, LAP-C331A, and LAP-R337A HeLa stable cell lines were treated as described in *(A)* before being fixed and costained with anti-GFP, anti-CREST, and anti- α -tubulin antibodies and the DNA dye Hoechst 33342. *C*, quantification of the percentage of cells with chromosome misalignment in metaphase (y-axis) for conditions shown in *(B)* (x-axis). *D*, LAP-only, LAP-ERK2-WT, and LAP-ERK2-2A HeLa stable cell lines were treated as described in *(A)* before being fixed and costained with anti-GFP, anti-CREST, and anti- α -tubulin antibodies and the DNA dye Hoechst 33342. *E*, quantification of the percentage of cells with chromosome misalignment in metaphase (y-axis) for conditions shown in *(D)* (x-axis). *F*, model of how DUSP7 regulates the abundance of active phospho-ERK2 to ensure the fidelity of chromosome alignment. See main text for details. Scale bars: 10 μ m. * p < 0.05, ** p < 0.01, ns indicates not statistically significant (unpaired two-tailed Student's *t*-test).

To further understand the phospho-ERK2 equilibrium regulated by MEK and DUSP7 during cell division, we asked if the ERK2-DUSP7 interaction was dependent on ERK2 phosphorylation. IP experiments using cell extracts from a U0126-treated LAP-DUSP7 stable cell line showed that ERK2 bound to DUSP7 in the absence of MEK kinase activity (Fig. S6C). Since ERK2 is phosphorylated by MEK at T185 and Y187 (33, 34), we generated the nonphosphorylation mimetic mutant ERK2-2A (T185,Y187A) (Fig. S2, I and J) and analyzed its binding to DUSP7. *In vitro* binding experiments showed that both ERK2 and ERK2-2A bound to DUSP7 (Fig. S6D). Similar results were observed in IP experiments from HeLa cell extracts (Fig. S6E). Together, these results showed that DUSP7's binding to ERK2 did not require ERK2 to be phosphorylated. Instead, D318 within the ERK2 common docking (CD) domain (24) was responsible for its binding to DUSP7 (Fig. S6F). Next, we examined if phosphorylation of ERK2 at T185 and Y187 was critical for cell division by analyzing cells overexpressing GFP-tagged ERK2 or the nonphosphorylation mimetic mutant ERK2-2A (Fig. 4A). Compared with the overexpression of ERK2, overexpression of ERK2-2A led to a significant increase in cells with chromosome alignment defects in metaphase (ERK2 = 28.7 ± 4.4 , $p = 0.1438$; ERK2-2A = 49.7 ± 3.0 , $p < 0.01$; compared with GFP control = 20.6 ± 6.4) (Fig. 4, D and E), which was consistent in U2OS cells (Fig. S6A) and HCT116 cells (Fig. S6B). These data indicated that the proper amount of phospho-ERK2 in cells was critical for chromosome alignment and segregation during mitosis.

Discussion

This study revealed a novel function for DUSP7 in mitotic chromosome alignment and established the MAPK/ERK pathway as being important for cell division. Our data are consistent with a model where, during a normal mitosis, MEK's kinase activity phosphorylates ERK2 and DUSP7's phosphatase activity dephosphorylates ERK2 to establish an equilibrium of active phospho-ERK2 (Fig. 4F middle panel). This phospho-ERK2 equilibrium is critical for ensuring the fidelity of chromosome alignment and segregation. Perturbing the balance of active phospho-ERK2 through MEK inhibition (Fig. 4F right panel), DUSP7 depletion (Fig. 4F left panel) or overexpression (Fig. 4F right panel) leads to defects in chromosome alignment. Together, these results establish DUSP7 as an important mitotic phosphatase that regulates the abundance of active phospho-ERK2 to ensure the fidelity of chromosome alignment and segregation.

Interestingly, although the DUSP7 KIM mutant R102A did not bind ERK2, it could still dephosphorylate it (Fig. 1F, Fig. S3, C–E). This is consistent with previous DUSP6 observations, where the DUSP6 KIM mutant R64A did not bind ERK2 but was able to dephosphorylate it (29). Therefore, it is possible that these mutants are capable of transiently interacting with ERK2, but that the interaction is undetectable in IP experiments.

With the exception of ERK2, there is little known about the repertoire of DUSP7 substrates, regulators, and interactors. The GO enrichment analyses of the DUSP7 protein association network and DUSP7 proximity protein network indicate that

DUSP7 is likely to associate with numerous proteins that carry out important functions related to a broad array of cellular processes including apoptosis, regulation of transcription, and cell division (Table S1). Therefore, future studies aimed at understanding the importance of these interactions will further aid our understanding of DUSP7's function in cell division and beyond.

Experimental procedures

Cell culture

Table S2 lists all reagents and tools used in this study. HeLa cells (ATCC) were grown in DMEM/Ham's F-12 with L-Glutamine (Genesee Scientific), U2OS (ATCC) and HCT116 cells were grown in McCoy's 5A (Gibco), with 10% FBS and 5% CO₂ at 37 °C. Detailed experimental procedures for cell synchronization, cell transfection, and inhibitor treatments are in the Supporting information.

Generation of vectors and cell lines

DUSP7 and ERK2 mutants were generated by QuikChange Lightning Site-Directed Mutagenesis (Agilent). cDNAs of GFP, DUSP7, DUSP7 KIM mutants, DUSP7 catalytic dead mutants, ERK2, ERK2-2A, and DUSP7 truncations were cloned into pGLAP1, pGBioID2, pCS2-HA, or pCS2-Flag *via* Gateway LR Clonase reaction (35). pGLAP1-only/DUSP7/DUSP7-C331A/DUSP7-R337A/ERK2/ERK2-2A/DUSP7-truncations and pGBioID2-only/DUSP7 were used to generate Dox inducible HeLa Flp-In T-REx LAP-GFP/DUSP7-C331A/DUSP7-R337A/ERK2/ERK2-2A/DUSP7-truncations and HeLa Flp-In T-REx BioID2-only/DUSP7 stable cell lines as described previously (36, 37) (see Supporting information).

LAP/BioID2 purifications and LC-MS/MS analyses

LAP purifications from Taxol arrested LAP-tagged inducible stable cell lines were as previously described (36). For BioID2 purifications, biotinylated proteins were purified from Taxol-arrested BioID2-tagged inducible stable cell lines as described previously (38, 39). Mass spectrometry analysis was performed on a Thermo Q Exactive Plus Orbitrap as described previously (40). Protein-protein interaction information was integrated from the Biological General Repository for Interaction Datasets (BioGRID v. 3.5) (41). Protein-complex information was derived from the Comprehensive Resource of Mammalian Protein Complexes (CORUM v. 3.0) (42). Selected GO terms (Gene Ontology release June 2019) (43) were used to analyze the protein-protein interactions based on cellular mechanisms. Affinity-based and proximity-based networks were generated with RCytoscapeJS (44, 45). See Supporting information and Table S3–S6 for details on purifications, mass spectrometry, quantification of data, and protein interaction and proximity networks.

Immunoprecipitations, *in vitro* binding assays, and immunoblot analyses

Immunoprecipitations, *in vitro* binding assays, and immunoblot analyses were performed as described previously (46) with minor modifications detailed in the Supporting information.

ACCELERATED COMMUNICATION: *DUSP7* regulates *ERK2* to promote cell division

Cell imaging

Fixed-cell and live-cell time-lapse microscopy was carried out as described previously (47), except that an ImageXpress XL imaging system (Molecular Devices) was used for live cell imaging. See [Supporting information](#) for details on imaging, quantification of data, and statistical analyses.

RT-qPCR

RNA from control or *DUSP7* siRNA transfected HeLa, U2OS, or HCT116 cells and *DUSP7* cell lines was isolated with Direct-zol RNA Miniprep Kits (Zymo Research) and reverse transcribed with UltraScript 2.0 cDNA Synthesis Kit (Genesee Scientific). qPCR was carried out with the synthesized cDNA, oligo(dT) primers, and qPCRBIOSyGreen Blue Mix Lo-ROX (Genesee Scientific) using a CFX Connect Real-Time PCR Detection System (Bio-Rad). qPCR data were analyzed with the Livak–Schmittgen method ($2^{-\Delta\Delta CT}$) (48).

Antibodies

See [Table S2](#) for a list of the antibodies used for immunoblotting and IF microscopy.

Data and code availability

Mass spectrometry data were deposited at the UCSD Center for Computational Mass Spectrometry MassIVE datasets <ftp://massive.ucsd.edu/MSV000085629/>. R scripts used to analyze and visualize LC-MS/MS results were deposited at GitHub <https://github.com/uclatorreslab/MassSpecAnalysis>. All remaining data are contained within this article.

Supporting information—This article contains supporting information (46, 49–51).

Acknowledgements—Figure 4F was created using BioRender.com.

Author contributions—X. G., I. R., Y. A. G., E. F. V., A. A. G., W. C., J. P. W., B. T., R. D., and J. Z. T. performed the experiments, discussed the results, and wrote the paper.

Funding and additional information—Work was supported by NIH-NIGMS R35GM139539, R01GM117475 (J. Z. T.); USHHS T32CA009056 (Y. A. G.); a grant to the University of California, Los Angeles from the HHMI through the James H. Gilliam Fellowships for Advanced Study Program and an MBI Whitcome Fellowship (E. F. V.); NIH P30DK063491 (J. P. W.) and NCI P30CA016042 (R. D.). The content is solely the responsibility of the authors and does not necessarily represent the official views of the National Institutes of Health.

Conflict of interest—The authors declare that they have no conflicts of interest with the contents of this article.

Abbreviations—The abbreviations used are: CT, C terminus; D7, *DUSP7*; DUSP, dual-specificity phosphatase; ERK, extracellular signal-regulated kinase; IF, immunofluorescence; IP, immunoprecipitation; KIM, kinase interaction motif; LAP, localization and

affinity purification; NC, negative control; NT, N terminus; OE, overexpression; PI, phosphatase inhibitor; WT, wild type; Thy, thymidine.

References

- Gordon, D. J., Resio, B., and Pellman, D. (2012) Causes and consequences of aneuploidy in cancer. *Nat. Rev. Genet.* **13**, 189–203
- Heim, A., Rymarczyk, B., and Mayer, T. U. (2017) Regulation of cell division. *Adv. Exp. Med. Biol.* **953**, 83–116
- Ong, J. Y., Bradley, M. C., and Torres, J. Z. (2020) Phospho-regulation of mitotic spindle assembly. *Cytoskeleton (Hoboken)* **77**, 558–578
- Saurin, A. T. (2018) Kinase and phosphatase cross-talk at the kinetochore. *Front. Cell Dev. Biol.* **6**, 62
- Magnaghi-Jaulin, L., Eot-Houllier, G., Gallaud, E., and Giet, R. (2019) Aurora A protein kinase: To the centrosome and beyond. *Biomolecules* **9**, 28
- Combes, G., Alharbi, L., Braga, L. G., and Elowe, S. (2017) Playing polo during mitosis: PLK1 takes the lead. *Oncogene* **36**, 4819–4827
- Bryja, V., Cervenka, L., and Cajanek, L. (2017) The connections of Wnt pathway components with cell cycle and centrosome: Side effects or a hidden logic? *Crit. Rev. Biochem. Mol. Biol.* **52**, 614–637
- Cuyas, E., Corominas-Faja, B., Joven, J., and Menendez, J. A. (2014) Cell cycle regulation by the nutrient-sensing mammalian target of rapamycin (mTOR) pathway. *Methods Mol Biol.* **1170**, 113–144
- Eblen, S. T. (2018) Extracellular-regulated kinases: Signaling from Ras to ERK substrates to control biological outcomes. *Adv. Cancer Res.* **138**, 99–142
- Wang, X. M., Zhai, Y., and Ferrell, J. E., Jr. (1997) A role for mitogen-activated protein kinase in the spindle assembly checkpoint in XTC cells. *J. Cell Biol.* **137**, 433–443
- Minshull, J., Sun, H., Tonks, N. K., and Murray, A. W. (1994) A MAP kinase-dependent spindle assembly checkpoint in *Xenopus* egg extracts. *Cell* **79**, 475–486
- Takenaka, K., Gotoh, Y., and Nishida, E. (1997) MAP kinase is required for the spindle assembly checkpoint but is dispensable for the normal M phase entry and exit in *Xenopus* egg cell cycle extracts. *J. Cell Biol.* **136**, 1091–1097
- Shinohara, M., Mikhailov, A. V., Aguirre-Ghiso, J. A., and Rieder, C. L. (2006) Extracellular signal-regulated kinase 1/2 activity is not required in mammalian cells during late G2 for timely entry into or exit from mitosis. *Mol. Biol. Cell* **17**, 5227–5240
- Meloche, S., and Pouyssegur, J. (2007) The ERK1/2 mitogen-activated protein kinase pathway as a master regulator of the G1- to S-phase transition. *Oncogene* **26**, 3227–3239
- Seternes, O. M., Kidger, A. M., and Keyse, S. M. (2019) Dual-specificity MAP kinase phosphatases in health and disease. *Biochim. Biophys. Acta Mol. Cell Res.* **1866**, 124–143
- Kim, H. S., Fernandes, G., and Lee, C. W. (2016) Protein phosphatases involved in regulating mitosis: Facts and hypotheses. *Mol. Cells* **39**, 654–662
- Patterson, K. L., Brummer, T., O'Brien, P. M., and Daly, R. J. (2009) Dual-specificity phosphatases: Critical regulators with diverse cellular targets. *Biochem. J.* **418**, 475–489
- Keyse, S. M. (2008) Dual-specificity MAP kinase phosphatases (MKPs) and cancer. *Cancer Metastasis Rev.* **27**, 253–261
- Owens, D. M., and Keyse, S. M. (2007) Differential regulation of MAP kinase signalling by dual-specificity protein phosphatases. *Oncogene* **26**, 3203–3213
- Dowd, S., Sneddon, A. A., and Keyse, S. M. (1998) Isolation of the human genes encoding the pyst1 and Pyst2 phosphatases: Characterisation of Pyst2 as a cytosolic dual-specificity MAP kinase phosphatase and its catalytic activation by both MAP and SAP kinases. *J. Cell Sci.* **111**(Pt 22), 3389–3399
- Caunt, C. J., Armstrong, S. P., Rivers, C. A., Norman, M. R., and McArdle, C. A. (2008) Spatiotemporal regulation of ERK2 by dual specificity phosphatases. *J. Biol. Chem.* **283**, 26612–26623

ACCELERATED COMMUNICATION: DUSP7 regulates ERK2 to promote cell division

22. Pfender, S., Kuznetsov, V., Pasternak, M., Tischer, T., Santhanam, B., and Schuh, M. (2015) Live imaging RNAi screen reveals genes essential for meiosis in mammalian oocytes. *Nature* **524**, 239–242
23. Tischer, T., and Schuh, M. (2016) The phosphatase Dusp7 drives meiotic resumption and chromosome alignment in mouse oocytes. *Cell Rep.* **17**, 1426–1437
24. Tanoue, T., Adachi, M., Moriguchi, T., and Nishida, E. (2000) A discordance docking motif in MAP kinases common to substrates, activators and regulators. *Nat. Cell Biol.* **2**, 110–116
25. Denu, J. M., and Dixon, J. E. (1995) A catalytic mechanism for the dual-specific phosphatases. *Proc. Natl. Acad. Sci. U. S. A.* **92**, 5910–5914
26. Zhang, Z. Y., Wang, Y., Wu, L., Fauman, E. B., Stuckey, J. A., Schubert, H. L., Saper, M. A., and Dixon, J. E. (1994) The Cys(X)5Arg catalytic motif in phosphoester hydrolysis. *Biochemistry* **33**, 15266–15270
27. Chen, P., Hutter, D., Yang, X., Gorospe, M., Davis, R. J., and Liu, Y. (2001) Discordance binding determinants for ERK2/p38alpha and JNK map kinases activate the phosphatase catalytically. *J. Biol. Chem.* **276**, 29440–29449
28. Slack, D. N., Seternes, O. M., Gabrielsen, M., and Keyse, S. M. (2001) Distinct binding determinants for ERK2/p38alpha and JNK map kinases mediate catalytic activation and substrate selectivity of map kinase phosphatase-1. *J. Biol. Chem.* **276**, 16491–16500
29. Nichols, A., Camps, M., Gillieron, C., Chabert, C., Brunet, A., Wilsbacher, J., Cobb, M., Pouyssegur, J., Shaw, J. P., and Arkininstall, S. (2000) Substrate recognition domains within extracellular signal-regulated kinase mediate binding and catalytic activation of mitogen-activated protein kinase phosphatase-3. *J. Biol. Chem.* **275**, 24613–24621
30. Favata, M. F., Horiuchi, K. Y., Manos, E. J., Daulerio, A. J., Stradley, D. A., Feeser, W. S., Van Dyk, D. E., Pitts, W. J., Earl, R. A., Hobbs, F., Copeland, R. A., Magolda, R. L., Scherle, P. A., and Trzaskos, J. M. (1998) Identification of a novel inhibitor of mitogen-activated protein kinase kinase. *J. Biol. Chem.* **273**, 18623–18632
31. Duncia, J. V., Santella, J. B., 3rd, Higley, C. A., Pitts, W. J., Wityak, J., Frieze, W. E., Rankin, F. W., Sun, J. H., Earl, R. A., Tabaka, A. C., Teleha, C. A., Blom, K. F., Favata, M. F., Manos, E. J., Daulerio, A. J., et al. (1998) MEK inhibitors: The chemistry and biological activity of U0126, its analogs, and cyclization products. *Bioorg. Med. Chem. Lett.* **8**, 2839–2844
32. Otori, M., Kinoshita, T., Okubo, M., Sato, K., Yamazaki, A., Arakawa, H., Nishimura, S., Inamura, N., Nakajima, H., Neya, M., Miyake, H., and Fujii, T. (2005) Identification of a selective ERK inhibitor and structural determination of the inhibitor-ERK2 complex. *Biochem. Biophys. Res. Commun.* **336**, 357–363
33. Haystead, T. A., Dent, P., Wu, J., Haystead, C. M., and Sturgill, T. W. (1992) Ordered phosphorylation of p42mapk by MAP kinase kinase. *FEBS Lett.* **306**, 17–22
34. Payne, D. M., Rossomando, A. J., Martino, P., Erickson, A. K., Her, J. H., Shabanowitz, J., Hunt, D. F., Weber, M. J., and Sturgill, T. W. (1991) Identification of the regulatory phosphorylation sites in pp42/mitogen-activated protein kinase (MAP kinase). *EMBO J.* **10**, 885–892
35. Torres, J. Z., Summers, M. K., Peterson, D., Brauer, M. J., Lee, J., Senese, S., Gholkar, A. A., Lo, Y. C., Lei, X., Jung, K., Anderson, D. C., Davis, D. P., Belmont, L., and Jackson, P. K. (2011) The STARD9/Kif16a kinesin associates with mitotic microtubules and regulates spindle pole assembly. *Cell* **147**, 1309–1323
36. Torres, J. Z., Miller, J. J., and Jackson, P. K. (2009) High-throughput generation of tagged stable cell lines for proteomic analysis. *Proteomics* **9**, 2888–2891
37. Bradley, M., Ramirez, I., Cheung, K., Gholkar, A. A., and Torres, J. Z. (2016) Inducible LAP-tagged stable cell lines for investigating protein function, spatiotemporal localization and protein interaction networks. *J. Vis. Exp.* <https://doi.org/10.3791/54870>
38. Gupta, G. D., Coyaud, E., Goncalves, J., Mojarad, B. A., Liu, Y., Wu, Q., Gheiratmand, L., Comartin, D., Tkach, J. M., Cheung, S. W., Bashkurov, M., Hasegan, M., Knight, J. D., Lin, Z. Y., Schueler, M., et al. (2015) A dynamic protein interaction landscape of the human centrosome-cilium interface. *Cell* **163**, 1484–1499
39. Kim, D. I., Jensen, S. C., Noble, K. A., Kc, B., Roux, K. H., Motamedchaboki, K., and Roux, K. J. (2016) An improved smaller biotin ligase for BioID proximity labeling. *Mol. Biol. Cell* **27**, 1188–1196
40. Patananan, A. N., Capri, J., Whitelegge, J. P., and Clarke, S. G. (2014) Non-repair pathways for minimizing protein isoaspartyl damage in the yeast *Saccharomyces cerevisiae*. *J. Biol. Chem.* **289**, 16936–16953
41. Stark, C., Breitkreutz, B. J., Reguly, T., Boucher, L., Breitkreutz, A., and Tyers, M. (2006) BioGRID: A general repository for interaction datasets. *Nucleic Acids Res.* **34**, D535–D539
42. Giurgiu, M., Reinhard, J., Brauner, B., Dunger-Kaltenbach, L., Fobo, G., Frishman, G., Montrone, C., and Ruepp, A. (2019) CORUM: The comprehensive resource of mammalian protein complexes-2019. *Nucleic Acids Res.* **47**, D559–D563
43. Ashburner, M., Ball, C. A., Blake, J. A., Botstein, D., Butler, H., Cherry, J. M., Davis, A. P., Dolinski, K., Dwight, S. S., Eppig, J. T., Harris, M. A., Hill, D. P., Issel-Tarver, L., Kasarskis, A., Lewis, S., et al. (2000) Gene ontology: Tool for the unification of biology. The Gene Ontology Consortium. *Nat. Genet.* **25**, 25–29
44. Franz, M., Lopes, C. T., Huck, G., Dong, Y., Sumer, O., and Bader, G. D. (2016) Cytoscape.js: A graph theory library for visualisation and analysis. *Bioinformatics* **32**, 309–311
45. Shannon, P., Markiel, A., Ozier, O., Baliga, N. S., Wang, J. T., Ramage, D., Amin, N., Schwikowski, B., and Ideker, T. (2003) Cytoscape: A software environment for integrated models of biomolecular interaction networks. *Genome Res.* **13**, 2498–2504
46. Cheung, K., Senese, S., Kuang, J., Bui, N., Ongpipattanakul, C., Gholkar, A., Cohn, W., Capri, J., Whitelegge, J. P., and Torres, J. Z. (2016) Proteomic analysis of the mammalian katanin family of microtubule-severing enzymes defines katanin p80 subunit B-like 1 (KATNBL1) as a regulator of mammalian katanin microtubule-severing. *Mol. Cell. Proteomics* **15**, 1658–1669
47. Gholkar, A. A., Senese, S., Lo, Y. C., Vides, E., Contreras, E., Hodara, E., Capri, J., Whitelegge, J. P., and Torres, J. Z. (2016) The X-linked-intellectual-disability-associated ubiquitin ligase Mid2 interacts with astrin and regulates astrin levels to promote cell division. *Cell Rep.* **14**, 180–188
48. Livak, K. J., and Schmittgen, T. D. (2001) Analysis of relative gene expression data using real-time quantitative PCR and the $2^{-\Delta\Delta Ct}$ method. *Methods* **25**, 402–408
49. Tighe, A., Johnson, V. L., and Taylor, S. S. (2004) Truncating APC mutations have dominant effects on proliferation, spindle checkpoint control, survival and chromosome stability. *J. Cell Sci.* **117**, 6339–6353
50. Rappsilber, J., Mann, M., and Ishihama, Y. (2007) Protocol for micro-purification, enrichment, pre-fractionation and storage of peptides for proteomics using StageTips. *Nat. Protoc.* **2**, 1896–1906
51. Ishihama, Y., Oda, Y., Tabata, T., Sato, T., Nagasu, T., Rappsilber, J., and Mann, M. (2005) Exponentially modified protein abundance index (empAI) for estimation of absolute protein amount in proteomics by the number of sequenced peptides per protein. *Mol. Cell. Proteomics* **4**, 1265–1272

Appendix Chapter 2

Inducible LAP-tagged Stable Cell Lines for Investigating Protein Function, Spatiotemporal Localization and Protein Interaction Networks

Video Article

Inducible LAP-tagged Stable Cell Lines for Investigating Protein Function, Spatiotemporal Localization and Protein Interaction Networks

Michelle Bradley¹, Ivan Ramirez¹, Keith Cheung¹, Ankur A. Gholkar¹, Jorge Z. Torres^{1,2,3}¹Department of Chemistry and Biochemistry, University of California, Los Angeles²Molecular Biology Institute, University of California, Los Angeles³Jonsson Comprehensive Cancer Center, University of California, Los AngelesCorrespondence to: Jorge Z. Torres at torres@chem.ucla.eduURL: <http://www.jove.com/video/54870>DOI: [doi:10.3791/54870](https://doi.org/10.3791/54870)

Keywords: Molecular Biology, Issue 118, TAP-tag, LAP-tag, Epitope-tag, Biochemical purifications, Affinity proteomics, Protein-protein interactions, Interactome, Protein interaction network, Protein localization

Date Published: 12/24/2016

Citation: Bradley, M., Ramirez, I., Cheung, K., Gholkar, A.A., Torres, J.Z. Inducible LAP-tagged Stable Cell Lines for Investigating Protein Function, Spatiotemporal Localization and Protein Interaction Networks. *J. Vis. Exp.* (118), e54870, doi:10.3791/54870 (2016).

Abstract

Multi-protein complexes, rather than single proteins acting in isolation, often govern molecular pathways regulating cellular homeostasis. Based on this principle, the purification of critical proteins required for the functioning of these pathways along with their native interacting partners has not only allowed the mapping of the protein constituents of these pathways, but has also provided a deeper understanding of how these proteins coordinate to regulate these pathways. Within this context, understanding a protein's spatiotemporal localization and its protein-protein interaction network can aid in defining its role within a pathway, as well as how its misregulation may lead to disease pathogenesis. To address this need, several approaches for protein purification such as tandem affinity purification (TAP) and localization and affinity purification (LAP) have been designed and used successfully. Nevertheless, in order to apply these approaches to pathway-scale proteomic analyses, these strategies must be supplemented with modern technological developments in cloning and mammalian stable cell line generation. Here, we describe a method for generating LAP-tagged human inducible stable cell lines for investigating protein subcellular localization and protein-protein interaction networks. This approach has been successfully applied to the dissection of multiple cellular pathways including cell division and is compatible with high-throughput proteomic analyses.

Video Link

The video component of this article can be found at <http://www.jove.com/video/54870/>

Introduction

To investigate the cellular function of an uncharacterized protein it is important to determine its *in vivo* spatiotemporal subcellular localization and its interacting protein partners. Traditionally, single and tandem epitope tags fused to the N or C-terminus of a protein of interest have been used to facilitate protein localization and protein interaction studies. For example, the tandem affinity purification (TAP) technology has enabled the isolation of native protein complexes, even those that are in low abundance, in both yeast and mammalian cell lines^{1,2}. The localization and affinity purification (LAP) technology, is a more recent development that modifies the TAP procedure to include a localization component through the introduction of the green fluorescent protein (GFP) as one of the epitope tags³. This approach has given researchers a deeper understanding of a protein's subcellular localization in living cells while also retaining the ability to perform TAP complex purifications to map protein-protein interaction networks.

However, there are many issues associated with the use of TAP/LAP technologies that has hampered their widespread use in mammalian cells. For example, the length of time that is necessary to generate a stable cell line expressing a TAP/LAP tagged protein of interest; which typically relies on cloning the gene of interest into a viral vector and selecting single cell stable integrants with the desired expression level. Additionally, many cellular pathways are sensitive to constitutive protein overexpression (even at low levels) and can arrest cells or trigger cell death over time making the generation of a TAP/LAP stable cell line impossible. These and other constraints have impeded LAP/TAP methodologies from becoming high-throughput systems for protein localization and protein complex elucidation. Therefore, there has been considerable interest in the development of an inducible high-throughput LAP-tagging system for mammalian cells that takes advantage of current innovations in cloning and cell line technologies.

Here we present a protocol for generating stable cell lines with Doxycycline/Tetracycline (Dox/Tet) inducible LAP-tagged proteins of interest that applies advances in both cloning and mammalian cell line technologies. This approach streamlines the acquisition of data with regards to LAP-tagged protein subcellular localization, protein complex purification and identification of interacting proteins⁴. Although affinity proteomics utilizes a wide range of techniques for protein complex elucidation⁵, our approach is beneficial for expediting the identification of these complexes and their native interaction networks and is amenable to high-throughput protein tagging that is necessary to investigate complex biological pathways that contain a multitude of protein constituents. Key to this approach are advancements in cloning strategies that enable high fidelity and expedited cloning of target genes into an array of vectors for gene expression *in vitro*, in various organisms like bacteria and baculovirus,

and in mammalian cells^{6,7}. Additionally, the ORFeome collaboration has cloned thousands of sequence validated open reading frames in vectors that incorporate these advances in cloning, which are available to the scientific community⁸⁻¹¹. In our system, the pGLAP1 LAP-tagging vector enables the simultaneous cloning of a large number of clones, which facilitates high-throughput LAP-tagging. This expedited cloning procedure is coupled to a streamlined approach for generating cell lines with LAP-tagged genes of interest inserted at a single pre-determined genomic locus. This makes use of cell lines that contain a single flippase recognition target (FRT) site within their genome, which is the site of integration for LAP-tagged genes. These cell lines also express the tetracycline repressor (TetR) that binds to Tet operators (TetO₂) upstream of the LAP-tagged genes and silences their expression in the absence of Dox/Tet. This allows for Dox/Tet inducible expression of the LAP-tagged protein at any given time. Having the capability of inducible LAP-tagged protein expression is critical, since many cellular pathways are sensitive to the levels of critical proteins governing the pathway and can arrest cell growth or trigger cell death when these proteins are constitutively overexpressed, even at low levels, making the generation of non-inducible LAP-tagged stable cell lines impossible¹².

Protocol

NOTE: An overview of the generation of inducible LAP-tagged stable cell lines for any protein of interest is illustrated in **Figure 1** and the overview of LAP-tagged protein expression, purification and preparation for mass proteomic analyses is illustrated in **Figure 3**.

1. Cloning the Open Reading Frame (ORF) of the Gene of Interest into the LAP-tag Vector

1. Cloning the ORF of the Gene of Interest into the Shuttle Vector.
 1. Use polymerase chain reaction (PCR) to amplify the ORF of interest with the appropriate attB1 and attB2 sites within the primers for either N-terminal fusion or C-terminal fusion. See **Table 1** for primer sequences and **Table 2** for PCR conditions.
 2. Gel purify the PCR products by resolving them on a 1% agarose gel. Excise the amplified band that is the correct size from the gel and extract it from the gel slice using a DNA gel extraction kit as per manufacturer's instructions.
 3. Incubate the purified attB containing PCR products with an attP containing shuttle vector and the recombinase that allows the PCR products to recombine into the vector as per manufacturer's instructions (see **Materials Table**).
NOTE: Empty shuttle vectors and LAP-tagging vectors contain the *ccdB* gene and have to be propagated in *ccdB* resistant bacterial cells (see **Materials Table**). However the *ccdB* gene is recombined out when an ORF is inserted into these vectors, hence use standard DH5 α *E. coli* cells when propagating vectors with cloned ORFs.
 4. Transform DH5 α *E. coli* cells with 1 μ l of the reaction product and plate the transformed cells onto a Luria broth (LB) agar plate with 50 mg/ml Kanamycin¹³.
 5. Select the Kanamycin resistant colonies.
 6. Grow the selected colonies in LB media with 50 mg/ml Kanamycin, make a DNA mini-prep and confirm gene integration by DNA sequencing using the sequencing primers listed in **Table 3**.
2. Transferring the Gene of Interest from the Shuttle Vector into the LAP-tag Vector.
 1. Incubate the shuttle vector containing the sequence verified gene of interest ORF with the LAP-tag vector (pGLAP1 for N-terminal fusion) and the recombinase that mediates the transfer of the gene of interest from the shuttle vector into the LAP-tag vector as per manufacturer's instructions (see **Materials**).
NOTE: A series of LAP/TAP vectors that can be used based on the desired promoter, epitope-tag, and N or C-terminal tagging can be found in **Table 4**.
 2. Transform DH5 α *E. coli* cells with 1 μ l of the reaction product and plate the transformed cells onto an LB agar plate with 100 mg/ml Ampicillin¹³.
 3. Select the Ampicillin resistant colonies.
 4. Grow the selected colonies in LB media with 100 mg/ml Ampicillin, make a DNA mini-prep, and confirm gene integration by DNA sequencing using the sequencing primers listed in **Table 5**.

2. Generation of an Inducible Stable Cell Line that Expresses the LAP-tagged Gene of Interest

1. Select the cell line best suited for the project of interest. Alternatively, create a host cell line from any existing cell line that constitutively expresses the TetR and contains a FRT site that allows the LAP-tagged gene of interest to be stably integrated into the genome (see **Materials**).
NOTE: This protocol uses a HEK293 cell line that contains the TetR and an FRT site, which is grown in -Tet DMEM/F12 media [made with 10% fetal bovine serum (FBS) that is devoid of Tetracycline (-Tet)]⁴.
2. Determine the minimum concentration of Hygromycin required to kill the host cell line within 1 to 2 weeks after drug addition. The concentration can vary between host cell lines, with most ranging between 100 μ g/ml and 800 μ g/ml.
NOTE: HEK293 cells grown in -Tet DMEM/F12 media with 100 μ g/ml Hygromycin at 37 °C and 5% CO₂ will die within 1-2 weeks.
3. Co-transfect the vector that expresses the flippase recombinase (mediates the integration of the LAP-tagged gene of interest into the FRT site within the genome of the cell) with the LAP-tagged vector into HEK293 cells using a transfection reagent as per manufacturer's instructions. Use a ratio of 4:1 of recombinase vector to LAP vector¹⁴.
NOTE: The optimal ratio is dependent on the host cell line and method of transfection, and may require a titration. A ratio of 4:1 works well for most cell lines. Include a mock-transfected plate as a negative control.
4. One day post-transfection, replace the -Tet DMEM/F12 media with fresh media.
5. Two days post-transfection, split cells to 25% confluence. Allow cells ~5 hr to attach, then add Hygromycin-containing -Tet DMEM/F12 media at the concentration predetermined in step 2.2. For HEK293 cells use 100 μ g/ml Hygromycin.

NOTE: The FRT containing HEK293 cell line also contains the TetR that is associated with Blasticidin resistance, therefore 5 µg/ml Blasticidin is used during the stable cell line selection process to select for the TetR and to minimize leaky expression.

6. Replace Hygromycin-containing -Tet DMEM/F12 media as needed until distinct cell foci appear that resemble opaque spots against the transparent plate.
7. Add 20 µl of trypsin on top of each cell foci and pipet up and down 2 times with a 200 µl pipet tip. Place cells in a 24 well plate and expand the cells by continual growth in Hygromycin-containing -Tet DMEM/F12 media.
8. Screen cells for inducible LAP-tagged protein expression by fixed-cell or live-cell fluorescence microscopy and/or Western blotting for the GFP tag within the LAP-tag¹⁵.

3. Purification of LAP-tagged Protein Complexes

NOTE: The following LAP-tagged protein purification protocol details recommendations on conditions and volumes used for a typical LAP-tagged protein purification based on previous experience. However, caution should be exercised to ensure that empirical optimization is carried out for any protein complex and protein expression level of interest to provide the best results.

1. Cell Growth and Cell Harvesting.
 1. Expand the validated LAP-tagged cell line for TAP isolation of protein complexes, by continually passaging all HEK293 cells into larger plates and/or roller bottles in -Tet DMEM/F12 media at 37 °C and 5% CO₂.
 2. For Tet/Dox inducible cell lines, induce for 10-15 hr at a concentration of 0.2 µg/ml Tet/Dox when the cells reach ~70% confluency, before harvesting cells.
NOTE: The concentration and induction time should be determined for each protein, a titration of 0.1-1 µg/ml Tet/Dox for 10-15 hr is recommended.
 3. Harvest cells by agitation or trypsinization and pellet cells at 875 x g for 5-10 min.
2. Coupling Anti-GFP Antibody to Protein A Beads
 1. Use 40 µg of antibody for immunoprecipitation from a lysate prepared from a 0.5 ml cell pellet, packed cell volume (PCV).
NOTE: The amount of antibody needed will depend on the abundance of the LAP-tagged protein, among other factors, and will require optimization. A titration of 10-40 µg is recommended.
 2. Equilibrate 160 µl packed volume (PV) Protein A beads into PBST (PBS + 0.1% Tween-20) in a 1.5 ml tube. Wash 3 times with 1 ml of PBST.
NOTE: All washes herein are carried out by centrifuging the beads at 5,000 x g for 10 sec.
 3. Resuspend beads in 500 µl PBST and add 80 µg of affinity-purified rabbit anti-GFP antibody to each tube of 160 µl beads. Mix for 1 hr at room temperature (RT).
 4. Wash beads 2 times with 1 ml of PBST. Then, wash beads 2 times with 1 ml of 0.2 M sodium borate, pH 9 (20 ml 0.2 M sodium borate + 15 ml 0.2 M boric acid). After the final wash, add 900 µl of the 0.2 M sodium borate, pH 9 to bring the final volume to 1 ml.
 5. Add 100 µl of 220 mM dimethylpiperimidate (DMP) to a final concentration of 20 mM. Rotate the tubes gently at RT for 30 min. For 220 mM DMP, resuspend contents of one 50 mg bottle in 877 µl of 0.2 M sodium borate, pH 9 and add immediately to the bead suspension.
 6. After incubation with DMP, wash beads 1 time with 1 ml of 0.2 M ethanolamine, 0.2 M NaCl pH 8.5 to inactivate the residual crosslinker. Resuspend beads in 1 ml of the same buffer and rotate for 1 hr at RT. Pellet beads and resuspend beads in 500 µl of 0.2 M ethanolamine, 0.2 M NaCl pH 8.5. Beads are stable for several months at 4 °C.
3. Preparation of Buffers for Cell Lysis and Complex Purification
 1. Prepare LAPX buffers (where X is the desired salt concentration [mM KCl]) of the LAP buffer; 300 mM for cell lysis, 200 mM for most bead washes, and 100 mM for washing beads prior to eluting proteins) by making a pH 7.4 solution containing 50 mM 4-(2-hydroxyethyl)-1-piperazineethanesulfonic acid (HEPES), X mM KCl, 1 mM ethylene glycol tetraacetic acid (EGTA), 1 mM MgCl₂, and 10% glycerol.
NOTE: The components of this buffer are used to approximate the environment in living cells. HEPES is used as a buffer in the pH range of 7.2-8.2. KCl is a salt used to maintain the ionic strength of the buffer. EGTA is a chelating agent that binds calcium ions to reduce the levels of calcium compared to magnesium. Glycerol and MgCl₂ are used to improve the stability of proteins.
 2. Prepare LAPX^N buffer by adding 0.05% nonyl phenoxypolyethoxyethanol to the LAPX buffer.
NOTE: Nonyl phenoxypolyethoxyethanol is a mild detergent that solubilizes proteins, but preserves protein-protein interactions, thus a higher concentration is used during the extraction process and it is then lowered during the binding and washing steps.
4. Preparation of Cell Lysates
 1. Resuspend 500 µl of PCV into 2.5 ml of LAP300 with 0.5 mM dithiothreitol (DTT) and protease inhibitors. Add 90 µl of 10% nonyl phenoxypolyethoxyethanol (0.3% final) and mix by inversion.
 2. Place on ice for 10 min. Centrifuge at 21,000 x g for 10 min. Collect this low speed supernatant (LSS). Take a 10 µl sample of the LSS for gel analysis.
 3. Transfer LSS to a TLA100.3 tube and spin at 100,000 x g for 1 hr at 4 °C. Collect this high speed supernatant (HSS), in a tube and place on ice. Take a 10 µl sample of the HSS for gel analysis.
NOTE: Avoid taking the top most lipid layer and the bottom most cell debris layer. The lipid layer should be removed by vacuum aspiration prior to collecting the HSS.
5. First Affinity Capture: Binding to Anti-GFP Beads
 1. Pre-elute antibody coupled beads (use 160 µl of beads per 0.5 ml cell pellet (PCV)) by washing them 3 times with 1 ml of elution buffer [3.5 M MgCl₂ with 20 mM Tris, pH 7.4] to get rid of uncoupled antibodies and reduce background. Do quickly. Do not leave beads in high salt for a long time.
 2. Wash beads 3 times with 1 ml of LAP200^N. Mix HSS extract with antibody beads for 1 hr at 4 °C. Centrifuge at 21,000 x g for 10 min. Take a 10 µl sample of the supernatant (*i.e.*, the flow through (FT)) for gel analysis.

3. Wash beads 3 times with 1 ml of LAP200^N with 0.5 mM DTT and protease inhibitors. Wash beads 2 times (5 min each) with 1 ml of LAP200^N with 0.5 mM DTT and protease inhibitors. Wash quickly 2 times with 1 ml of LAP200^N with 0.5 mM DTT and no protease inhibitors before adding the tobacco etch virus (TEV) protease.
6. TEV Cleavage
 1. Dilute 10 µg TEV protease in 1 ml of LAP200^N and rotate tubes at 4 °C overnight.
NOTE: This step can be optimized for any LAP-tagged protein to be completed in a few hours by adjusting the concentration of TEV protease, which can aid the preservation of LAP-tagged protein complexes.
 2. Pellet beads and transfer supernatant to a fresh tube. Rinse beads twice with 160 µl LAP200^N with 0.5 mM DTT and protease inhibitors (triple concentration) to remove any residual protein. Take a 10 µl sample of the supernatant for gel analysis.
7. Second Affinity Capture: Binding to S Protein Agarose
 1. Wash 1 tube of 80 µl S protein agarose slurry (40 µl packed resin) 3 times with 1 ml of LAP200^N.
NOTE: S protein binding to the S-tag will reconstitute an active RNase and an alternative second epitope tag should be considered for RNA containing protein complexes.
 2. Add TEV eluted supernatant to S protein agarose beads and rock for 3 hr at 4 °C. Pellet beads and wash 3 times with 1 ml of LAP200^N with 0.5 mM DTT and protease inhibitors. Wash beads 2 times with 1 ml of LAP100.
8. Protein Elution
 1. Elute proteins off S protein agarose by adding 50 µl of 4x Laemmli sample buffer and heat at 97 °C for 10 min.
NOTE: Proteins can also be eluted from the beads with elution buffer (3.5 M MgCl₂ with 20 mM Tris, pH 7.4).

4. Identify Interacting Proteins by Mass Spectrometry Analysis

1. Test the quality of the purification by analyzing the collected samples by sodium dodecyl sulfate polyacrylamide gel electrophoresis (SDS-PAGE), silver staining the gel (see **Materials Table**) and by immunoblotting the eluates and probing with anti-GFP antibodies to ensure that the LAP-tagged purification worked¹⁶, see **Figure 4**.
2. To identify stoichiometric and substoichiometric co-purifying species, take the final elution sample and separate it by SDS-PAGE. Stain the gel with a mass spectrometry compatible protein stain. Excise the most prominent bands and the space in between them from the gel and process them for analysis by mass spectrometry separately¹⁶.
NOTE: There are numerous approaches for separating the final purification eluates and preparing them for mass spectrometry⁵. For example, LAP-purified complexes can be eluted from S-protein beads by using high salt (3.5 M MgCl₂) and the entire protein population en masse can be analyzed by mass spectrometry¹⁷. Alternatively, final eluates can be separated for 1 mm by SDS-PAGE and a single 1 mm band can be excised and analyzed. This clears the complex mixture of any beads or particulate matter that will interfere with the analysis.

Representative Results

To highlight the utility of this system, the open reading frame (ORF) of the Tau microtubule binding protein was cloned into the shuttle vector by amplifying the Tau ORF with primers containing attB1 and attB2 sites (**Table 1**) and incubating the PCR products with the shuttle vector and a recombinase that mediates the insertion of the PCR products into the shuttle vector. The reaction products were used to transform DH5α bacteria¹³ and plasmid DNA from Kanamycin resistant colonies was sequenced to ensure Tau insertion. A sequence validated shuttle-Tau vector was then used to transfer the Tau ORF into the pGLAP1 vector, which fused Tau in frame with the LAP (EGFP-TEV-S-Protein) tag, by incubating the shuttle-Tau vector with the pGLAP1 vector and the recombinase that mediates the transfer of the ORF from the shuttle vector to pGLAP1. The reaction products were used to transform DH5α bacteria¹³ and plasmid DNA from Ampicillin resistant colonies was sequenced to ensure that the LAP-Tau fusion was in frame. Sequence validated pGLAP1-LAP-Tau was then co-transfected with a vector that expresses the flippase recombination enzyme into HEK293 cells that contained a single flippase recognition target (FRT) site within their genome, which is the site of integration for LAP-tagged genes¹⁴. This cell line also expressed the TetR that binds to Tet operators upstream of the LAP-tagged genes and silences their expression in the absence of Tet/Dox. Stable integrants were selected with -Tet DMEM/F12 media with 100 µg/ml Hygromycin for 5 days. Individual Hygromycin resistant cell foci were harvested by adding 20 µl of trypsin on top and pipetting up and down 2 times. Cells were placed in a 24 well plate and expanded by continual growth in -Tet DMEM/F12 media.

To verify that the Hygromycin resistant cells were capable of expressing LAP-Tau, HEK293 LAP-Tau cells were induced with 0.1 µg/ml Dox for 15 hr and protein extracts were prepared from non-induced and Dox-induced cells. These extracts were separated by SDS-PAGE, transferred to a PVDF membrane, and immunoblotted for GFP and Tubulin as loading control. As seen in **Figure 4A**, LAP-Tau (visualized with anti-GFP antibodies) was only expressed in the presence of Dox. To validate that LAP-Tau was properly localized to the mitotic microtubule spindle during mitosis, as had been previously shown for endogenous Tau¹⁸, HEK293 LAP-Tau cells were induced with 0.1 µg/ml Dox for 15 hr and cells were fixed with 4% paraformaldehyde and co-stained for DNA (Hoechst 33342) and microtubules (anti-Tubulin antibodies). Consistently, LAP-Tau was localized to the mitotic spindle during metaphase of mitosis (**Figure 4B**). To verify that LAP-Tau and its interacting proteins could be purified with this system, HEK293 LAP-Tau cells were grown in roller bottles to ~70% confluency, induced with 0.1 µg/ml Dox for 15 hr, harvested by agitation, lysed with LAP300 buffer, and LAP-Tau was purified using the above protocol. Eluates from the LAP-Tau purification were resolved by SDS-PAGE and the gel was silver stained. **Figure 4C** shows the LAP-Tau purification, marked with an asterisk is LAP-Tau and several other bands indicative of Tau interacting proteins can be seen.

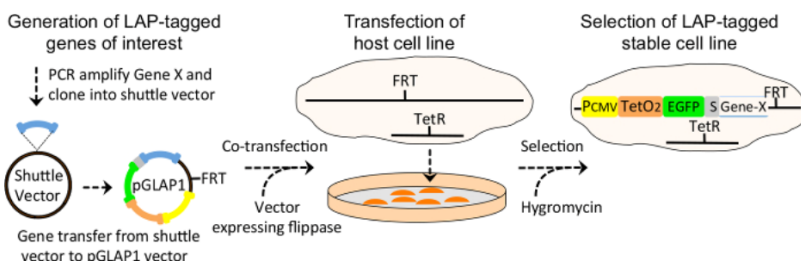


Figure 1: Overview of the Generation of LAP-tagged Inducible Stable Cell Lines for any Protein of Interest. The open reading frame (ORF) of genes of interest are amplified with attB1 and attB2 sites flanking the 5' and 3' end sequences, respectively (primer sequences are given in **Table 1**) and cloned into the shuttle vector. Sequence verified shuttle vectors with the gene of interest are then used to transfer the gene of interest into the pGLAP1 vector. The sequence verified pGLAP1 vector with the gene of interest is then co-transfected with the vector containing the flippase recombinase into the desired cell line that contains a single flippase recognition target (FRT) site within their genome, which is the site of integration for LAP-tagged genes. These cell lines also express the Tet repressor (TetR) that binds to Tet operators (TetO₂) upstream of the LAP-tagged genes and silences their expression in the absence of Tet/Dox. The LAP-tagged gene of interest is then recombined into the FRT site and stable integrants are selected with Hygromycin. [Please click here to view a larger version of this figure.](#)

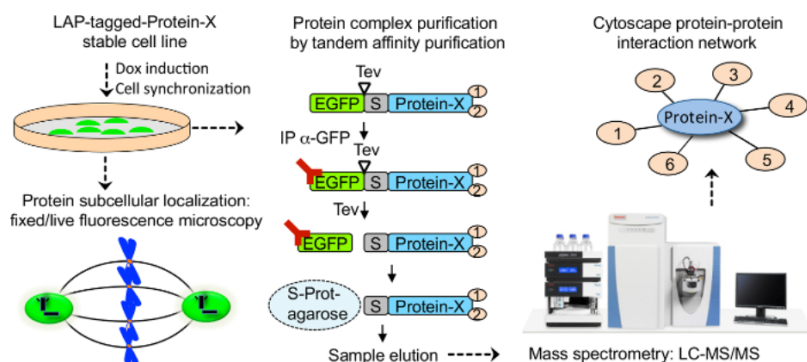


Figure 2: Overview of the Applications for LAP-tagged Stable Cell Lines. LAP-tagged inducible stable cell lines are induced to express the LAP-tagged protein of interest by Dox addition and can be synchronized at various stages of the cell cycle or can be stimulated with chemicals or ligands to activate any desired signaling pathway. The subcellular localization of the LAP-tagged protein of interest can be analyzed by live cell or fixed cell imaging. LAP-tagged proteins can also be tandem affinity purified and their interacting proteins can be identified by liquid chromatography tandem mass spectrometry (LC-MS/MS). Finally, Cytoscape can be used to generate a protein-protein interaction network of the bait protein. Dox indicates Doxycycline, IP indicates immunoprecipitate, EGFP indicates enhanced green fluorescent protein, Tev indicates TEV protease cleavage site, and S indicates S-tag. [Please click here to view a larger version of this figure.](#)

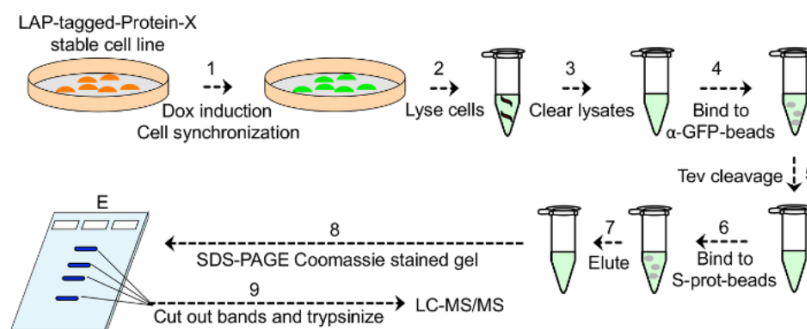


Figure 3: Overview of LAP-tagged Protein Expression, Purification and Preparation for Mass Spectrometry. The protocol has 9 steps: 1) growth and induction of LAP-tagged protein expression, 2) cell harvesting and lysis, 3) the preparation of lysates, 4) the binding of lysates to anti-GFP beads, 5) TEV protease cleavage of the GFP-tag, 6) the binding of lysates to S-protein beads, 7) the elution of the bait protein and interacting proteins, and 8-9) the preparation of samples for mass spectrometry-based proteomic analyses. [Please click here to view a larger version of this figure.](#)

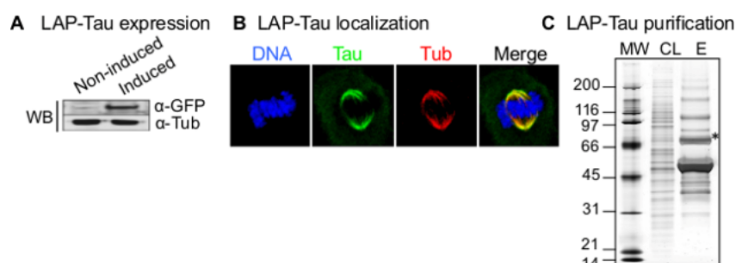


Figure 4: Verification of LAP-Tau expression. (A) Western blot (WB) analysis of protein samples from non-induced and Dox induced LAP-Tau HEK293 cells probed with anti-GFP and anti-Tubulin antibodies to detect the LAP-tagged Tau protein and the Tubulin loading control, respectively. Note that LAP-Tau is only expressed when the cells are induced with Dox. (B) Mitotic cells expressing LAP-Tau were fixed and co-stained for DNA (Hoechst 33342) and Tubulin (Tub) with anti-tubulin antibodies and the subcellular localization of LAP-tau was analyzed by fluorescence microscopy. Note that LAP-Tau localizes to the mitotic spindle and spindle poles during mitosis. (C) Silver stained gel of the LAP-Tau purification. MW indicates molecular weight, CL indicates cleared lysates, and E indicates final eluates. Samples were run on a 4-20% SDS-PAGE and the gel was silver stained to visualize the purified proteins. Note that a band corresponding to LAP-Tau is marked with an asterisk and several other bands corresponding to co-purifying proteins can be seen. [Please click here to view a larger version of this figure.](#)

N-terminal fusion	
Forward	5'- GGG GACAAGT TGTACAAAAAGCAGGCTTCATG-(>18gsn)-3'
Reverse	5'-GGG GACCACTTTGTACAAGAAAGCTGGGT T TTATCA-(>18gsn)-3'
C-terminal fusion	
Forward	5'-GGG GACAAGTTTGTACA AAAAAGCAGGCTTCACC-(>18gsn)-3'
Reverse	5'-GGG GACCACTTTGTACA AGAAAGCTGGGTG-(>18gsn)-3'

Table 1: Forward and Reverse Primers for Amplifying ORFs or Interest for Insertion into the Shuttle Vector. The attB sites are highlighted in bold letters, gsn denotes that more than 18 gene specific nucleotides are added to the primer.

Step	Temperature	Time
Initial denaturation	94 °C	2 min
PCR Amplification Cycles (35)	Denature	94 °C
	Anneal	55 °C (depending on the primer T _m)
	Extend	72 °C
Hold	4 °C	indefinitely

Table 2: PCR Conditions for Amplification of the ORFs of Interest.

Vector	Forward Sequencing Primer	Reverse Sequencing Primer
Shuttle Vector	5'-TGTAACGACGGCCAGT-3'	5'-CAGGAAACAGCTATGAC-3'

Table 3: Forward and Reverse Sequencing Primers for the Shuttle Vector.

ID	Structure	Parental	Promoter	Bac Res	Mam Res	Tet reg?
pGLAP1	N-term EGFP-TEV-S peptide	pcDNA5/FRT/TO	CMV	Amp	Hyg	Yes
pGLAP2	N-term Flag-TEV-S peptide	pcDNA5/FRT/TO	CMV	Amp	Hyg	Yes
pGLAP3	N-term EGFP-TEV-S peptide; C-term V5	pEF5/FRT-V5	EF1a	Amp	Hyg	No
pGLAP4	N-term Flag-TEV-S peptide; ; C-term V5	pEF5/FRT-V5	EF1a	Amp	Hyg	No
pGLAP5	C-term S peptide-PreProt x2-EGFP	pEF5/FRT-V5	EF1a	Amp	Hyg	No

Table 4: List of Available LAP/TAP Vectors with Variable Promoters, Epitope-tags, and Dox Inducible Expression Capabilities for N or C-terminal Protein Tagging. Vectors are commercially available. Bac Res indicates bacterial resistance marker, Mam Res indicates mammalian cell resistance marker, Tet reg? indicates whether expression is Tet/Dox regulatable.

Vector	Forward Sequencing Primer	Reverse Sequencing Primer
pGLAP1	5'-ATCACTCTCGGCATGGACGAGCTGTACAAG-3'	5'-TGGCTGGCAACTAGAAGGCACAGTCGAGGC-3'
pGLAP2	5'-CGAACGCCAGCACATGGACAGGG-3'	5'-TGGCTGGCAACTAGAAGGCACAGTCGAGGC-3'
pGLAP3	5'-AGAAACCCTGCTGCTAA-3'	5'-TAGAAGGCACAGTCGAGG-3'
pGLAP4	5'-AGACCCAAGCTGGCTAGGTAAGC-3'	5'-TAGAAGGCACAGTCGAGG-3'
pGLAP5	5'-CGTAATACGACTCACTATAG-3'	5'-TCCAGGGTCAAGGAAGGCACGG-3'

Table 5: Forward and Reverse Sequencing Primers for pGLAP Vectors.

Discussion

The outlined protocol describes the cloning of genes of interest into the LAP-tagging vector, the generation of inducible LAP-tagged stable cell lines, and the purification of LAP-tagged protein complexes for proteomic analyses. With respect to other LAP/TAP-tagging approaches, this protocol has been streamlined to be compatible with high-throughput approaches to map protein localization and protein-protein interactions within any cellular pathway. This approach has been widely applied to the functional characterization of proteins critical for cell cycle progression, mitotic spindle assembly, spindle pole homeostasis, and ciliogenesis to name a few and has aided the understanding of how misregulation of these proteins can lead to human diseases^{15,16,19,20}. For example, our group recently utilized this system to define the function and regulation of the STARD9 mitotic kinesin (a candidate cancer target) in spindle assembly^{15,21}, to define a new molecular link between the Tctex1d2 dynein light chain and short rib polydactyly syndromes (SRPS)¹⁹, and to define a new molecular link to understanding how mutation of the Mid2 ubiquitin ligase can lead to X-linked intellectual disabilities¹⁶. Other laboratories have also successfully applied this method, including one that determined that Tctn1, a regulator of mouse Hedgehog signaling, was a part of a ciliopathy-associated protein complex that regulated ciliary membrane composition and ciliogenesis in a tissue-dependent manner^{22,23}. Therefore, this protocol can be broadly applied to the dissection of any cellular pathway.

A critical step in this protocol is the selection of LAP-tagged stable cell lines that are Hygromycin resistant. Special care should be taken to ensure that all cells in the control plate are dead before selecting foci in the experimental plate for amplification. Hygromycin can also be added during routine cell culturing of LAP-tagged stable cell lines to further ensure that all cells maintain the LAP-tagged gene of interest at the FRT site. We caution that not all LAP-tagged proteins will be functional and that it is important to have assays in place that can be used to test protein function. Examples of assays used to test protein function include the rescue of siRNA-induced phenotypes and *in vitro* activity assays. To address any potential problems with the addition of a large LAP-tag, we have previously generated TAP-tag vectors compatible with this system that contain smaller tags, like FLAG, which are less likely to inhibit the function and localization of the protein of interest⁴. In addition, LAP-tagging vectors exist for generating C-terminal LAP-tagged proteins or C-terminal TAP-tagged proteins that are compatible with this system, which can be used in cases where a LAP/TAP tag is not tolerated at the N-terminus of a protein. Additionally, the salt and detergent concentrations of the purification buffers (LAPX⁴) can be modified to increase or decrease the purification stringency if none or too many interactions are observed. Similarly, the tandem affinity purification procedure is more stringent than single purification procedures and weak interactors may be lost, thus a single purification scheme can be used when few or no interactors are identified.

It is important to note that other GFP epitope tagging approaches exist that allow large scale GFP protein tagging for protein localization and purification studies^{24,25}. These include the BAC TransgenOmics approach that utilizes bacterial artificial chromosomes to express GFP-tagged genes of interest from their native environment that contains all the regulatory elements, which mimics endogenous gene expression²⁴. More recently, CAS9/single-guided RNA (sgRNA) ribonucleoprotein complexes (RNPs) have been used to endogenously tag genes of interest with a split-GFP system that allows the expression of GFP-tagged genes from their endogenous genomic loci²⁵. Although both of these approaches enable the expression of tagged proteins under endogenous conditions, compared to the LAP-tagging protocol described here, they do not allow for inducible and tunable expression of the tagged genes of interest. Additionally, they have yet to be applied to tandem epitope tagging for TAP.

It is also important to note that other tagging systems can also be modified to become compatible with the system described here for generating inducible epitope-tagged stable cell lines. For example, proximity-dependent biotin identification (BioID) has garnered considerable attention due to its ability to define spatial and temporal relationships among interacting proteins²⁶. This technique exploits protein fusions to a promiscuous strain of the *Escherichia coli* biotin ligase BirA, which biotinylates any protein within a ~10 nm radius of the enzyme. The biotinylated proteins are then affinity purified using biotin-affinity capture and analyzed for composition by mass spectrometry. BirA will biotinylate any protein in close proximity, even transiently, which makes it especially suited for detecting weaker interacting partners within a complex²⁷. Additionally, the purification scheme does not necessitate that endogenous protein-protein interactions remain intact and can be carried out under denaturing conditions, thus reducing the rate of false positives. Within our current protocol, the substitution of the pGLAP1 vector by a BirA-tagging vector could transform this system from identifying protein-protein interactions based on affinity to detecting them based on proximity. Such a system would be highly advantageous for detecting transient protein interactions as is the case between many enzyme-substrate interactions and for mapping the spatiotemporal protein-protein interactions within defined structures as has been carried out for the centrosome and cilia^{26,28}.

Disclosures

The authors have nothing to disclose.

Acknowledgements

This work was supported by a National Science Foundation Grant NSF-MCB1243645 (JZT), any opinions, findings, and conclusions or recommendations expressed in this material are those of the authors and do not necessarily reflect the views of the National Science Foundation. The funders had no role in study design, data collection and analysis, decision to publish, or preparation of the manuscript.

References

- Rigaut, G. *et al.* A generic protein purification method for protein complex characterization and proteome exploration. *Nat Biotechnol.* **17**, 1030-1032 (1999).
- Puig, O. *et al.* The tandem affinity purification (TAP) method: a general procedure of protein complex purification. *Methods.* **24**, 218-229 (2001).
- Cheeseman, I. M., & Desai, A. A combined approach for the localization and tandem affinity purification of protein complexes from metazoans. *Sci STKE.* **2005**, p11 (2005).
- Torres, J. Z., Miller, J. J., & Jackson, P. K. High-throughput generation of tagged stable cell lines for proteomic analysis. *Proteomics.* **9**, 2888-2891 (2009).
- LaCava, J. *et al.* Affinity proteomics to study endogenous protein complexes: pointers, pitfalls, preferences and perspectives. *Biotechniques.* **58**, 103-119 (2015).
- Landy, A. Dynamic, structural, and regulatory aspects of lambda site-specific recombination. *Annu Rev Biochem.* **58**, 913-949 (1989).
- Hartley, J. L., Temple, G. F., & Brasch, M. A. DNA cloning using in vitro site-specific recombination. *Genome Res.* **10**, 1788-1795 (2000).
- The ORFeome Collaboration: a genome-scale human ORF-clone resource. *Nat Methods.* **13**, 191-192 (2016).
- Brasch, M. A., Hartley, J. L., & Vidal, M. ORFeome cloning and systems biology: standardized mass production of the parts from the parts-list. *Genome Res.* **14**, 2001-2009 (2004).
- Lamesch, P. *et al.* hORFeome v3.1: a resource of human open reading frames representing over 10,000 human genes. *Genomics.* **89**, 307-315 (2007).
- Rual, J. F. *et al.* Human ORFeome version 1.1: a platform for reverse proteomics. *Genome Res.* **14**, 2128-2135 (2004).
- Fiering, S., Kim, C. G., Epner, E. M., & Groudine, M. An "in-out" strategy using gene targeting and FLP recombinase for the functional dissection of complex DNA regulatory elements: analysis of the beta-globin locus control region. *Proc Natl Acad Sci U S A.* **90**, 8469-8473 (1993).
- Sambrook, J., Fritsch, E. F., & Maniatis, T. *Molecular cloning: a laboratory manual*. 2nd ed. edn, Cold Spring Harbor Laboratory, (1989).
- Uyttersprot, N., Costagliola, S., & Miot, F. A new tool for efficient transfection of dog and human thyrocytes in primary culture. *Mol Cell Endocrinol.* **142**, 35-39 (1998).
- Senese, S. *et al.* A unique insertion in STARD9's motor domain regulates its stability. *Mol Biol Cell.* **26**, 440-452 (2015).
- Gholkar, A. A. *et al.* The X-Linked-Intellectual-Disability-Associated Ubiquitin Ligase Mid2 Interacts with Astrin and Regulates Astrin Levels to Promote Cell Division. *Cell Rep.* **14**, 180-188 (2016).
- Graumann, J. *et al.* Applicability of tandem affinity purification MudPIT to pathway proteomics in yeast. *Mol Cell Proteomics.* **3**, 226-237 (2004).
- Connolly, J. A., Kalnins, V. I., Cleveland, D. W., & Kirschner, M. W. Immunofluorescent staining of cytoplasmic and spindle microtubules in mouse fibroblasts with antibody to tau protein. *Proc Natl Acad Sci U S A.* **74**, 2437-2440 (1977).
- Gholkar, A. A. *et al.* Tctex1d2 associates with short-rib polydactyly syndrome proteins and is required for ciliogenesis. *Cell Cycle.* **14**, 1116-1125 (2015).
- Cheung, K. *et al.* Proteomic Analysis of the Mammalian Katanin Family of Microtubule-severing Enzymes Defines Katanin p80 subunit B-like 1 (KATNBL1) as a Regulator of Mammalian Katanin Microtubule-severing. *Mol Cell Proteomics.* **15**, 1658-1669 (2016).
- Torres, J. Z. *et al.* The STARD9/Kif16a Kinesin Associates with Mitotic Microtubules and Regulates Spindle Pole Assembly. *Cell.* **147**, 1309-1323 (2011).
- Garcia-Gonzalo, F. R. *et al.* A transition zone complex regulates mammalian ciliogenesis and ciliary membrane composition. *Nat Genet.* **43**, 776-784 (2011).
- Chih, B. *et al.* A ciliopathy complex at the transition zone protects the cilia as a privileged membrane domain. *Nat Cell Biol.* **14**, 61-72 (2012).
- Leonetti, M. D., Sekine, S., Kamiyama, D., Weissman, J. S., & Huang, B. A scalable strategy for high-throughput GFP tagging of endogenous human proteins. *Proc Natl Acad Sci U S A.* **113**, E3501-3508 (2016).

25. Poser, I. *et al.* BAC TransgeneOmics: a high-throughput method for exploration of protein function in mammals. *Nat Methods*. **5**, 409-415 (2008).
26. Firat-Karalar, E. N., & Stearns, T. Probing mammalian centrosome structure using BioID proximity-dependent biotinylation. *Methods Cell Biol.* **129**, 153-170 (2015).
27. Roux, K. J., Kim, D. I., & Burke, B. BioID: a screen for protein-protein interactions. *Curr Protoc Protein Sci.* **74**, Unit 19 23 (2013).
28. Gupta, G. D. *et al.* A Dynamic Protein Interaction Landscape of the Human Centrosome-Cilium Interface. *Cell*. **163**, 1484-1499 (2015).